SPRINGER BRIEFS IN PHYSICS

Vladimir G. Plekhanov

Isotope-Based Quantum Information

Springer

SpringerBriefs in Physics

For further volumes:
http://www.springer.com/series/8902

Vladimir G. Plekhanov

Isotope-Based Quantum Information

Springer

Vladimir G. Plekhanov
Mathematics and Physics Department
Computer Science College
Erika Street 7a
10416 Tallinn
Estonia

ISSN 2191-5423 ISSN 2191-5431 (electronic)
ISBN 978-3-642-28749-7 ISBN 978-3-642-28750-3 (eBook)
DOI 10.1007/978-3-642-28750-3
Springer Heidelberg New York Dordrecht London

Library of Congress Control Number: 2012937298

Printed on acid-free paper

Springer is part of Springer Science+Business Media (www.springer.com)

Preface

During the past decades the field of *quantum information* processing has experienced extremely rapid progress. This book provides an introduction to the main ideas and techniques of the rapid progressing field of quantum information and quantum computation using *isotope-mixed* materials. This book is divided into four chapters. Chapter 2 presents the introduction to the physics of isotope effect in solids. My goal here is to give an elementary introduction which is accessible not only to physics, but also to mathematicians and computer scientists desiring an initiation into subject. In this chapter isotope *low-dimensional structures* are very shortly described. The reader might understand the material presented in this chapter without the need for consulting other texts. Chapter 3 is devoted to the description of classical and quantum information. The rest of the chapter has presented the concepts and models of quantum computers. There are discussed not only different algorithms of quantum computation but also are presented the different models of *quantum computers*. The quantum error corrections is very briefly discussed. We did not attempt to make our small book self-contained by explaining every concept which is needed only occasionally. We do hope, however, that we have succeded in explaining the basic concepts from quantum mechanics and computer science which are used throughout the book and the whole field of quantum information and *quantum computation*.

With numerous illustrations this small book will be of great interest to undergraduate and graduate students taking courses in *mesoscopic* physics or nanoelectronics as well as quantum information, and academic and industrial researchers working in this field.

The bibliography at the end of the each chapter includes many of the key papers in the area and points to other books and survey papers on the subject.

Tallinn Vladimir G. Plekhanov

Acknowledgments

Many thanks are due to Prof. W. Reder for carefully reading the manuscript as well as Dr. N. Write for improving my English. I appreciate that invaluable help given by Mr. M. T. Kivi (Dr. of Medicine) during my difficult period. Again it is pleasure to thank the Staff of Springer, in particular Dr. C. Ascheron and Elke Sauer, for the continued excellent cooperation. I deeply thank the authors and publishers who have kindly permitted us to reproduce figures and tables from their papers and books.

In a few cases I have been unable to contact the authors, and I would be grateful if they would nevertheless retrospectively give me the necessary permission. I wish to express me deep gratitude my family for their patience during long preparation of this book.

Contents

Chapter 1
Introduction

Investigation, manufacture, and application of *isotopes* are highly variable and is determined by the different areas of science and technique. The range of the application of isotopes is exclusively wide: starting with the investigation of universal principle of the structure matter and common normality evolution of *Universe* [1–3] and finished by different biochemical process in living organisms as well as special technical applications [4]. The presence of isotopes and isotope effect in nature serves the bright illustration of the mutual connection between simplicity and complexity in science [5].

The paramount meaning has the role of isotopes in the fundamental natural science investigations. This includes not only the study of nature's nuclear interactions and, in this way, the origin of *isotope effect*, but also the reconstructions of nucleogenesis process of the Universe, which could explain the observable in nature relative to spreading of chemical elements [1–3].

Investigations of the *atomic nucleus*, and the fundamental forces that determine *nuclear* structure, as is well known, offer fascinating insights into the nature of the physical world. We all well known that the history of the nuclear physics dates from the latter years of the nineteenth century when Henry Becqeurel in 1896 discovered the radioactivity. He was working with compounds containing the element uranium. Becqeurel found that photographic plates covered to keep out light became fogged, or partially exposed, when these uranium compounds were anywhere near the plates. Two years after Becquerel's discovery, Pierre and Marie Curie in France and Rutherford in England succeeded in separating a naturally occurring radioactive element, radium ($Z = 88$) from the ore. It was soon revealed that there are three, distinctly different types of radiation emitted by radioactive substances. They were called *alpha* (α), *beta* (β) and *gamma* (γ) rays—terms which have been retained in ours days. When a *radioactive source* was placed in a magnetic field, it was found that there were three different types of activity, as the trajectories of some of the rays emitted were deflected to one direction, some to the opposite direction, and some not affected at all. Subsequently it was found that α-rays consist of positively charged ^{4}He nuclei, β-rays are made of electrons (positrons) and γ-rays are nothing

V. G. Plekhanov, *Isotope-Based Quantum Information*, SpringerBriefs in Physics,
DOI: 10.1007/978-3-642-28750-3_1, © The Author(s) 2012

but electromagnetic radiation that carries no net charge. The existence of the nucleus as the small central part of an atom was first proposed by Rutherford in 1911. Rutherford proposed that the atom does consist of a small, heavy positively charged center surrounded by orbiting electrons which occupy the vast bulk of the atoms volume. The simplest atom—hydrogen—consisted of a proton and a single orbital electron. Later, in 1920, the radii of a few heavy nuclei were measured by Chadwick and were found to be in the order of 10^{-14} m., much smaller than the order of 10^{-10} m for atomic radii (for details, see e.g. [6] and references therein).

The building blocks of nuclei are *neutrons* and *protons*, two aspects, or quantum states, of the same particle, the nucleon. Since a neutron does not carry any net electric charge and is unstable as an isolated particle (see, below), it was not discovered until 1932 by Chadwick, whose existence has been anticipated by Rutherford as early as 1920. Since only positive charges (protons) are present in nucleus, the electromagnetic force inside a nucleus is repulsive and the *nucleons* cannot be held together unless there is another source of force that is attractive and stronger than Coulomb's.

Studies of the structure of the nucleus have shown that it is composed of protons and neutrons, and more recently studies (see, e.g. [6]) of very high energy collisions have shown that these protons and neutrons are themselves composed of elusive particles called *quarks.* Particle physics deals with the world of the quarks and all other particles still thought to be fundamental.

Thus, our present knowledge of physical phenomena suggests that there are four types of forces between physical objects:

(1) gravitational;
(2) electromagnetic;
(3) strong, and
(4) weak.

Both gravitational and electromagnetic forces are infinite in range and their interaction strength diminish with the square of the distance of separation. Clearly, nuclear force cannot follow the same radial dependence. Being much stronger, it would have pulled the nucleons in different nuclei together into a single unit and destroyed all the atomic structure we are familiar with. In fact, nuclear force has a very short distance.

If in the nuclear physics the meaning of isotope is establishing one then application isotope effect in atomic and molecular physics allows to get the results, which are difficult to overestimate so far as owing to this results it was to construct the "building" of the science of the twentieth century-the *quantum mechanics* (see, also [6]). During the last fifty years the isotope effect is one of the modern and power methods for investigation of structure and properties of solids. This conclusion supports the numerous reviews (see, e.g. [7–9]) and first monographs [4, 10] dedicated to isotope effect of stable isotopes. In the last years the more and more investigations of *solid-state physics* are conducted by using *radioactive* isotopes, which give evidence of the already comprehensive list of references (see, for instance [11–15]).

This book consists of four part. First one is the traditional introduction of the subject written. The second part devotes to the short description of the ground of

nature of isotope effect. With this aim the detailed analysis of the neutron and proton structure and their mutual transformation in the weak interaction process was conducted. Note that the main characteristics of isotope effect—the mass of free particles (proton and neutron) does not conserve in the *weak interaction* process. This contradiction is removed although partly if take into account the modern presentation [16] that the mass of proton (neutron) is created from quark condensate (not from constituent quarks [17–19]) which is the coherent superposition of the states with different chirality. Thus the elucidation of the reason of origin of the nucleon mass is taken down to elucidation of the reason to break down the chiral symmetry in *Quantum Chromodynamics* [20–27]. In this part of the book the manifestation of isotope effect in phonon and electron (exciton) states of solids is considered. With comparison to the change of corresponding characteristics (for example: the lines shift in *absorption, scattering, emission* spectra) in the isotope effect in atomic physics and condensed matter physics on two orders more in solid (see, for example [28]). It is underlined that taking into account only linear part of electron–phonon interaction is not sufficient for the description of the experimental facts on the elementary excitations of systems consisting of light elements with isotope effect.

The subject of *quantum information* brings together ideas from quantum physics, classical information theory, and computer science. This topic is devoted the third part of book. It is very significant that information can be expressed in different ways without losing its essential nature, since this leads to the possibility of the automatic manipulation of information—a machine needs only to be able to manipulate quite simple things like integers in order to do surprisingly powerful information processing. It is easy to do from document preparation to differential calculus and even to translating between human languages.

We should recall that quantum mechanics has developed originally as a theory to explain behavior of large number (ensembles) of microscopic objects, such as atoms or electrons [29–31]. However, over the last decades, considerable interest in the application of quantum theory to individual systems—mesoscopic and even macroscopic systems where a small number of collective degree of freedom show genuine quantum behavior (see, e.g. [32, 33]). One exciting aspect of this developing fundamental research is its technological potential. Its results that might be termed quantum information technology. As we know well, the first deep insight into quantum information theory came with Bell's 1964 analysis [34, 35] of the paradoxical thought experiment by Einstein and co-workers in 1935 [36]. Bell's inequality draws attention to the importance of correlations between separated quantum objects which have interacted in the past, but which no longer influence one another. In essence, his argument shows that the degree of correlation which can be present in such systems exceeds that which could be predicted on the basis of any law of physics which describes particles in terms of classical variables rather than quantum states. The next link between quantum mechanics and information theory came about when it was realized that simple properties of quantum systems, such as the unavoidable disturbance involved in measurement, could be put to practical use in quantum cryptography (see, e.g. review [38] and references therein). Quantum cryptography covers several ideas, of which the most firmly established is quantum

key distribution. This is an ingenious method in which transmitted quantum states are used to perform a very particular communication task. The significant feature is that the principles of quantum mechanics guarantee a type of conservation of quantum information, so that if the necessary quantum information arrives at the parties wishing to establish a random key. They can be sure it has not gone elsewhere, such as to spy. This part of the book considers not only the theory of *cryptography*but also its practical application [38].

References

1. E.M. Burbidge, G.R. Burbidge, W.A. Fowler, F. Hoyle, Synthesis of the elements in Stars. Rev. Mod. Phys. **29**, 547–652 (1957)
2. G. Wallerstein, I. Jhen Jr, P. Parker et al., Synthesis of the elements in stars:forty years in progress. Rev. Mod. Phys. **69**, 995–1084 (1997)
3. S. Esposito, Primordial Nucleosynthesis: Accurate Prediction for Light Element Abundances, ArXiv:astro-ph/ 9904411
4. V.G. Plekhanov, *Applications of the Isotopic Effect in Solids* (Springer, Heidelberg, 2004)
5. M. Gell-Mann, *The Quark and the Jaguar (Adventures in the Simple and the Complex)* (W.H. Freeman and Co., New York, 1997)
6. V.G. Plekhanov, Manifestation and origin of the isotope effect, ArXive: gen. phys/0907.2024 (2009) p. 1–192
7. V.G. Plekhanov, Elementary excitations in isotope-mixed crystals. Phys. Reports **410**, 1–235 (2005)
8. M. Cardona, M.L.W. Thewalt, Isotope effect on the optical spectra of semiconductors. Rev. Mod. Phys. **77**, 1173–1224 (2005)
9. V.G. Plekhanov, Fundamentals and applications of isotope effect in solids. Progr. Mat. Science **51**, 287–426 (2006)
10. V.G. Plekhanov, *Giant Isotope Effect in Solids* (Stefan-University Press, La Jola, 2004). (USA)
11. V.G. Plekhanov, Applications of isotope effects in solids. J. Mater. Science **38**, 3341–3429 (2003)
12. G. Schatz, A. Weidinger, A. Gardener, *Nuclear Condensed Matter Physics*, 2nd edn. (Wiley, New York, 1996)
13. D. Forkel-Wirth, Exploring solid state physics with radioactive isotopes. Rep. Progr. Phys. **62**, 527–597 (1999)
14. D. Forkel-Wirth, M. Deicher, Radioactive isotopes in solid state physics, Nucl. Phys. A **693**, 327–341 (2001)
15. V.G. Plekhanov, Isotope-Mixed Crystals: Fundamentals and Applications (2011, in press)
16. F. Halzen, D. Martin, *Quarks and Leptons* (Wiley, New York, 1984)
17. E.H. Simmons, Top Physics, ArXiv, hep-ph/0011244 (2000)
18. C.D. Froggatt, The origin of mass. Surveys High Energ. Phys. **18**, 77–99 (2003)
19. B.L. Ioffe, The origin of mass, Usp. Fiz. Nauk (Moscow) **176**, 1103–1104 (2006) (in Russian)
20. D.W. Lee, *Chiral Dynamics* (Gordon and Breach, New York, 1972)
21. S. Coleman, *Aspects of Symmetry* (Cambridge University Press, Cambridge, 1985)
22. G. Ecker, Chiral Perturbation Theory, ArXiv:hep-ph/9501357 (1995)
23. A. Pich, 1995, Chiral Perturbation Theory, ArXiv:hep-ph/9502366
24. S.R. Bean, P.F. Bedaque, W.C. Haxton, in *At the Frontier of Particle Handbook of QCD*, ed. by M. Shifman (World Scientific, Singapore, 2001)
25. W. Weise, Yukawa's Pion, Low-Energy QCD and Nuclear Chiral Dynamics, ArXiv: nucl-th/ 0704.1992 (2007)
26. J. Bijens, Chiral Perturbation Theory Beyon One Loop, ArXiv: hep-ph/0604043

27. J. Bijens, Progr. Part. Nucl. Phys. **58**, 521–563 (2007)
28. V.G. Plekhanov, Isotopic and disorder effects in large exciton spectroscopy, Uspekhi-Phys. (Moscow) **167**, 577–604 (1997) (in Russian)
29. P.A.M. Dirac, *The Principles of Quantum Mechanivs* (Oxford University Press, U.K., 1958)
30. R.P. Feyman, R.P. Leighton, M. Sands, *The Feyman Lecture in Physics*, vol. 3 (Addison-Wesley, Reading, MA, 1965)
31. L.D. Landau, E.M. Lifshitz, *Quantum Mechanics (Nonrelativistic Theory)* (Pergamon, New York, 1977)
32. H. Grabert, H. Horner, Eds. Special issue on single charge tunneling. Z. Phys. **B85**(3), 317–467 (1991)
33. T. Basche, W.E. Moerner, U.P. Wild (eds.), *Single-Molecule Optical Detection (Imaging and Spectroscopy* (VCH, Weinheim, 1996)
34. J.S. Bell, On the EPR paradox. Physics **1**, 195–200 (1964)
35. J.S. Bell, On the problem of hidden variables in quantum mechanics, Rev. Mod. Phys. **38**, 447–452 (1966)
36. A. Einstein, B. Podolsky, N. Rosen, Can quantum mechanics description reality considered complete? Phys. Rev. **47**, 777–780 (1935)
37. N. Gisin, G. Ribvordy, W. Tittel, H. Zbinden, Quantum cryptography. Rev. Mod. Phys. **74**, 145–195 (2002)
38. G. Gibbert, M. Amrick, 2000, Practical Quantum Cryptography; A Comprehensive Analysis, ArXiv: quant-ph/ 0009027

Chapter 2
Introduction to Isotope Effect

2.1 The Nucleons and its Constituents

An atom consists of an extremely small, positively charged nucleus (see Fig. 2.1) surrounded by a cloud of negatively charged electrons. Although typically the nucleus is less than one ten-thousandth the size of the atom, the nucleus contains more than 99.9% of the mass of the atom. Atomic nucleus is the small, central part of an atom consisting of A-nucleons, Z-protons, and N-neutrons (Fig. 2.2). The atomic mass of the nucleus, A, is equal to Z+N. A given element can have many different isotopes, which differ from one another by the number of neutrons contained in the nuclei [1, 2]. In a neutral atom, the number of electrons orbiting the nucleus equals the number of protons in the nucleus. As usually nuclear size is measured in fermis ($1\,\text{fm} = 10^{-15}\,\text{m}$, also called femtometers). The basic properties of the atomic constituents can be read in Table 2.1.

As we can see from Table 2.1, protons have a positive charge of magnitude $e = 1.6022 \times 10^{-19}\,\text{C}$ (Coulombs) equal and opposite to that of the *electron*. *Neutrons* are uncharged. Thus a neutral atom (A, Z) contains Z electrons and can be written symbolically as ${}^{A}_{Z}\text{X}_{N}$ (see also Fig. 2.2). Here X is chemical symbol and N is neutron number and is equal $\text{N} = \text{A} - \text{Z}$. The masses of *proton* and neutron are almost the same, approximately 1836 and 1839 electron masses (m_e), respectively. Apart from electric charge, the proton and neutron have almost the same properties. This is why there is a common name of them: *nucleon*. Both the proton and neutron are nucleons. As we well know the proton is denoted by letter p and the neutron by n. Chemical properties of an element are determined by the charge of its atomic *nucleus*, i.e., by the number protons (electrons). It should be added, that although it is true that the neutron has zero net charge, it is nonetheless composed of electrically charged quarks (see below), in the same way that a neutral atom is nonetheless composed of protons and electrons. As such, the neutron experiences the *electromagnetic interaction*. The net charge is zero, so if we are far enough away from the neutron that it appears to occupy no volume, then the total effect of the electric force will add up to zero. The

V. G. Plekhanov, *Isotope-Based Quantum Information*, SpringerBriefs in Physics,
DOI: 10.1007/978-3-642-28750-3_2, © The Author(s) 2012

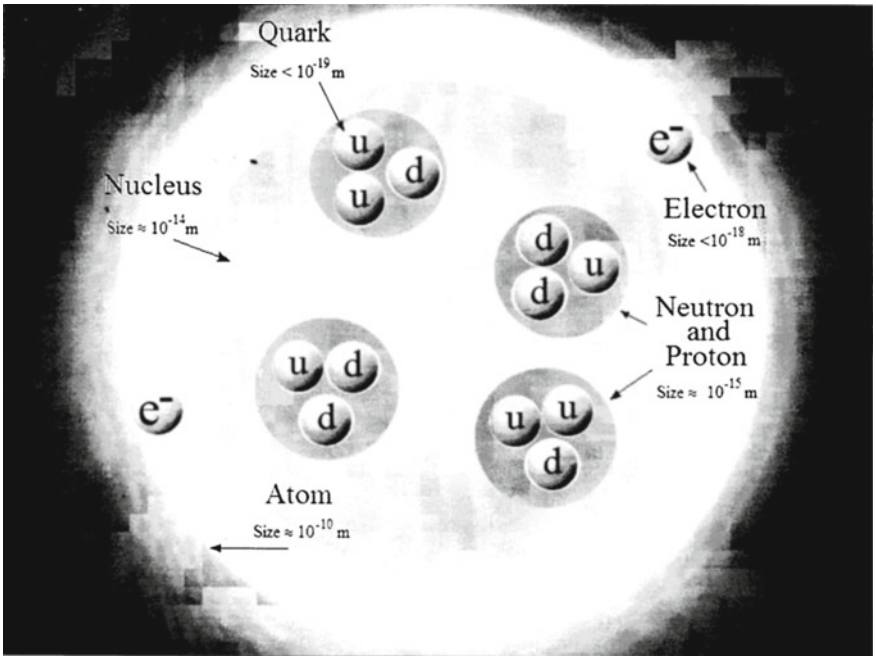

Fig. 2.1 Structure within the atom. If the *protons* and *neutrons* in this picture were 10 cm across, then the quarks and electrons would be less than 0.1 mm in size and the entire atom would be about 10 km across (after http://www.lbl.gov/abc/wallchart/)

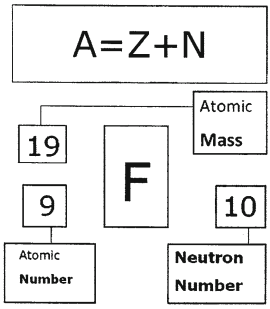

Fig. 2.2 Atomic nomenclature

movement of the charges inside the neutrons does not cancel, however, and this is what gives the neutron its nonzero *magnetic moment*.

Each of the atomic constituents a spin 1/2 in units of $\hbar\,(=\mathrm{h}/2\pi)$ and is an example of the class of particles of half-integer spin known as *fermions*. Fermions obey the exclusion principle of Pauli, which determines the way electrons can occupy atomic energy states. The same rule applies, as will be shown below, to nucleons in nuclei. Associated with the spin is a magnetic dipole moment. Compared with the magnetic moment of *electron*, nuclear moment is very small. However, they play an important

Table 2.1 The basic properties of the atomic constituents

Particle	Charge	Mass (u)	Spin ($\hbar$)	Magnetic moment (JT^{-1})
Proton	e	1.007276	1/2	1.411×10^{-26}
Neutron	0	1.008665	1/2	-9.66×10^{-27}
Electron	−e	0.000549	1/2	9.28×10^{-24}

role in the theory of *nuclear* structure. It may be surprising that the uncharged neutron has a magnetic moment. This reflects the fact that it has an underlying quark substructure (see, e.g. [3]), consisting of charged components. Electron scattering off these basic nuclear constituents (proton and neutron) makes up for the ideal probe to obtain a detailed view of the internal structure. A very detailed analysis using the best available data has been carried out recently by Kelly [4]; these data originate from recoil or target polarizations experiments. In Fig. 2.3 the proton charge and magnetization distribution are given. What should be noted is the softer charge distribution compared to the magnetic one for proton. These resulting densities are quite similar to Gaussian density distributions that can be expected starting from *quark picture* (for details, see below) and, at the same time more realistic than the exponential density distributions [5–10]. The neutron charge and magnetization are also given in Fig. 2.3. What is striking is that magnetization distribution resembles very closely the corresponding *proton* distribution. Since scattering on neutrons normally carries the larger error, the neutron charge distribution is not precisely fixed. Nonetheless, one notices that the interior charge density is balanced by a negative charge density, situated at the neutron surface region, thereby making up for the integral vanishing of the total charge of the *neutron*.

We should recall from atomic physics that the quantity e$\hbar$/2m is called *magneton*. For atomic motion we use the *electron mass* and obtain the Bohr's magneton $\mu_B = 5.7884\times10^{-5}$ eV/T. Putting in the proton mass we have the nuclear magneton $\mu_N = 3.1525\times10^{-8}$ eV/T. Note that $\mu_N \ll \mu_B$ owing to the difference in the masses, thus under most circumstances atomic magnetism has much larger effects than nuclear magnetism. Ordinary magnetic interactions of matter (ferromagnetism, for example) are determined by *atomic magnetism*.
We can write

$$\mu = g_l l \mu_N \tag{2.1}$$

where g_l is the g-factor associated with the orbital angular momentum l. For protons $g_l = 1$, because neutrons have no electric charge; we can use Eq. (2.1) to describe the orbital motion of neutrons if we put $g_l = 0$. We have thus been considering only the orbital motion of *nucleons*. Protons and neutrons, like electrons, as mentioned above also have intrinsic or spin magnetic moments, which have no classical analog but which we write in the same form as Eq. (2.1):

$$\mu = g_s s \mu_N \tag{2.2}$$

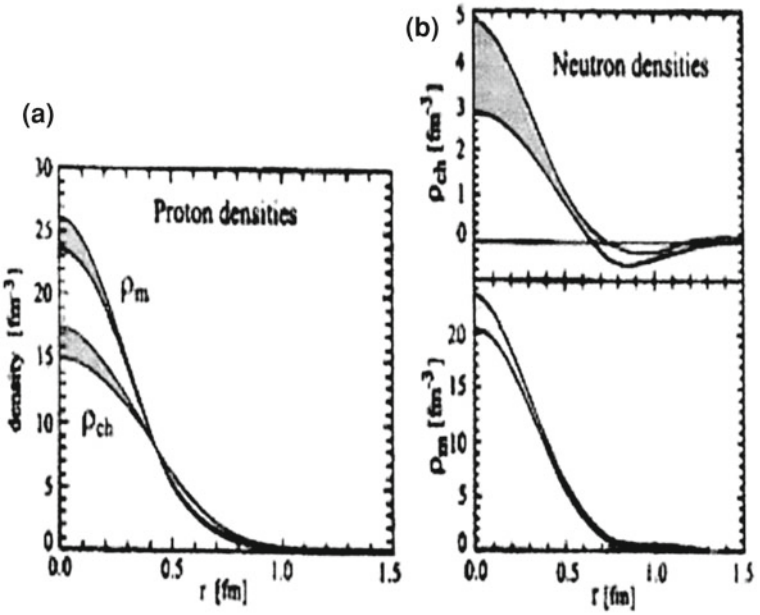

Fig. 2.3 Comparison between charge (ρ_{ch}) and magnetization (ρ_m) for the proton (**a**) and neutron (**b**). Both densities are normalized to $\int \mathrm{d}r r^2 \rho(r) = 1$ (after [5–7])

where $s = 1/2$ for protons, neutrons, and electrons (see Table 2.1). The quantity g_s is known as the spin g-factor and is calculated by solving a relativistic quantum mechanics equation (see, also [8–10]). For free nucleons, the experimental values are far from the expected value for point particles: proton–$g_s = 5.5856912 \pm 0.0000022$ and neutron $-g_s = 3.8260837 \pm 0.0000018$.

2.1.1 Mass and Nuclear Binding Energy

Inside a *nucleus*, neutrons and protons interact with each other and are bound within the nuclear volume under the competing influences of attractive nuclear and repulsive electromagnetic forces. This binding energy has a direct effect on the mass of an atom. It is therefore not possible to separate a discussion of *nuclear binding energy*; if it were, then nucleon would have masses given by $Z_{m_p} + Z_{m_n}$ and the subject would hardly be of interest.

As is well known, in 1905, Einstein presented the equivalence relationship between mass and energy: $E = mc^2$. From this formula, we see that the speed of light c is very large and so even a small mass is equivalent to a large amount of energy. This is why in nuclear physics it is more convenient to use a much smaller unit called megaelectronvolt ($1\,\mathrm{MeV} = 1.602 \times 10^{-13}\,\mathrm{J}$). On the atomic

scale, 1 au is equivalent to 931.5 MeV/c^2, which is why energy changes in atoms of a few electron volt cause insignificant changes in the mass of atom. *Nuclear* energies, on the other hand, are millions of electron volts and their effects on atomic mass are easily detectable. For example, the theoretical mass of $^{35}_{17}$Cl is $17 \times 1.00782503 + 18 \times 1.00866491 = 35.28899389$ amu. Its measured (see below) mass is only 34.96995 amu. Therefore, the mass defect and binding energy of $^{35}_{17}$Cl are

$$\Delta = 0.32014389 \text{ amu.}$$
$$\mathrm{E}_B = \frac{0.32014389 \times 931.5}{35} = 8.520 \text{ MeV/nucleon} \tag{2.3}$$

and in common sense the binding energy is determined by next relation

$$\mathrm{E}_B = \mathrm{Z}m_p + \mathrm{N}m_n - \mathrm{B/c}^2 \tag{2.4}$$

where B/c^2 is the actual nuclear mass.

As we can see, the *binding energy* of the atoms of most elements have values ranging from about 7.5 to 8.8 MeV [11]. The binding energy per nucleon rises slightly with increasing mass number and reaches a maximum value for ^{62}Ni. Thereafter the binding energies decline slowly with increasing mass number. The binding energies of the atoms of H, He, Li, and Be are lower than the binding energies of the other elements (see, also Fig. 2.5 below).

The measurement of *nuclear masses* occupies an extremely important place in the development of nuclear physics. *Mass spectrometry* (see, e.g. [12–15]) was the first technique of high precision available to the experimenter, since the mass of a nucleus increases in a regular way with the addition of one proton or neutron. In mass spectrometers, a flux of identical nuclei (ions), accelerated to a certain energy, is directed to a screen (photoplate) where it makes a visible mark. Before striking the screen, this flux passes through magnetic field, which is perpendicular to velocity of the nuclei. As a result, the flux is deflected to certain angle. The greater the mass, the smaller the angle. Thus, measuring the displacement of the mark from the center of the screen, we can find the deflection angle and then calculate the mass. The example of a mass spectrum of different isotopes of krypton is shown in Fig. 2.4. From the relative areas of the peaks it can determine the abundance of the stable isotopes of krypton (for details see [12–15]).

Relative masses of *nuclei* can also be determined from the results of nuclear reactions or nuclear decay. For example, if a nucleus is radioactive and emits an α-particle, we know from energy conservation that its mass must be greater than that of decay products by the amount of energy released in the decay. Therefore, if we measure the letter, we can determine either of the initial or the final nuclear masses if one of them is unknown. An example of this is presented briefly below. At present we shall illustrate some typical reactions, bridging the gap between "classical" methods and the more advanced "high-energy" types of experiments [4–7].

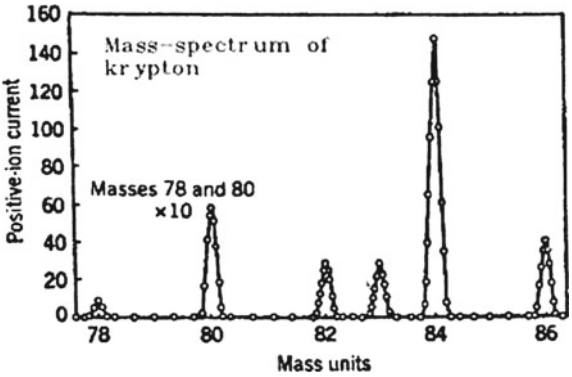

Fig. 2.4 A *mass-spectrum* analysis of krypton. The ordinates for the peaks at mass positions 78 and 80 should be divided by 10 to show these peaks in their true relation to the others (after [11])

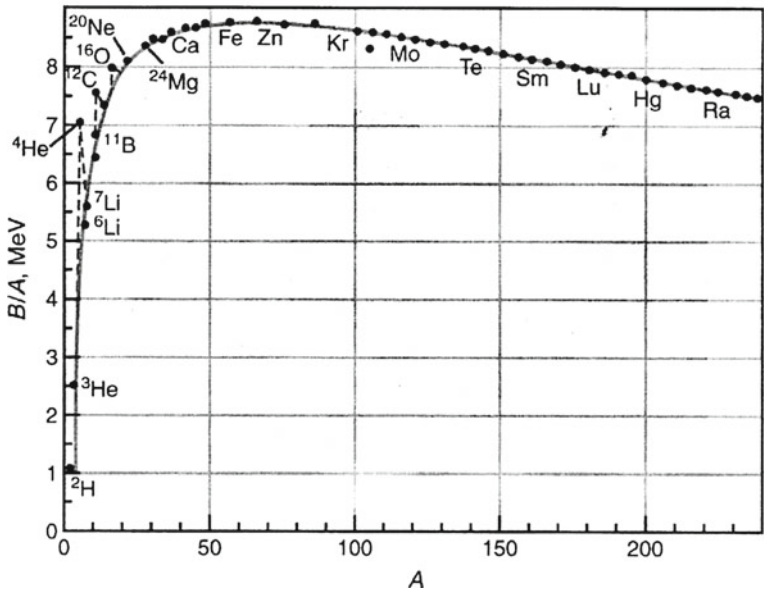

Fig. 2.5 The *binding energy* per *nucleon* B/A as a function of the nuclear mass number A (after [16])

The possible, natural decay processes can also be brought into the class of reaction processes with the conditions: no incoming light particle α and $Q > 0$. We list them in the following sequence:

α-decay:

$$ {}^{A}_{Z}\mathrm{X}_{N} \rightarrow {}^{A-4}_{Z-2}\mathrm{Y}_{N-2} + {}^{4}_{2}\mathrm{He}_{2} \tag{2.5} $$

Table 2.2 Masses of electron, nucleons and some nuclei (after [11])

Particle	Number of protons	Number of neutrons	Mass (MeV)
e	0	0	0.511
p	1	0	938.2796
n	0	1	939.5731
$^{2}_{1}$H	1	1	1876.14
$^{3}_{1}$H	1	2	2808.920
$^{3}_{2}$He	2	1	2808.391
$^{4}_{2}$He	2	2	3728.44
$^{7}_{3}$Li	3	4	6533.832
$^{9}_{4}$Be	4	5	8392.748
$^{12}_{6}$C	6	6	11174.860
$^{16}_{8}$O	8	8	14895.077
$^{238}_{92}$U	92	146	221695.831

β-decay:

$$^{A}_{Z}\mathrm{X}_{N} \rightarrow {}^{A}_{Z-1}\mathrm{Y}_{N+1} + \mathrm{e}^{+} + \nu_e \quad (\mathrm{p} \rightarrow \mathrm{n\text{-}type}) \tag{2.6}$$

$$^{A}_{Z}\mathrm{X}_{N} \rightarrow {}^{A}_{Z+1}\mathrm{Y}_{N-1} + \mathrm{e}^{-} + \overline{\nu}_e \quad (\mathrm{n} \rightarrow \mathrm{p\text{-}type}) \tag{2.6'}$$

$$^{A}_{Z}\mathrm{X}_{N+\mathrm{e}^{-}} + \mathrm{e}^{-} \rightarrow {}^{A}_{Z-1}\mathrm{Y}_{N+1} + \nu_e \quad (\mathrm{e}^{-}\text{-capture}) \tag{2.6''}$$

Here e^{-}, e^{+}, ν_e and $\overline{\nu}_e$ are *electron, positron, neutrino and antineutrino*.
γ-decay:

$$^{A}_{Z}X^{*}_{N} \rightarrow {}^{A}_{Z}\mathrm{X}_{N} + \mathrm{h}\nu \tag{2.7}$$

Here X^{*} is excited nuclei. Nuclear fission:

$$^{A}_{Z}\mathrm{X}_{N} \rightarrow {}^{A_1}_{Z_1}\mathrm{Y}_{N_1} + {}^{A_2}_{Z_2}\mathrm{U}_{N_2} + \mathrm{x{\cdot}n}. \tag{2.8}$$

Since mass and energy are equivalent (see Einstein formula above), in nuclear physics it is customary to measure masses of all particles in the units of energy (MeV). Examples of masses of subatomic particles are given in Table 2.2.

As was noted above, nuclear binding energy increases with the total number of nucleons A and, therefore, it is common to quote the average binding energy per nucleon (B/A). The variation of B/A with A is shown in Fig. 2.5. Several remarkable features are immediately apparent. First of all, the curve is relatively constant except for the very *light nuclei*. The average binding energy of most nuclei is, to within 10%, about 8 MeV per nucleon. Second, we note that the curve reaches peak near $\mathrm{A} = 60$, where the nuclei are most tightly bound, light and very *heavy nuclei* are containing less bound nucleons. Thus, the source of energy production in fusion of light nuclei or fusion of very heavy nuclei can be source of energy [16, 17].

The interactions between two nucleons (NN) is one of the central questions in physics and its importance goes beyond the properties of nuclei. Nucleons can combine to make four different few-nucleon systems, the deuteron ($p + n$), the triton

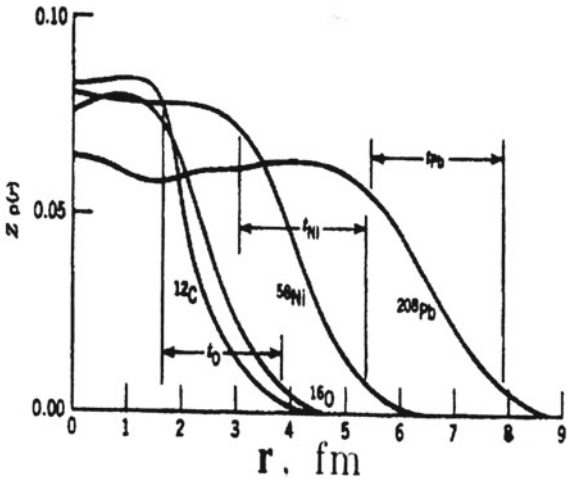

Fig. 2.6 Coulomb potential used for defining the nuclear radius R

$(p + 2n)$, the helion $(2p + n)$ and the α-particle $(2p + 2n)$ (see, e.g. [18–21]). These particles are grouped together because they are stable (excluding from the radioactive triton which has a half-life of about 12 years and so may be treated as a stable entity for most practical purpose), have no bound excited states (except the α-particles which have two excited states at about 20 and 22 MeV), and are frequently used as projectiles in nuclear investigations. The absence of stable particles of mass of five provides a natural boundary between few nucleon systems and heavier nuclei [20]. Few nucleon systems provide the simplest systems to study nuclear structure. The deuteron provides important information about the nucleon–nucleon interaction. Below we have indicated a few of the properties of the N–N force:

1. At short distances it is stronger than the Coulomb's force; the nuclear force can overcome the Coulomb's repulsion (see also Fig. 2.6) of protons in the nucleus.
2. At long distances, of the order of atomic sizes, the nuclear force is negligibly feeble. The interaction among nuclei in a molecule can be understood based only on the Coulomb's force.
3. Some fundamental particles are immune from the nuclear force. At present time we have no evidence from atomic structure, for example, that electrons feel the nuclear force at all.
4. The N–N force seems to be nearly independent of whether the nucleons are neutrons or protons. As is well known this property is called charge independence.
5. The N–N force depends on whether the spins of the nucleons are parallel or antiparallel.
6. The N–N force includes a repulsive term, which keeps the nucleons at a certain average separation.
7. The N–N force has a noncentral or tensor component. This part of the force does not conserve orbital angular momentum, which is a constant of the motion under central forces.

2.2 Manifestation Isotope Effect in Condensed Matter

Studies of vibrational properties of crystals containing impurities (defects of various type [22]) were described in detail in a number of excellent review [23, 24]. The main characteristics of a *phonon* spectrum are the *dispersion* relation $\omega(\vec{q})$ and the frequency distribution function $g(\omega)$ [25]. Both are mainly determined in experiments on the scattering of thermal neutrons, provided it turns out to be possible to separate coherent and incoherent scattering [26]. An important role of neutrons in studying lattice dynamics is related to the fact that the energy of thermal neutrons ($k_B T \sim 10^{-1} - 10^{-2}$ eV) is of the same order as the energy of phonons. At the same time their de Broglie wavelength is comparable with the interatomic distance in crystals [27, 28].

The simplest defects in a crystalline lattice that distort its translational symmetry are *isotopes* of the elements forming a crystal. If the impurity concentration (isotopes) in a crystal is high enough that the interaction between impurity atoms (ions) plays an important role, such a system is called a mixed crystal with a various degree of *disorder*. There are two types of disordered systems: disordered alloys (isotopic mixtures) or mixed crystals and glassy substances, which possess a more pronounced spatial disorder than configurational disorder. The first theoretical dynamic model of mixed crystals was a linear chain, which represented the development of the virtual model (Nordheim, 1931; Pant and Joshi, 1969 (see, e.g. [47])). Despite its simplicity, this model adequately described general features of lattice dynamics of mixed alkali-halide crystals. This model uses two independent force constants f_0 and f_0', which are obtained, as a rule, from the observed frequencies of LO phonons in pure substances, according to the expression $f = \omega^2 mM/2(m+M)$, *where* m and M (M′) are masses of crystal-forming particles. The dependence of the force constant on concentration was described by equation $F = f_0 x - (f_0' - f_0)x$ by assuming a linear dependence of f_0 (f_0') on concentration x (see, also [22] and references therein). A more complex concentration dependence of the force constant was considered in detail in comprehensive reviews [29–33], where the cluster model and isodisplacement model in lattice dynamics, based on the *Coherent Potential Approximation* (CPA) or averaging of the T-matrix, were also described.

2.2.1 Isotope Effect in Phonon Spectra

a. First-order Raman Spectra

In view of the obvious mass dependence of *phonon frequencies*, dynamic lattice properties have been studied intensively, mainly by *Raman scattering*. In addition to changes in the average atomic mass, mass fluctuation due to isotopic disorder as will be shown below also affects phonon frequencies and line-widths. Elemental *semiconductors* (C, Si, Ge, α-Sn) with *diamon-like structure* are an ideal object to

study the isotopic effects by the method of the Raman scattering. At the present time the high-quality isotopically enriched indicated crystals are also available. In this part we describe our understanding of the first-order Raman spectra of the *isotope-mixed elemental and compound semiconductors* (CuCl, GaN, GaAs) with zinc-blend structure.

The materials with *diamond* structure discussed here have a set of threefold-degenerate phonons (frequency ω_0) at the centre ($\vec{k} = 0$, Γ-point) of the Brillouin zone (BZ) (see, also [26]). These phonons are Raman active but infrared inactive [34]. Let us consider the case of Ge, with the five isotopes [35–37]. The uninitiated will ask himself whether one should see five phonons (or more if he knows that there are two atoms per *primitive cell* (PC)) corresponding to the five different masses, or only one corresponding to the average mass. The reason why the Raman spectrum (see, Fig. 2.7) of natural Ge does not show the local modes of the individual isotopes is that the scattering potentials for the phonons due to the mass-defects (mass fluctuations) are too small to induce bound states (i.e., *Anderson localization* of the phonons [38, 39]). Really a three-dimensional crystal fluctuations in the parameters of the secular equation lead to localization if these fluctuation (measured in units of frequency, i.e., $(\Delta M/M)\omega_0$) are larger than the bandwidth of the corresponding excitations. For optical phonons in Ge this bandwidth is $\sim 100\,\mathrm{cm}^{-1}$ (see, e.g. [40]) while $(\Delta M/M)\omega_0 \leq 0.4 \times 300 = 12\,\mathrm{cm}^{-1}$). Hence no phonon localization (with lines corresponding to all pairs of masses) is expected, in agreement with the observation of only line at $304\,\mathrm{cm}^{-1}$ ($\sim 80\,\mathrm{K}$) for natural Ge.

Figure 2.7a demonstrates the dependence of the shape and position of the first-order line of *optical phonons* in germanium crystals on the isotope composition at liquid nitrogen temperatures [36, 37]. The lines in these spectra are fully resolved instrumentally (the experimental resolution was better than $0.1\,\mathrm{cm}^{-1}$) and their width is caused by homogeneous broadening. The centroid of the *Raman line shifts* following relation $\omega_0 \sim M^{-1/2}$. This behavior is expected within *harmonic approximation*. Additional frequency shifts are observed [41] for the natural and alloy samples which arise from their *isotope* mass disorder. This additional shift is $0.34 \pm 0.04\,\mathrm{cm}^{-1}$ in natural Ge and $1.06 \pm 0.04\,\mathrm{cm}^{-1}$ (Fig. 2.8) in the $^{70/76}$Ge alloy sample, which has nearly the maximum *isotopic disorder* possible with natural isotopes.

As it is well known, the natural diamond exhibits a single first-order Raman's peak at $\omega_{\mathrm{LTO}}(\Gamma) = 1332.5\,\mathrm{cm}^{-1}$. Figure 2.7b shows the first-order *Stokes Raman spectra* for several samples with different isotope ratios [43]. The Raman energy is found to increase continuously, but nonlinear, with decreasing x. The energy difference between the extreme compositions is $52.3\,\mathrm{cm}^{-1}$, which is consistent with the isotope mass ratio. Analogous structures of first-order light scattering spectra and their dependence on isotope composition has now been observed many times, not only in elementary Si [44] and α-Sn [45], but also in compound CuCl and GaN semiconductors (for more details see reviews [45–47]). Already this short list of data shows a large dependence (see, also Fig. 2.8) of the structure of first-order light scattering spectra in *diamond* as compared to other crystals (Si, Ge).

Figure 2.9 compares the composition of the Raman frequency in the *VCA* and *CPA* according to Hass et al. [48] and Spitzer et al. [49]. The present Raman data

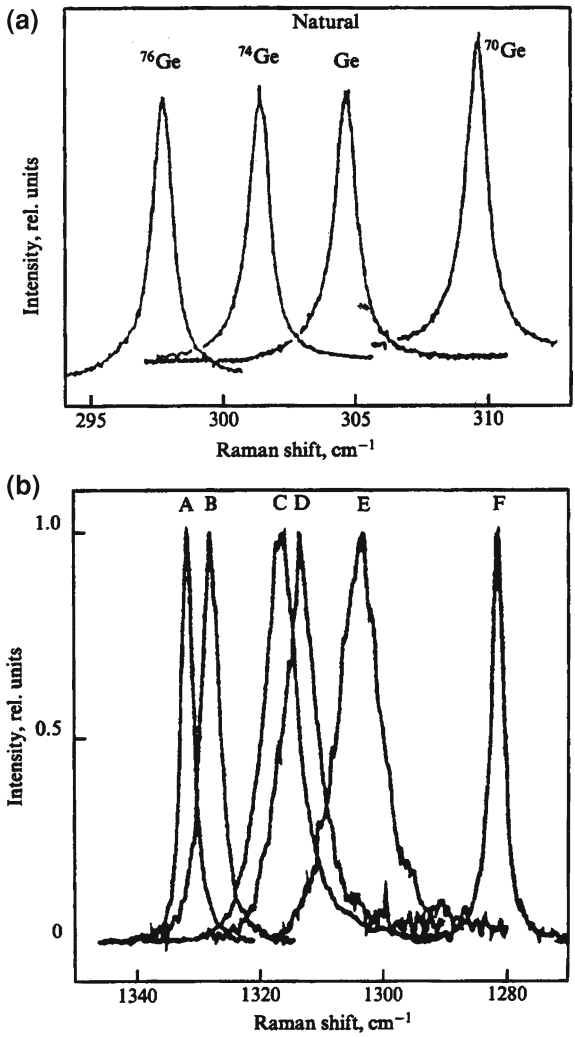

Fig. 2.7 **a** First-order Raman scattering spectra in Ge with different *isotope* contents [36, 37]; **b** First-order Raman scattering spectra in isotopically mixed *diamond* crystals $^{12}C_x^{13}C_{1-x}$. The peaks *A*, *B*, *C*, *D*, *E*, and *F* correspond to x = 0.989; 0.90; 0.60; 0.50; 0.30; and 0.001 [43]

in Fig. 2.9 are in excellent agreement with those of Chrenko [50] and Hanzawa et al. [43]. Both sets of data exhibit a pronounced bowing (nonlinearity) relative to the VCA that is described very well by CPA. Hass et al. concluded that the bowing is a direct consequence of the scattering due to isotopic disorder. Similar nonlinearity are observed in many other properties of alloy systems (e.g., the band gaps of semiconductor alloys and isotope-mixed crystals [51]. The deviation from linearity is approximately 5 cm^{-1} near the middle of the composition range. This is much larger than the experimental uncertainties (about the size of the data points) and should certainly be considered if the Raman frequency is to be used as a measure of *isotopic composition* (for details see [26]).

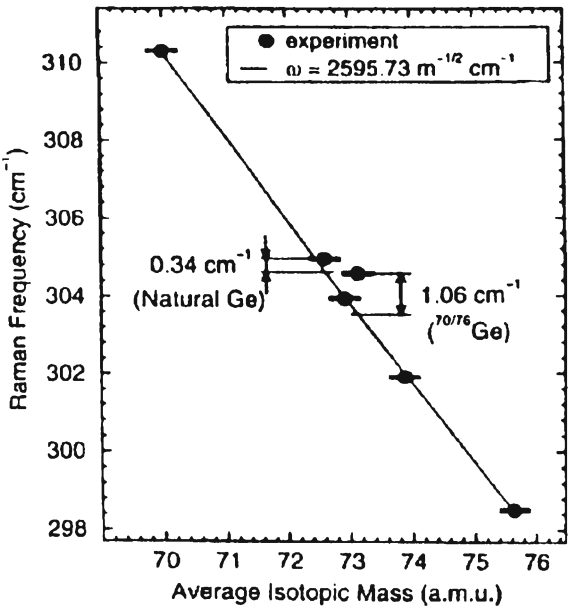

Fig. 2.8 Raman frequency as a function of the average mass, measured at 10 K, for *isotopically enriched* and disordered Ge samples. The *solid line* is a calculation with $\omega = 2595{,}73/\sqrt{\mathrm{M}}\ \mathrm{cm}^{-1}$ (after [41])

The measured Raman linewidth (Fig. 2.9b) is larger near the center of the composition range than near the end points. The variation is not symmetric in x and $(1-\mathrm{x})$ and the maximum width occurs at approximately 70% at ^{13}C. The CPA curves represent intrinsic contributions to the Raman linewidth due to the disorder-induced broadening of the zone-center optic mode. The observed widths, according to Hass et al. [48], contain additional contributions due to instrumental resolution ($\sim 1.8\,\mathrm{cm}^{-1}$) and *anharmonic* decay [47, 51]. The anharmonic broadening of the Raman line has been calculated for diamond by Wang et al. [45] to be on the order of $1\,\mathrm{cm}^{-1}$ at 300 K. Contributions other than disorder thus account well for the observed widths near $x = 0$ and 1. Assuming that such contributions are reasonably constant across the entire composition range, we see that both CPA calculations account very well for the qualitative trend in the data, including the peak near $x = 0.7$.

Detail calculations of the self-energy and the first-order Raman lineshape were performed by Spitzer et al. [49]. They obtained a qualitative agreement with experimental results. Comparing the Raman lineshape of Ge and C, the presence of a large isotopic broadening for *diamond*, contrary to the small broadening observed for Ge should be noted. The reason lies in the fact that $\vec{k} = 0$ is not the highest point of the phonon dispersion relation in the case of diamond [52]. This maximum lies somewhat off $\vec{k} = 0$, resulting in a nonvanishing density of states at ω_0, considerably larger than that found from relation $\mathrm{N}_d \sim \mathrm{Re}\left(\omega_0 - \omega + \mathrm{i}\frac{\Delta\omega_0}{2}\right)^{1/2}$ [46]. This density of states is strongly asymmetric about ω_0, a fact which yields an asymmetric phonon lineshape [49]. This asymmetry also results in a lopsided dependence of

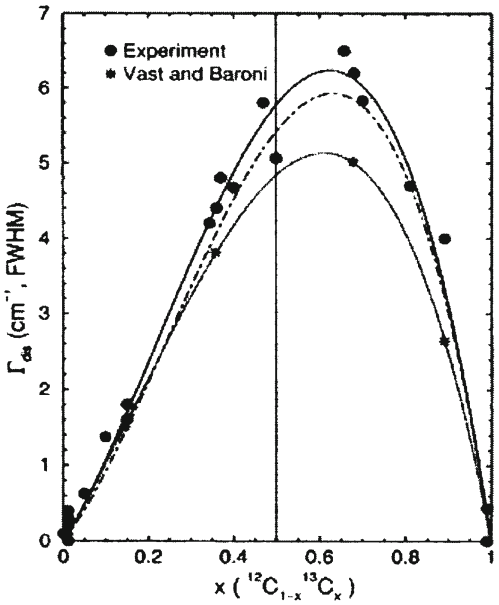

Fig. 2.9 **a** Disorder-induced shift of the Raman phonon of *diamond* as a function of the ^{13}C concentration. The open symbols are Raman experimental data , whereas the asterisks correspond to ab initio calculations. The solid line is a fit with Eq. (2.40) for $n = 2, 3$ to all experimental data [60]. The *dotted* and *dot–dashed lines* represent the fits to theoretical values obtained from ab initio and CPA calculations, respectively (after [69]); *b Disorder-induced broadening* of the Raman phonon of diamond as a function of the ^{13}C concentration. The filled circles have been obtained from the Raman data by taking into account the corresponding instrumental resolutions and substracting the anharmonic broadening $\Gamma_{anh} \approx 2\text{cm}^{-1}$ (FWHM). The solid line is a fit with Eq. (2.40) for $n = 2, 3$ to these points [60]. The *dotted* and *dot–dashed lines* are the corresponding fits to the values obtained from ab initio and CPA calculations, respectively (after [69])

the linewidth versus concentration (Fig. 2.9), which disagrees with the symmetric dependence expected from the proportionality to mass fluctuation parameter g [22].

Thus, depicted in Figs. 2.7–2.9 experimental results are testified the nonlinear dependence Raman frequency shift on the *isotope concentration*.

b. Second-order Raman Spectra

The *second-order* Raman spectra for a natural and isotope-mixed crystals of diamond were investigated by Chrenko [50] and Hass and cowokers [48]. Second-order Raman spectra for the synthetic diamonds are shown in Fig. 2.10 . The second-order spectra were measured by Hass and cowokers with slightly lower resolution ($\sim 4\,\text{cm}^{-1}$) than the first-order spectra because of the much lower count rate. The results of Hass et al. for 1.1 at. % ^{13}C agree well with previous measurements for natural diamond [53]. The spectra for 0.07 and 99 at % ^{13}C also look similar, if one ignores the shifts that

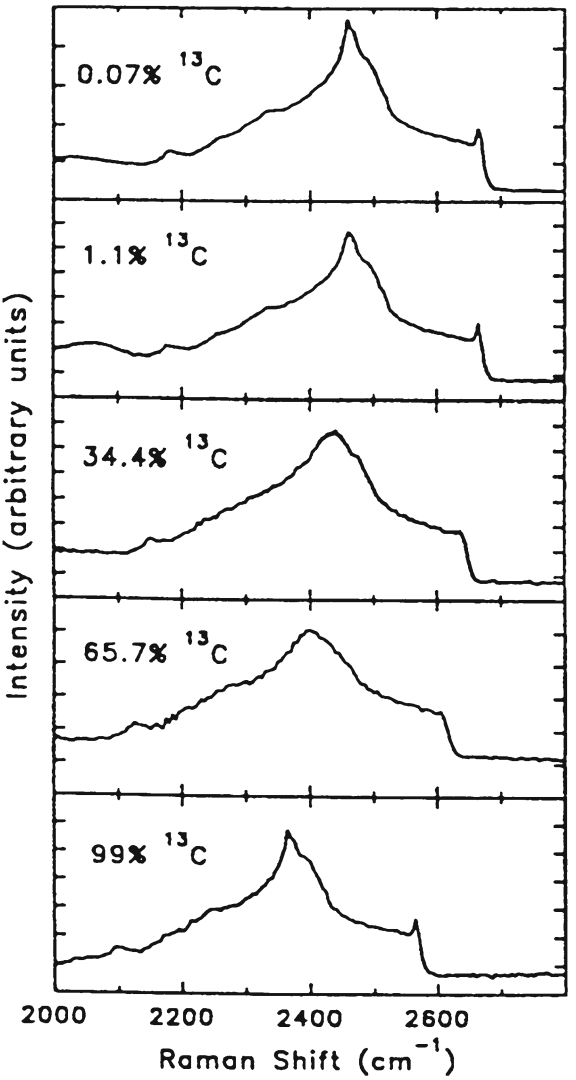

Fig. 2.10 Second-order Raman spectra for *synthetic diamond* with identicated compositions at room temperature (after [48])

occur as a result of differences in M. More significant differences are observed for the more heavily mixed crystals: the 34.4 and 65.7 at % ^{13}C results are noticeably broader and do not appear to exhibit the sharp peak near the high-frequency cutoff. As was shown above, it is this peak at the top of the second-order spectrum (2667 cm $^{-1}$ for 1.1. at % ^{13}C) that has been the subject of intense controversy. Chrenko [50] also examined the second-order spectra of his samples and claims that he was able to see this peak at all composition except 68 % ^{13}C. His measurements may have been of somewhat higher resolution than in paper of Hass et al. but it is clear that even in his

89 at % ^{13}C spectrum (which is the only raw data presented), some broadening of this peak has occurred.

The *IR absorption* in *mixed crystals* can change in two ways, depending on the concentration: *one-mode* and *two-mode* (see, for example, review Elliott et al. [30]). In the case of one-mode behavior, the spectrum always exhibits a single band whose maximum gradually shifts from one extreme position to another. The two-mode behavior corresponds to the presence of two bands in the spectrum, which are characteristic for each of the components of a mixed crystal. As the concentration of components changes, these bands shift, and their intensities undergo a strong redistribution. In principle, the same system can exhibit different types of behavior at the opposite ends [29]. This classification is only a qualitative one, and it is seldom realized in its pure form (for details see review [22]). The appearance of the *localized mode* in the limit of the isolated defect is considered the most important necessary condition for the two-mode behavior of phonons (and also for electrons [32]). In review of Elliott et al. [30], a simple quantitative criterion was suggested for determining the type of behavior of the IR absorption in a crystal of NaCI type [32]. Because the square of the frequency of the TO (Γ) phonon is inversely proportional to the reduced mass of the unit cell M, the shift caused by the defect is equal to

$$\Delta = \omega_{TO}^2 (l - \bar{M}/\bar{M}') \tag{2.9}$$

This shift is compared in paper of Elliott and others with the width of the phonon optical zone. This width in the parabolic dispersion approximation, neglecting the acoustic branches, is equal to

$$\mathrm{W} = \omega_{TO}^2 \frac{\varepsilon_0 - \varepsilon_\infty}{\varepsilon_0 + \varepsilon_\infty}. \tag{2.10}$$

The localized or gap mode appears provided $|\Delta| > \mathrm{W}/2$. However, as was noted by Elliott et al. [30], in order for the two peaks to be retained up to a concentration of about 0.5, the stricter condition of $|\Delta| > \mathrm{W}$ should be satisfied. The substitution of numerical values into (2.9) and (2.10) shows that the relation

$$|\Delta| > \frac{1}{2}\mathrm{W} \tag{2.11}$$

for LiH (LiD) is always valid, because $|\Delta| = 0.44\omega_{TO}^2$ and $\mathrm{W} = 0.58\omega_{TO}^2$. This means that the *localized mode* should be observed at low concentrations. This conclusion agrees with the experimental data described above (Fig. 26 in Ref. [22]). As for the second theoretical relation $|\Delta| > \mathrm{W}$, as noted above, for LiH (LiD) crystals, the reverse relation $\mathrm{W} > |\Delta|$ is always valid [54, 55]. We will consider this question in more detail in review [22]. Figure 2.11 shows the second-order Raman spectra of mixed $\mathrm{LiH}_x\mathrm{D}_{1-x}$ crystals at room temperature [54, 55]. Along with the properties of Raman spectra at high concentrations discussed in the review of Plekhanov [56], note also that as the hydrogen concentration further increases ($x > 0.15$), the

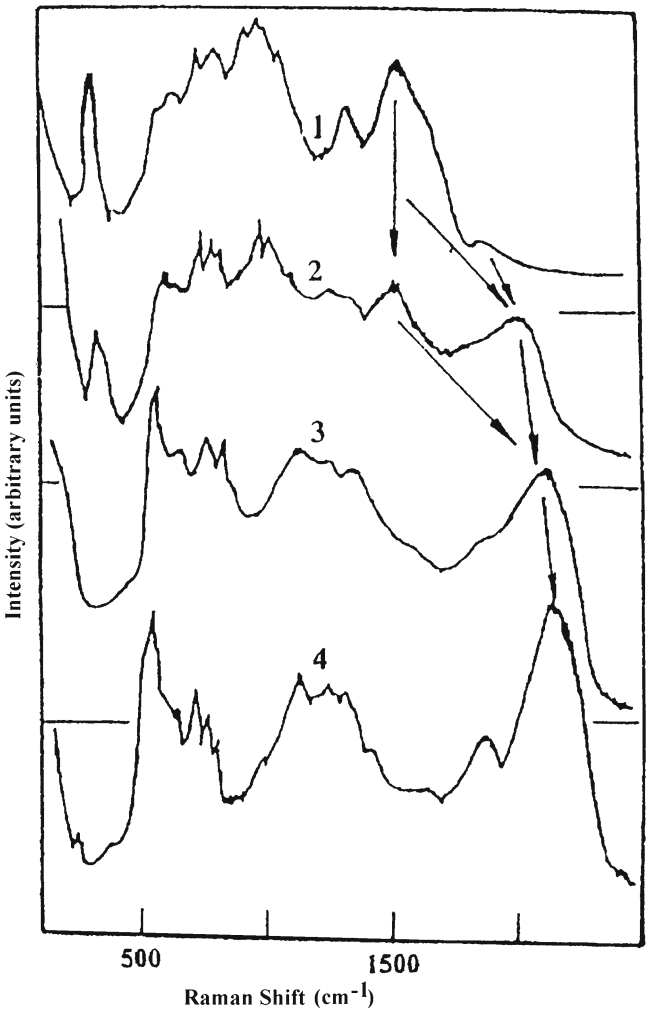

Fig. 2.11 Second-order Raman spectra of mixed LiH_xD_{1-x} crystals excited at λ + 488.0 nm at room temperature, x = 0.0 (*1*); x = 0.42 (*2*); x = 0.76 (*3*); x = 1 (*4*). The *arrows* show the bands corresponding to LO(Γ) phonons (after [54, 55])

intensity of the 2LO (Γ) phonon peak in a LiD crystal decreases, while the intensity of the highest frequency peak in mixed LiH_xD_{1-x} crystals increases. The latter peak is related to the renormalized LO (Γ) modes in a mixed crystal. Thus, comparison of Raman spectra 1 and 2 in Fig. 2.11 shows that in the concentration range of $0.1 < x < 0.45$, the Raman spectrum exhibits LO (Γ) phonon peaks of a pure LiD and mixed LiH_xD_{1-x} crystal. A further increase in $x > 0.45$ is accompanied by two effects observed in the Raman spectra of mixed crystals. The first effect is manifested in a substantial rearrangement of the acousto-optical part of the spectrum

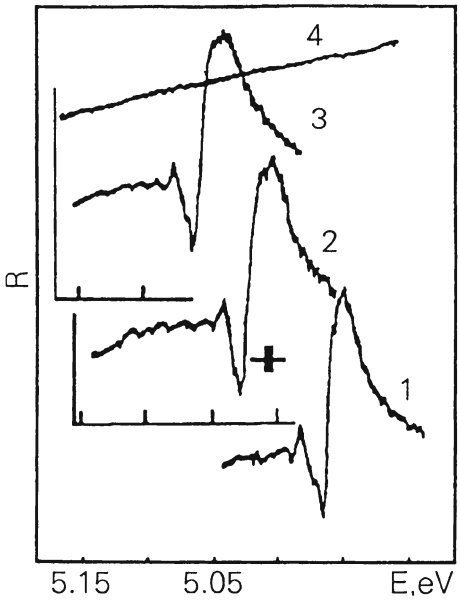

Fig. 2.12 Mirror *reflection* spectra of crystals: 1-LiH; 2-LiH_xD_{1-x}; 3-LiD at 4,2 K. Light source without crystals, curve 4 (after [57])

(spectra 1–3 in Fig. 2.11), and the second one consists in a further blue shift of the highest frequency LO (Γ) phonon peak. This peak shifts up to the position of peak 12 in the spectrum of a pure LiH crystal [56]. This is most clearly seen from comparison of spectra 2 and 4 in Fig. 2.11 (for details see reviews [22, 56]).

2.2.2 Renormalization of Electron (Exciton) States

In this section we will briefly discuss the variation of the *electronic gap* (E_g) and *exciton binding energy* of *insulating* and *semiconducting* crystals with isotope composition. As is well known *isotopic substitution* only affects the wavefunction of phonons; therefore, the energy values of electron levels in the Schrödinger equation ought to have remained the same. This, however, is not so, since isotopic substitution modifies not only the phonon spectrum, but also the constant of electron–phonon interaction. It is for this reason that the energy values of purely electron transition in molecules of hydride and deuteride are found to be different. This effect is even more prominent when we are dealing with a solid [57]. Intercomparison of *absorption* spectra for thin films of LiH and LiD at room temperature [58] revealed that the long-wave maximum (as we know now, the exciton peak) moves 64.5 meV toward the shorter wavelengths when H is replaced with D.

The mirror *reflection* spectra of mixed and pure LiD crystals cleaved in liquid helium are presented in Fig. 2.12. For comparison, on the same diagram we have

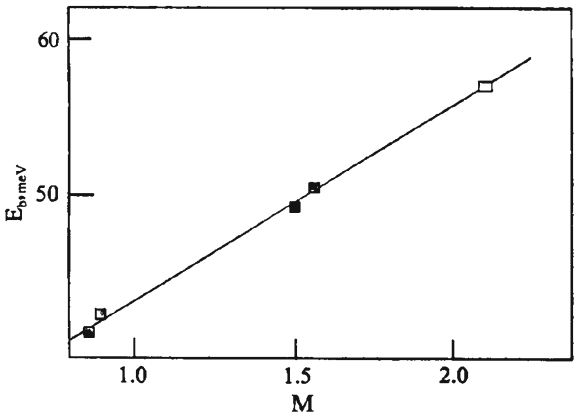

Fig. 2.13 Binding energy of Wannier–Mott excitons as a function of *reduced mass* of ions. Based on values of the reduced mass of ions for ^{6}LiH; ^{6}LiD; ^{7}LiH; ^{7}LiD and ^{7}LiT (after [57])

also plotted the reflection spectrum of LiH crystals with clean surface. All spectra have been measured with the same apparatus under the same conditions. As the *deuterium* concentration increases, the long-wave maximum broadens and shifts toward the shorter wavelengths. As can clearly be seen in Fig. 2.12, all spectra exhibit a similar long-wave structure. This circumstance allows us to attribute this structure to the excitation of the ground (1*s*) and the first excited (2*s*) *exciton* states. The energy values of exciton maxima for pure and mixed crystals at 2 K are presented in Table 21 of Ref. [51]. The binding energies of excitons E_b, calculated by the hydrogen-like formula, and the energies of interband transitions E_g are also given in Table 21 of Ref. [51].

Going back to Fig. 2.12, it is hard to miss the growth of Δ_{12} , [57], which in the *hydrogen-like model* causes an increase of the exciton Rydberg with the replacement of isotopes (see Fig. 2.13). When hydrogen is completely replaced with deuterium, the exciton Rydberg (in the Wannier–Mott model) increases by 20% from 40 to 50 meV, whereas E_g exhibits a 2% increase, and at $2 \div 4.2$ K is $\Delta E_g = 103$ meV. This quantity depends on the temperature, and at room temperature is 73 meV, which agrees well enough with $\Delta E_g = 64.5$ meV as found in the paper of Kapustinsky et al. [58].

The dependence of the *exciton binding energy* on the *isotope* mass presents in Fig. 2.13. From Fig. 2.13 we see that when hydrogen is completely replaced with deuterium, the binding energy of the exciton exhibits a 20% increase from 42 to 52 meV [51]. It is easy to see that in the model of virtual crystal the binding energy of the exciton in LiT crystals must be equal to 57 meV (see Fig. 2.13). Hence it follows that in the linear approximation the isotopic dependence of binding energy of Wannier–Mott excitons may be expressed as

$$E_b = E_b(0)\,(1 + \gamma)\,, \tag{2.12}$$

where $E_b(0)$ is purely the coulombic binding energy of the exciton (in the *frozen lattice*), which in our case is equal to 31.5 meV, and the angular coefficient is $\beta = 12.18\,\text{meV/M}$, where M is the *reduced mass* of ions of lithium and hydrogen (deuterium, tritium) ions; $\gamma = \beta M/E_b\,(0)$ (see also Plekhanov [51]). From the standard equation for the *Coulomb's binding energy* of the exciton

$$E_b = \frac{e^4 \mu}{\hbar^2 \varepsilon_\infty^2}, \tag{2.13}$$

we get the dimensionless constant of the Coulomb's interaction:

$$\eta^2 = \frac{E_b\,(0)}{\hbar\omega_{LO}} = 0.47. \tag{2.14}$$

Comparing the value of $\eta^2 = 0.47$ and the constant of *Fröhlich exciton–phonon interaction* $g^2 = 0.33$ [51] we see that they are close enough. This implies that both the Fröhlich and the Coulomb interactions between electrons (holes) and LO phonons in exciton must be treated with equal attention, as has already been emphasized in Klochikhin's paper [59]. This paper deals from the start with 'bare' *electrons* and *holes*, and all renormalizations are calculated in the two-particle configuration. Such an approach enables us to avoid the considerable difficulty which arises when polarons [60] are used as start-up particles. This difficulty is primarily associated with the fact that the momentum of each particle is conserved when the particles are treated separately, whereas it is the center-of-mass momentum that is conserved when a pair moves as a whole. As demonstrated in Klochikhin [59], this approach also makes it possible to calculate the higher order corrections to the exciton–phonon interaction. It was also shown that the use of the pole parts of polaron *Green functions* in place of complete expressions leads to a situation when the corrections of the order of $\eta^2 g^2$ and g^4 to the potential energy are lost because the corrections to the vertex parts and Green functions cancel out. The quantity lost is of the same order (g^2) as the correction to the residue but has the opposite sign [60]. The approach developed in Klochikhin [59] allowed the calculation of corrections of the order $\eta^2 g^2$ and g^4, the latter is comprised of the correction to the Fröhlich vertex and the correction to the Green functions in the exciton–phonon loop. It is important that the latter have opposite sign and cancel out exactly in the limit $E_b \ll \hbar\omega_{LO}$. As a result, because of the potential nature of the start-up Coulomb interaction, the correction to the Coulomb's vertex of the order $\eta^2 g^2$ does not vanish. As a result, the following expression was obtained in Klochikhin's paper for the binding energy E_b of Wannier–Mott *exciton* when $E_b \ll \hbar\omega_{LO}$ (the spectrum of exciton remains hydrogen like):

$$E_b = \hbar\omega_{LO}\left[\frac{\eta^2 - g^2 + \eta^2 g^2\,(c + v)}{2}\right]^2 \tag{2.15}$$

where c, v = $(m_{c,v}/\mu)^{1/2}$, and m_c, m_v are the electron and hole masses. Now E_b depends explicitly on g^2 (the Fröhlich constant of exciton–phonon interaction), and hence depends on the isotopic composition of the lattice, whereas the standard expression for the binding energy $E_b = \hbar\omega_{LO}\left(\eta^2 - g^2\right) = e^4\mu/\varepsilon_0^2\,\hbar^2$, which describes the exciton spectrum of many semiconductors accurately enough, exhibits no dependence on the isotopic effect. In the case of Eq. (2.15) the exciton spectrum remains hydrogen like. When the higher order corrections are taken into account, Eq. (2.15) becomes

$$E_b = \frac{e^4\mu}{2\varepsilon_0\hbar^2}\left[1 + g^2\varepsilon_0\frac{m_c+m_v}{\varepsilon_\infty} + g^4\frac{\varepsilon_0}{\varepsilon_\infty}\left(\zeta_1+\zeta_2\frac{1-\varepsilon_\infty}{\varepsilon_0}\right)(m_c+m_v)\right]. \qquad (2.16)$$

The order-of-magnitude evaluation of the coefficients ζ_1, ζ_2 gives $\zeta_1 \approx 0.15$ and $\zeta_2 \approx 0.02$; when $g^2(m_c + m_v) \ll 3.3$, the correction of the order $\eta^2 g^4$ is much less than the term of the order $\eta^2 g^2$ (see, e.g. [51] and references therein). Setting $m_v/m_c = 3.5$ and $g^2/\eta^2 = I - \varepsilon_0/\varepsilon_\infty$, and $(\varepsilon_\infty/\varepsilon_0) = (\omega_{TO}/\omega_{LO}) = 1/3.5)$, in paper [59] it was found that E_b $_{(theor)} = 48$ and 42 meV for LiD and LiH, respectively. Comparing these results with the experimental values (see Table 21 of Ref. [51]) we observe good agreement between theory and experiment. Hence follows a natural conclusion that the isotopic dependence of the *exciton binding energy* is primarily due to the *Fröhlich interaction* mechanism between excitons and phonons.

The single-mode nature of exciton reflection spectra of mixed crystals LiH_xD_{1-x} agrees qualitatively with the results obtained with the *virtual crystal model* (see e.g. Elliott et al. [30]; Onodera and Toyozawa [61, 62]), being at the same time its extreme realization, since the difference between ionization potentials ($\Delta\zeta$) for this compound is zero. According to the virtual crystal model, $\Delta\zeta = 0$ implies that $\Delta E_g = 0$, which is in contradiction with the experimental results for LiH_xD_{1-x} crystals. The change in E_g caused by *isotopic substitution* has been observed for many broad-gap and narrow-gap *semiconductor* compounds.

All of these results are documented in Table 21 of Ref. [51], where the variation of E_g, E_b, is shown at the isotope effect. We should highlight here that the most prominent isotope effect is observed in LiH crystals, where the dependence of $E_b = f(C_H)$ is also observed and investigated. To end this section, let us note that E_g decreases by 97 cm^{-1} when ^{7}Li is replaced with ^{6}Li.

Further, we will briefly discuss of the variation of the *electronic gap* (E_g) of *semiconducting* crystals with its isotopic composition. In the last time, the whole row of semiconducting crystals were grown. These crystals are diamond, copper halides, germanium, silicon, CdS, and GaAs. All numerated crystals show the dependence of the electronic gap on the isotope masses (see, reviews [60, 96]).

Before we complete the analysis of these results we should note that before these investigations, studies were carried out on the *isotopic effect* on exciton states for a whole range of crystals by Kreingol'd et al. (see, also [51]). First, the following are the classic crystals Cu_2O [63, 64] with the substitution $^{16}O \rightarrow {}^{18}O$ and $^{63}Cu \rightarrow {}^{65}Cu$. Moreover, there have been some detailed investigations of the isotopic

effect on ZnO crystals , where E_g was seen to increase by $55\,cm^{-1}$ ($^{16}O \rightarrow {}^{18}O$) and $12\,cm^{-1}$ (at $^{64}Zn \rightarrow {}^{68}Zn$) [65, 66]. In [67] it was shown that the substitution of a heavy ^{34}S isotope for a light ^{32}S isotope in CdS crystals resulted in a decrease in the *exciton Rydberg* constant (E_b), which was explained tentatively by the contribution from the nearest electron energy bands, which however are absent in LiH crystals.

More detailed investigations of the exciton *reflectance* spectrum in CdS crystals were done by Zhang et al. [68]. Zhang et al. studied only the effects of Cd substitutions, and were able to explain the observed shifts in the *bandgap* energies, together with the overall temperature dependence of the bandgap energies in terms of a two-oscillator model provided that they interpreted the energy shifts of the *bound excitons* and $n = 1$ polaritons as a function of average S mass reported as was noted above, earlier by Kreingol'd et al. [67] as shifts in the bandgap energies. However, Kreingol'd et al. [67] had interpreted these shifts as resulting from isotopic shifts of the free *exciton binding energies* (see, also [51]), and not the band gap energies, based on their observation of different energy shifts of features which they identified as the $n = 2$ free exciton states (for details see [67]). The observations and interpretations, according Meyer at al. [69], presented by Kreingol'd et al. [67] are difficult to understand, since on the one hand a significant bandgap shift as a function of the S mass is expected [68], whereas it is difficult to understand the origin of the relatively huge change in the free exciton binding energies which they claimed. Meyer et al. [69] reexamine the optical spectra of CdS as function of average S mass, using samples grown with natural Cd and either natural S ($\sim$95% ^{32}S), or highly enriched (99% ^{34}S). These author observed shifts of the bound excitons and the $n = 1$ free exciton edges consistent with those reported by Kreingol'd et al. [67], but, contrary to their results, Meyer et al. observed essentially identical shifts of the free exciton excited states, as seen in both *reflection* and *luminescence* spectroscopy. The reflectivity and photoluminescence spectra in polarized light ($\vec{E} \perp \vec{C}$) over the A and B exciton energy regions for the two samples depicted in Fig. 2.14. For the $\vec{E} \perp \vec{C}$ polarization used in Fig. 2.14 both A and B excitons have allowed transitions, and therefore reflectivity signatures. Figure 2.14 also reveals both reflectivity signatures of the $n = 2$ and 3 states of the A exciton as well as that of the $n = 2$ state of the B exciton.

In Table 2.3 Meyer et al. summarized the energy differences $\Delta E = E(Cd^{34}S) - E(Cd^{nat}S)$, of a large number of bound exciton and free exciton transitions, measured using *photoluminescence*, absorption, and *reflectivity* spectroscopy, in CdS made from natural S ($Cd^{nat}S$, 95% ^{32}S) and from highly isotopically enriched ^{34}S ($Cd^{34}S$, 99% ^{34}S) [51]. As we can see, all of the observed shifts are consistent with a single value, $10.8 \pm 0.2\,cm^{-1}$. Several of the donor bound exciton photoluminescence transitions, in paper [69] can be measured with high accuracy, reveal shifts which differ from each other by more than the relevant uncertainties, although all agree with the $10.8 \pm 0.2\,cm^{-1}$ average shift. These small differences in the shift energies for donor *bound exciton* transitions may reflect a small isotopic dependence of the donor binding energy in CdS. This value of $10.8 \pm 0.2\,cm^{-1}$ shift agrees well with the value of $11.8\,cm^{-1}$ reported early by Kreingol'd et al. [67] for the $B_{n=1}$ transition,

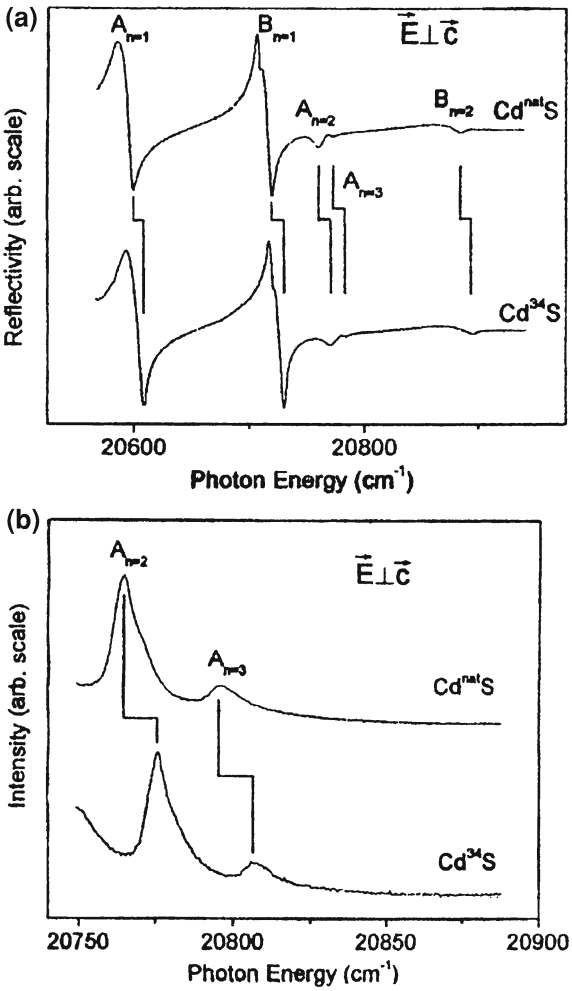

Fig. 2.14 **a** Reflection spectra in the A and B excitonic *polaritons* region of $Cd^{nat}S$ and $Cd^{34}S$ at 1.3 K with incident light in the $\vec{E} \perp \vec{C}$. The *broken vertical lines* connecting peaks indicate measured ene rgy shifts reported in Table 2.3. In this polarization, the n = 2 and 3 excited states of the A exciton, and the n = 2 excited state of the B exciton, can be observed. **b** Polarized photoluminescence spectra in the region of the $A_{n=2}$ and $A_{n=3}$ free exciton recombination lines of $Cd^{nat}S$ and Cd ^{34}S taken at 1.3 K with the $\vec{E} \perp \vec{C}$. The *broken vertical lines* connecting peaks indicate measured energy shifts reported in Table 2.3 (after [69])

particularly when one takes into account the fact that enriched ^{32}S was used in that earlier study, whereas Meyer et al. have used natural S in place of an *isotopically enriched* Cd^{32} S (for details see [51, 69]).

Authors [69] conclude that all of the observed shifts arise predominantly from an *isotopic dependence* of the band gap energies, and that the contribution from any isotopic dependence of the free exciton binding energies is much smaller. On the basis of the observed temperature dependencies of the excitonic transitions energies, together with a simple two-oscillator model, Zhang et al. [68] earlier calculated such a difference, predicting a shift with the S isotopic mass of 950 μeV/amu for the A exciton and 724 μeV/amu for the B exciton. Reflectivity and photoluminescence study of $^{nat}Cd^{32}S$ and $^{nat}Cd^{34}S$ performed by Kreingol'd et al. [67] shows that for

Table 2.3 The energy shifts of all of the transitions studied in [56] are given in terms of the $Cd^{34}S$ minus the $Cd^{nat}S$ energy, ΔE

Transition	Method	ΔE (cm^{-1})
I_2	PL	10.6 ± 0.1
I_2^z	PL	11.1 ± 0.1
I_2^a	PL	10.6 ± 0.1
$A_{n=1}$ (Γ_6)	A$\parallel$	10.8 ± 0.2
$A_{n=1}$ (Γ_5^L)	PL	11.0 ± 0.2
$A_{n=1}$ (Γ_5^L)	R$\perp$	10.9 ± 0.2
$A_{n=2}$	PL$\parallel$	11.3 ± 0.4
$A_{n=2}$	PL$\perp$	11.1 ± 0.4
$A_{n=2}$	R$\perp$	10.2 ± 0.5
$A_{n=3}$	PL$\parallel$	11.8 ± 1.1
$A_{n=3}$	PL$\perp$	10.9 ± 0.6
$A_{n=3}$	R$\perp$	10.7 ± 0.6
$B_{n=1}$ (Γ_1)	R$\parallel$	10.9 ± 0.3
$B_{n=1}$ ($\Gamma_5^L + \Gamma_5^T$)	R$\perp$	10.6 ± 0.4
$B_{n=2}$	R$\parallel$	9.4 ± 1.2
$B_{n=2}$	R$\perp$	9.8 ± 1.2
$C_{n=1}$ (Γ_1)	R$\parallel$	15 ± 6
$C_{n=1}$ (Γ_5)	R$\perp$	14 ± 5

The methods used were photoluminescence spectroscopy (*PL) and reflection spectroscopy (R). For measurements made using polarized light, the $\parallel$ or $\perp$ specifies the orientation of the **E** vector vesus the c axis

anion isotope substitution the ground state ($n = 1$) energies of both A and B excitons have a positive energy shifts with rate of $\partial E/\partial M_S = 740\,\mu$ eV/amu. Results of Meyer et al. [69] are consistent with a shift of $\sim 710\,\mu$eV/amu for both A and B excitons. Finally, it is interesting to note that the shift of the *exciton* energies with Cd mass is $56\,\mu$eV/amu [68], an order of magnitude less than found for the S mass.

In concluding this part we should note that recent high-resolution spectroscopic studies of excitonic and impurity transition in high-quality samples of isotopically enriched Si have discovered the broadening of bound exciton emission (absorption) lines connected with isotope-induced disorder as well as depend on their binding energy on the isotope mass [70–75]. The last effect was early observed on the bound excitons in diamond [56, 51], and earlier on the *free excitons* [76] in $LiH_x\ D_{1-x}$ mixed crystals (see, e.g. [77] and references therein).

2.3 Isotope Low-Dimensional Structure

The advances in epitaxial thin film homo and hetero-structures synthesis, which have been achieved through a variety of *epitaxial* techniques [78–80], have led to a vast array of new solid-state structures with many fascinating properties (see, e.g. [81–83]). *Isotope hetero-structures* has been studied only in last two

decades [81–89]. In combination with the well-established *neutron transmutation* doping (NTD [90]) technique, isotope hetero-structures appear to represent a family of solid-state structures, which offer new possibilities and numerous advantages over the traditional multilayer structures (see above). The formation of a doped *isotope* multilayer structure can be broken down into two independent steps: growth of the structure with isotopically pure or deliberately mixed layers and selective doping with the NTD process [93–95]. The formation of an isotope multilayer structure differs from the traditional methods in only that isotopically pure and deliberately mixed sources must be used, and, the most important, that no dopants are introduced during the growth process. The absence of any dopants during the growth process automatically eliminates all dopant-induced effects including autodoping and dopant interdiffusion between adjacent layers [88]. In principle all the established epitaxial techniques can be applied to the growth of isotope multilayer structures. The only requirement is the availability of *semiconductor* grade pure isotopes. The doping of an isotope heterostructures is achieved with the NTD [90] techniques after growth process has been completed. The NTD technique is isotope selective and therefore it can be used superlatively for the creation of the low-dimensional structure. The *cross-section* for thermal neutron capture and the subsequent nuclear processes of practically every stable isotope of all elements have been measured, studied, and documented (see also [90] and references therein).

As we all know breaking the crystal *translational* symmetry without strongly influencing its *electronic* band structure can be done by means of a modification in the mass of one or more atoms composing the crustal. Without translational symmetry, the wave vector conservation requirements can be circumvented. Ideal models for most studies of elementary excitations are represented by isotopically pure crystals. A new field offering interesting physical studies is opened with the growth of isotopically tailor-made single crystals. The translational symmetry operations can be removed in part by artificial fabricating isotopic superlattice in which layers of two isotopically enriched materials alternate periodically. MBE of *isotopically controlled* germanium has enabled studies of low-dimensional *phonons* in *isotope superlattice* [86–89] and *quantum dots* [91].

In this paragraph we describe the results of Raman measurements on novel kind of heterostructures, a series of isotopic superlattice' of germanium and silicon [86–91]. These samples represent an excellent model system to study the vibrionic properties of superlattice because the electronic structure should be affected only weakly by changes in the isotopic mass (see, e.g. reviews [60, 96]).

Since these changes are the only difference between the superlattice' constituents, *Raman spectroscopy* is the only non-destructive method to investigate their structural properties. Experimental data are compared with the results of planar force-constant model [86]. Let us consider the case of Ge, with the five *isotopes* of it [29]. The readers will ask themselves one should see five phonons (or more if they know that there are two atoms per primitive cell), corresponding to the five different masses, or only one corresponding to the average mass. We all know that the latter is true. The transition from the average mass vibrations to those localized at all possible pairs is an example of the *Anderson localization* phenomenon [38, 39], which is

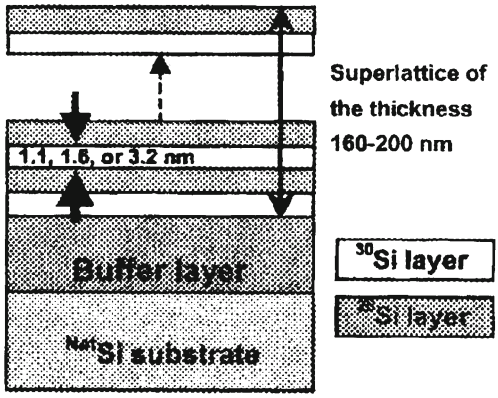

Fig. 2.15 Schematics of Si *isotope superlattices*. Thickness of each isotope layer are 1.1; 1.6; and 3.2 for $^{28}Si_8/^{30}Si_8$; $^{28}Si_{12}/^{30}Si_{12}$ and $^{28}Si_{24}/^{30}Si_{24}$ samples, respectively. Low index denotes the thickness of each isotope layer in atomic monolayers, each 0.136 nm thick (after [92])

observed in Raman experiments on LiH_xD_{1-x} system (for details see [47]). In a three-dimensional crystal, fluctuations in the parameters of the secular equation lead to localization (measured in units of frequency, i.e. $(\Delta M/M)\omega_0$) are larger than the bandwidth of the corresponding excitations. For optical phonons in Ge this bandwidth is $100\,cm^{-1}$ while $(\Delta M/M)\omega_0 \leqslant 0.04 \times 300 = 12cm^{-1}$ (see also above). Hence no phonon localization (with lines corresponding to all pairs of masses) is expected, in agreement with the observation of only one line at $304\,cm^{-1}$ (at 77 K) for natural Ge (see Fig. 2.7). For comparison we indicate that the bandwidth in the LiH_xD_{1-x} mixed crystal is more than $500\,cm^{-1}$, therefore, the *crystal* and *localized phonons* are coexist (for details see [47]).

In *superlattice* composed, for example, of n layers of ^{70}Ge and m layers of ^{76}Ge repeated periodically, one would expect to find optical modes localized or nearly localized in each of two constituents. Schematics of Si isotope superlattice are depicted in Fig. 2.15 [92]. Koijma et al. have grown three kinds of silicon isotope superlattice ($^{28}Si_n/^{30}Si_n$, with n = 8, 12 and 24) using the solid-source MBE technique [79, 97]. In this paper n denotes the thickness of each isotope layer in atomic monolayers, each 0.136 nm thick. The periodicity, i.e., the number $^{28}Si/^{30}Si$ pair layers stacked vertically, is 80, 50, and 30 for n = 8, 12, and 24 samples, respectively. The resulting total thickness of the superlattice is 160–200 nm (see, Fig. 2.15). The source for the ^{28} Si layer is actually ^{nat}Si which is composed of 92.2% ^{28}Si. The source for the ^{30}Si layer is a single Si crystal isotopically enriched to ^{30}Si(~98.74% [93–95]). In MBE, individual effusion cells equipped with crucibles made of high purity tantalum. The crucible are temperature is maintained at 1400° C for a growth rate of ~0.01 nm/s. The base pressure of the vacuum is 5×10^{-10} torr and the pressure during growth is $\sim 10^{-9}$ Torr Fig. 2.15.

As was shown [98], the E versus k dispersion of *phonons* in the superlattice is *zone folded* due to the new periodicity, na, introduced by the $(^{28}Si)_n$–$(^{30}Si)_n$ unit where a is the periodicity of the bulk Si. Because Raman spectroscopy, to first order, probes phonons situated at k ~ 0 in the dispersion relation, while only one longitudinal optical (LO) phonon peak is observed with bulk Si, multiple LO phonon peaks

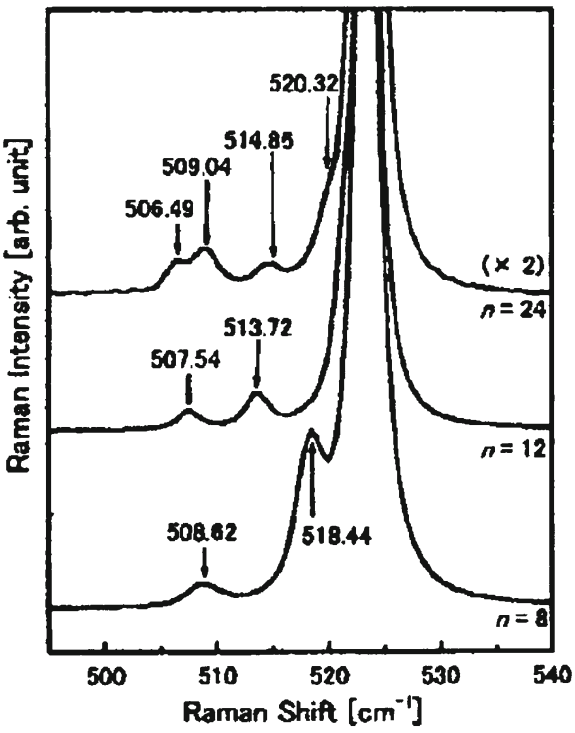

Fig. 2.16 Raman spectra of the $^{28}Si_n/^{30}Si_n$ samples with $n = 8$, 12 and 24 (after [92])

should appear for isotope superlattice due to the zone folding or *phonon localization* (see, e.g. [99]). Figure 2.16 shows the Raman spectra of Si superlattice. As expected, many peaks are observed on the shoulders of the large ^{nat}Si substrate LO peak around 523.5 cm^{-1}. The wave numbers of the identified peaks are indicated in Fig. 2.16 for comparison with theoretical predictions fulfilled in the planar bond-charge model for Si (see [100]). As was shown in paper [93–95] theoretical curves are not smooth due to anticrossings. In general, the agreement between the experimental and theoretical results is excellent, except for the one detail: while LO_1 (^{28}Si) peaks in n = 12 and 24 samples are hidden in the large substrate peak, the LO_1 (^{28}Si) peak is observed experimentally for the n = 8 sample and its position deviates from the calculation (for details see Fig. 4 in [92]).

Raman spectra of a serial of isotopic $^{70}(Ge)_n^{74}(Ge)_n$ *superlattice* with $2 \leq n \leq 32$ ($8 \leq n \leq 24$) was published in papers [87, 88]. Three modes could be observed (see Fig. 2.17) for the $^{70}(Ge)_{16}^{74}(Ge)_8$ "as-grown" superlattice as theoretically predicted [86]. We should underline that the excellent agreement between results of papers [87, 88].

In concluding this paragraph we should stressed that *isotopic superlattice* represents an excellent model system for the investigation of *confinement* of optical phonons. Both frequencies and relative intensities of the measured spectra are in

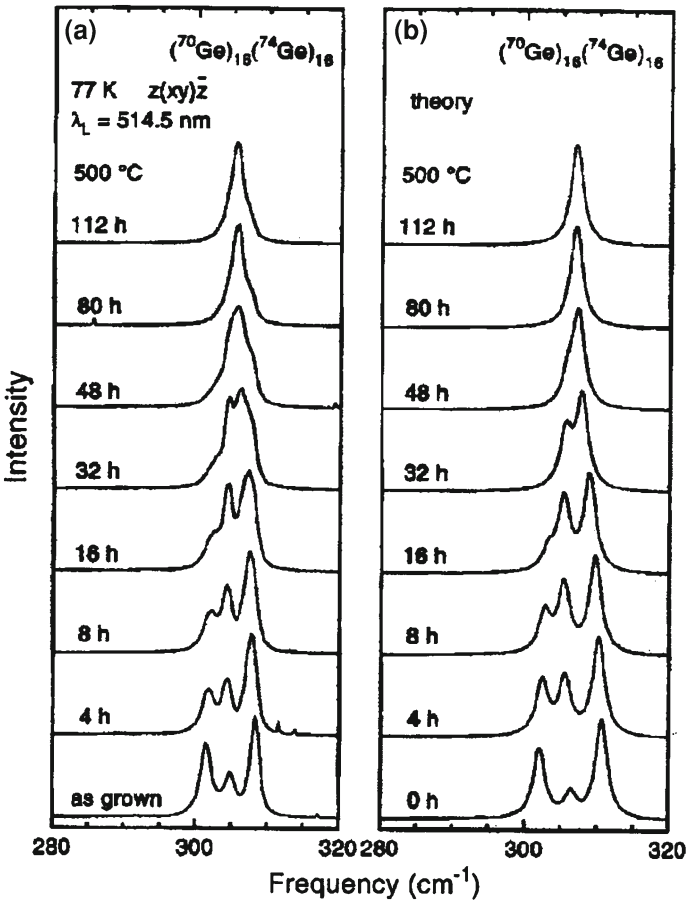

Fig. 2.17 **a** Experimental Raman spectra of a $(^{70}Ge)_{16}(^{74}Ge)_{16}$ superlattice for different annealing steps at 500°C. **b** Calculated Raman spectra for the same superlattice using the same parameters (after [88])

good agreement with calculations based on a planar *bond-charge model* and the bond-polarizability approach (for details see [93–95].

2.4 Excitons and Biexcitons in Quantum Dots

When a *semiconductor (insulator)* of *direct bandgap* E_g is shone with near-bandgap light, *electron-hole pairs* are created. If the electron and the hole were noninteracting only photon energies $\hbar\omega > E_g$ would be absorbed and E_g would be the absorption edge. The *Coulombic electron-hole interaction* greatly modifies this picture. The electron-hole attraction gives rise to bound states of the relative motion of the exciton.

The appearance of intense, narrow absorption lines below the fundamental absorption edge is the manifestation of these bound states.

In the case of confined systems for electrons and holes, such as *quantum wells (QWs), quantum wires (QWRs) and quantum dots (QDs)*, the *excitonic effects* are much more important than in *bulk solids*. In effect, as will be shown below, the binding energy of the electron- hole systems forming an excitons are much higher in quantum confined systems than in the case of solids, and, therefore, the excitonic transitions can be observed even at temperatures close to room temperature, as closed to the bulk case for which low temperatures are needed. This makes the role played by *excitons* in many optoelectronic devices of nanoscale very important.

It is perhaps easier to deal with a finite barrier *quantum dot* (QD) with spherical rather than cuboid symmetry. The approach is rather similar to that derived earlier for the circular *cross-section quantum wire* (QWr). Given the *spherical symmetry* of the potential, then the wave function would also be expected to have spherical symmetry, hence the Schrödinger equation for a constant *effective mass* could be written (see, e.g. [101, 103])

$$-\frac{\hbar^2}{2m^*}\left(\frac{\partial^2}{\partial x^2}+\frac{\partial^2}{\partial y^2}+\frac{\partial^2}{\partial z^2}\right)\Psi(r)+V(r)\Psi(r)=E_r\Psi(r), \tag{2.17}$$

where the index on E_r has been added just to indicate that this energy is associated with the *confinement* along the radius. In this case:

$$r=\sqrt{x^2+y^2+z^2}. \tag{2.18}$$

The transition can be made from Cartesian (x, y, z) to spherical polar coordinates, in effect just r, in the same way above. Using Eq. (93) of Ref. [102], each of the three *Cartesian axes* gives an equation of the following form:

$$\frac{\partial^2}{\partial x^2}\Psi(r)=\frac{1}{r}\frac{\partial}{\partial r}\Psi(r)-\frac{x^2}{r^3}\frac{\partial}{\partial r}\Psi(r)+\frac{x^2}{r^2}\frac{\partial^2}{\partial r^2}\Psi(r) \tag{2.19}$$

Therefore, the complete $\nabla^2\Psi(r)$ is given by:

$$\left(\frac{\partial^2}{\partial x^2}+\frac{\partial^2}{\partial y^2}+\frac{\partial^2}{\partial z^2}\right)\Psi(r) =\frac{3}{r}\frac{\partial}{\partial r}\Psi(r)-\frac{(x^2+y^2+z^2)}{r^3}\frac{\partial}{\partial r}\Psi(r)+\frac{(x^2+y^2+z^2)}{r^2}\frac{\partial^2}{\partial r^2}\Psi(r). \tag{2.20}$$

and

$$\left(\frac{\partial^2}{\partial x^2}+\frac{\partial^2}{\partial y^2}+\frac{\partial^2}{\partial z^2}\right)\Psi(r)=\frac{2}{r}\frac{\partial}{\partial r}\Psi(r)+\frac{\partial^2}{\partial r^2}\Psi(r). \tag{2.21}$$

Substituting into the Schrödinger equation then:

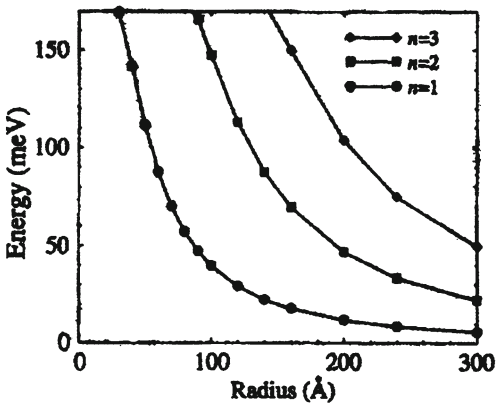

Fig. 2.18 The *confinement* energy in a *spherical* GaAs quantum dot surrounded by a $Ga_{0.8}Al_{0.2}As$ barrier (after [103])

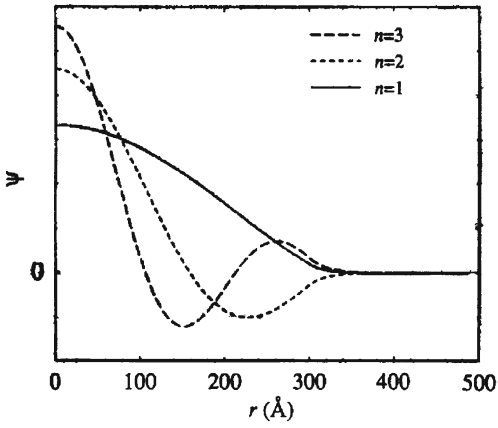

Fig. 2.19 The wave functions of the three lowest energy states in the 300 Å spherical quantum dot (after [103])

$$-\frac{\hbar^2}{2m^*}\left(\frac{2}{r}\frac{\partial}{\partial r}+\frac{\partial^2}{\partial r^2}\right)\Psi(r)+V(r)\Psi(r)=E_r\Psi(r). \tag{2.22}$$

Such spherical symmetric Schrödinger equations have been investigated before (see, e.g. [8–10]). The last equation, is numerically solved and Fig. 2.18 shows the results of calculations of the three lowest energy levels of a spherical GaAs QD surrounded by a finite barrier composed of $Ga_{0.8}Al_{0.2}As$, with a sharp boundary. In fact, the formalism above, as that of the *circular cross - section* QWr, is applicable for any radial potential profile V(r), e.g., it is also valid for diffused interfaces [103] Again, the behavior of the energies as a function of the spatial dimension, as shown in Fig. 2.18, is as expected in *confined* systems, namely the confinement energy decreases as the size of the system increases. Figure 2.19 displays the corresponding radial components of the wave functions. It can be seen that they all have a maximum at the centre of the potential and that as the principal quantum number n increases, then the number of nodes increases.

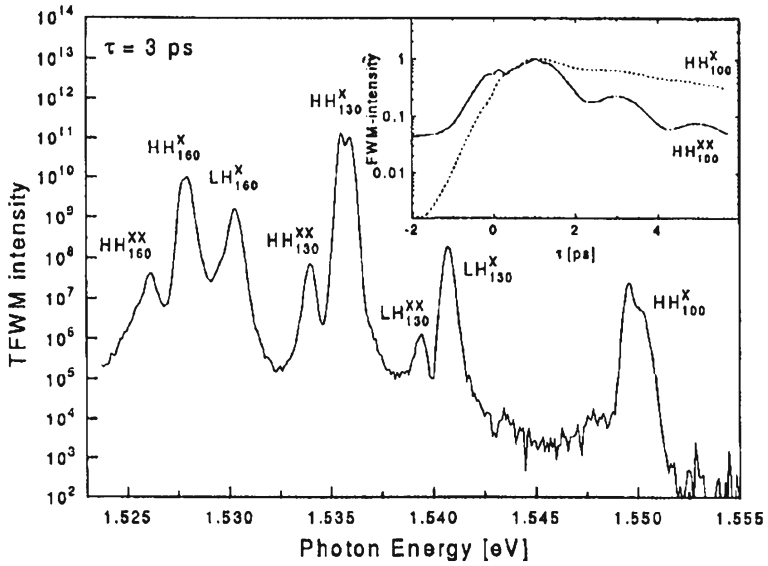

Fig. 2.20 Spectrally resolved four-wave mixing at $\tau = 3$ ps showing the heavy hole and light hole biexcitons. Insert shows the four-wave mixing intensity of the heavy hole exciton and biexciton as a function of delay (after [110])

In 1958, Moskalenko [104] and Lampert [105] suggested that in crystals besides excitons more complex electronic quasi particles might exist, made up of three or four carriers. The latter one, consisting of two electrons and two holes, is well known as *biexcitons* or *excitonic molecules* [106]. As the density of excitons is increased, biexcitons are formed by increasing the light intensity. Biexcitons can be generated either through ordinary excitation of the crystal or by two-photon absorption each photon having an energy

$$\mathrm{h}\nu = \mathrm{E}_x - \frac{\mathrm{E}_{B_{xx}}}{2}, \tag{2.23}$$

where $\mathrm{E}_{B_{xx}}$ is the *biexciton binding energy* and E_x is the *exciton energy*

$$\mathrm{E}_x = \mathrm{E}_\mathrm{g} - \mathrm{E}_{B_x} + \frac{\hbar^2 \mathrm{k}^2}{2\mathrm{m}_x}. \tag{2.24}$$

In the last relation E_g is the bandgap energy, E_{B_x} is the exciton binding energy and $\frac{\hbar^2 \mathrm{k}^2}{2\mathrm{m}_x}$ is the kinetic energy with which an exciton moves through the crystal (see, also [107]).

Compared to the bulk material, an increased stability of biexcitons due to the two-dimensional carrier confinement is observed for typical III–V structures such as GaAs/AlGaAs QWs [108–110] (see Fig. 2.20) or for wide bandgap II–VI materials such as CdZnSe/ZnSe [111]. As a consequence of the enhanced biexciton binding

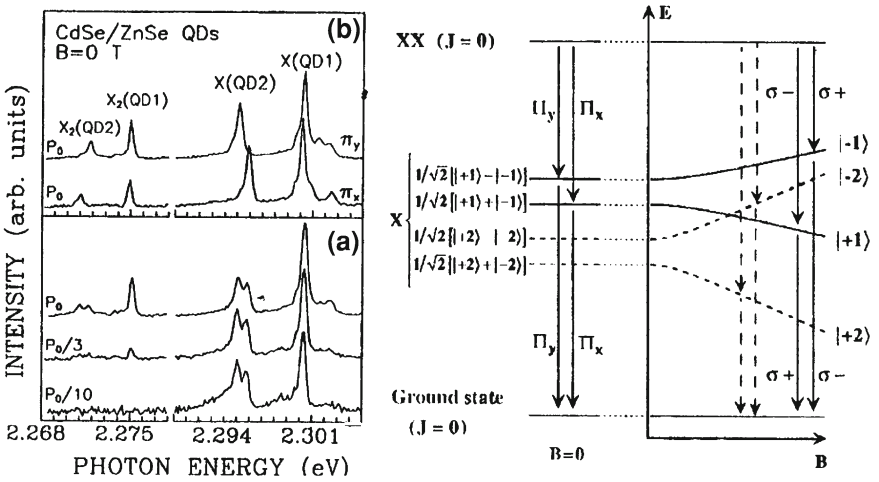

Fig. 2.21 *Left side Excitonic* (X) and *biexcitonic* (X_2) emission from two individual CdSe/ZnSe SQDs for different excitation powers. The PL spectra shown in the lower panel are unpolarized, the data presented in the upper panel represent linearly polarized PL spectra (π_x and π_y, respectively). *Right side* Energy level scheme for the biexciton–exciton cascade in a QD (after [111])

energy, a variety of optical properties, such as the photoluminescence(PL) spectrum, the optical gain or the four-wave mixing signal especially in wide bandgap II–VI QWs are strongly influenced by *biexcitons* (see [111] and references therein).

Below we briefly review some results obtained from *optical spectroscopy* on epitaxially grown single SQDs based on II–VI and II–N compounds. As was indicated above the biexciton (XX or X_2) is a four-particle state. In its lowest energy state configuration, two electrons and two holes with antiparallel spins occupy the first quantized state of the *conduction* and the *valence band* in the SQDs, respectively (see, e.g. [112]) We should add that the QDs in the material systems described here are quite small with diameters in the order of 10 nm and heights of a few nm. The biexciton state is therefore a singlet state with a total spin of $J = 0$. Thus, the exciton state X represents the final state for the biexciton recombination [113]. In II–VI semiconductors, as in III–V materials with a zincblende crystal lattice, *Coulomb interaction* leads to positive biexciton binding energies (see Eq. (2.24)), i.e., the energetic distance between XX (X_2) and X smaller than the energy difference between the first exciton state and the ground state. A typical optical fingeprint for the X_2 is therefore an additional PL line at the low energy side of the exciton *emission* X that exhibits a strong (quadratic) dependence on the excitation power [107]. This behavior is clearly visible in left panel of Fig. 2.21. At low excitation density, the PL spectrum of CdSe/ZnSe SQDs consists of emission peaks stemming from *exciton* recombination of two individual QDs. With rising excitation density additional lines emerge, red shifted by about 24 meV with respect to the excitonic emission X, and rapidly increasing in intensity, which can be attributed to biexciton emission X_2. The biexciton binding energy is obviously much larger than in III. As-based QDs

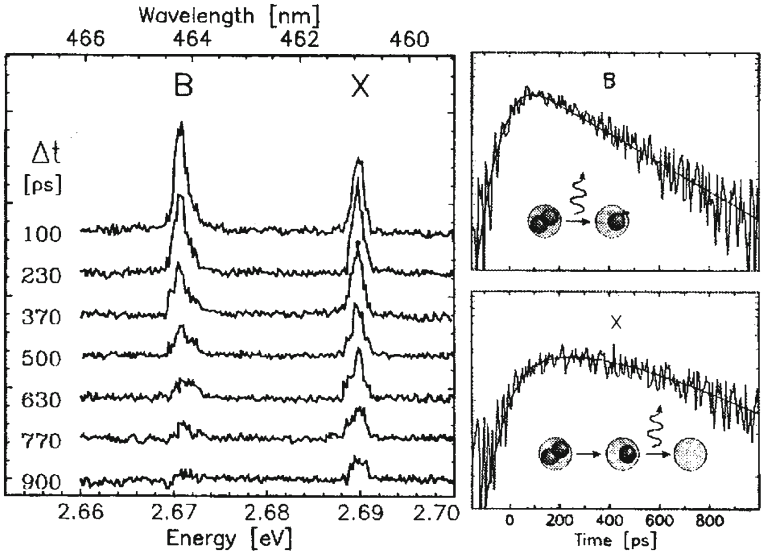

Fig. 2.22 *Left panel* Transient PL spectra from a single CdSe/ZnSe QD showing the single exciton X and the *biexciton* transition (here denoted by B = X_2). *Right panel* Decay curves for the exciton and the biexciton PL signal (for details see text) (after [111])

where a typical values of a few meV (∼2 meV [110]) have been determined (see, also [108, 109, 114]). When having a closer look on the PL spectra presented in Fig. 2.21, some more information can be extracted. One should have in mind that in QDs, the light hole level is shifted to higher energies due to strain and *confinement* and thus, excitons are formed between electrons and heavy holes. The ground state of a heavy hole exciton in a SQD is a spin quadruplet, which can be by the z-component (= component, according [111] in growth direction) of the total exciton spin J_z. If the z-component of the electron spin, $s_z = \pm$ 1/2, and the z-component of the total angular momentum of the heavy hole $j_z = \pm$ 3/2 are antiparallel, in such case, we get $J_z = s_z + j_z = \pm 2$ (the *dark exciton states* [113]).

In II–VI QDs the energy difference Δ_0 between *bright and dark exciton states* that is given by the isotropic electron-hole interaction energy, amounts to about 1 meV and more which is nearly an order of magnitude larger than in InAs/GaAs QDs [101]. As can be seen in Fig. 2.21, the exciton fine structure is reflected both in the exciton and in the biexciton recombination: SQD1 does not show a significant splitting of the exciton PL signal, while SQD2 exhibits a doublet with an energy separation of almost 1 meV indicating a reduced QD symmetry. Exactly the same behavior is observed in the corresponding biexciton lines. Moreover, the high energy component of the X emission in SQD2 (π_x polarized) corresponds to the low energy component of the X_2 emission and vice versa, in agreement with energy level scheme (see Fig. 2.20). All these effects are easily accessible in wide bandgap II–VI QDs because the characteristic energy splitting are significantly enhanced with respect to

III-As semiconductor QDs. We may expect more significant value of the exchange splitting for exciton and biexciton states in QD of *isotope-mixed crystals* (see, also [60, 93–95]). Thanks to the large biexciton binding energy, II–VI QDs were the first, where the biexciton–exciton cascade could be traced directly in the time domain on SQD level [115]. Figure 2.22 depicts transient PL spectra (left) of both *emission* lines and the time-dependent intensity of the exciton and the biexciton signal (right panel). The biexciton emission shows a monoexponential decay with a time constant of 310 ps. The exciton reveals a more complex behavior: the onset of the exciton line ids delayed, resulting in "plateau-like" characteristics of the exciton decay curve. The excitation density according authors of this experiment was set to a value where an average number of two electron-hole pairs per excitation pulse in the SQD was generated. Model calculations taking into account the biexciton state, the *bright*, and the *dark exciton states* and the "empty" QD (corresponding to a QD population with 2, 1 and 0 excitons, respectively) confirm that the exciton state is feeded by the biexciton recombination causing the delayed onset and the "plateau-like" characteristics of the *exciton emission dynamics* (for details see [101] and references therein).

References

1. F. Soddy, Intra-atomic charge. Nature (London) **92**, 399–400 (1913)
2. F. Soddy, The structure of the atom. Nature (London) **92**, 452–452 (1913)
3. H. Frauenfelder, E.M. Henley, *Subatomic Physics* (Prentice Hall, New York, 1991)
4. J.J. Kelly, Nucleon charge and magnerization densities from Sachs form factors. Phys. Rev. **C66**, 065203–065206 (2002)
5. G.A. Miller, A.K. Opper, E.J. Stephenson, Charge symmetry breaking and QCD, ArXiv: nucl-ex/0602021
6. G.A. Miller, Charge densities of the neutron and proton. Phys. Rev. Lett. **99**, 112001–112004 (2007)
7. G.A. Miller, J. Arringfton, The neutron negative central charge density: an inclusive–exclusive connection, ArXiv: nucl-th/0903.1617
8. P.A.M. Dirac, *The Principles of Quantum Mechanivs* (Oxford University Press, UK, 1958)
9. R.P. Feyman, R.P. Leighton, M. Sands, *The Feyman Lecture in Physics*, vol. 3 (Addison Wesley, Reading, MA, 1965)
10. L.D. Landau, E.M. Lifshitz, *Quantum Mechanics (Nonrelativistic Theory)* (Pergamon, New York, 1977)
11. V.G. Plekhanov, Manifestation and origin of the isotope effect, ArXive: gen. phys/0907.2024 (2009) pp. 1–192
12. F.W. Aston, *Mass-Spectra and Isotopes* (Science, Moscow, 1948). (in Russian)
13. K. Blaum, High accuracy mass spectrometry with stored ions. Phys. Reports **425**, 1–783 (2006)
14. K. Blaum, W. Geithnar, J. Lassen, Nuclear moments and charge radii of argon isotopes between the neutron-shell closures N = 20 and N = 28, Nucl. Phys. **799**, 30–45 (2008)
15. M. Glaser, M. Borys, Precision mass measurements. Rep. Prog. Phys. **72**, 126101–126131 (2009)
16. S.M. Wong, *Introductory Nuclear Physics* (Wiley, New York, 1998)
17. Ju.M. Schirokov, N.P. Judin, *Nuclear Physics* (Science, Moscow, 1980). (in Russian)
18. W.F. Hornyack, *Nuclear Structurs* (Academic Press, New York, 1975)
19. B.M. Brink, *Nuclear Forces* (Pergamon, New York, 1965)

20. J. Carlson, R. Schiavilla, Structure and dynamics of few—nucleon systems. Rev. Mod. Phys. **70**, 743–841 (1998)
21. C. Davies, S. Collins, Physics, (World, August, 2000), pp. 35–40
22. V.G. Plekhanov, Isotope effect on the lattice dynamics in crystals. Mater. Sci. Eng. **R35**, 139–237 (2001)
23. I.M. Lifshitz, *Selected Papers Physics of Real Crystals and Disordered Systems* (Science, Moscow, 1987). (in Russian)
24. A.A. Maradudin, E.W. Montroll, G.H. Weiss, I.P. Iopatova, *Theory of Lattice Dynamics in the Harmonic Approximation* (Academic Press, New York, 1971)
25. M. Born, K. Huang, *Dynamical Theory of Crystal Lattice* (Oxford University Press, London, 1968)
26. V.G. Plekhanov, Lattice-dynamics of isotope-mixed crystals, ArXiv: cond-mat/1007.5125 (2010)
27. G. Dolling, in *Neutron Spectroscopy and Lattice Dynamics*, ed. by G.K. Horton, A.A. Maradudin, Dynamical Properties of Solids, vol 1, (North-Holland, Amsterdam, 1974) Chap. 10, pp. 543–629
28. G. Dolling, A.D.B. Woods, *Thermal Vibrations Crystal Lattice*, in ed. by P.A. Egelstaff, Thermal Neutron Scattering, (Academic Press, New York, 1965), pp. 178–262
29. A.S. Barker Jr, A.J. Sievers, Optical studies of the vibrational properties of disordered solids. Rev. Mod. Phys. **47**(Suppl. 2), S1–S179 (1975)
30. R.J. Elliott, J.A. Krumhansl, P.L. Leath, The theory and properties of randomly disordered crystals and physical systems. Rev. Mod. Phys. **46**, 465–542 (1974)
31. R.J. Elliott, I.P. Ipatova (eds.), *Optical Properties of Mixed Crystals* (North-Holland, Amsterdam, 1988)
32. I.P. Ipatova, Universal parametrs in mixed crystals in [30] Chap. 1, pp. 1–34
33. D.W. Taylor, Phonon response theory and the infrared and Raman experiments in [30] Chap. 2, pp. 35–132
34. M. Lax, E. Burstein, Infrared lattice absorption in ionic and homopolar crystals. Phys. Rev. **97**, 39–52 (1955)
35. V.F. Agekyan, A.M. Asnin, V.M. Kryukov et al., Isotope effect in germanium, Fiz. Tverd. tela (St. Petersburg) **31**, 101–104, (1989). (in Russian)
36. H.D. Fuchs, G.H. Grein, C. Thomsen et al., Comparison of the phonon spectra of ^{70}Ge and ^{nat}Ge crystals: effects of isotopic disorder. Phys. Rev. **B43**, 483–491 (1991)
37. H.D. Fuchs, S.H.Grein, R.I. Devlen, et al., Anharmonic decay time, isotopic scattering time, and inhomogeneous line broadening optical phonons in ^{70}Ge, ^{76}Ge and natural Ge crystals ibid **B44**, 8633–8642, (1991)
38. P.W. Andersen, Absence of diffusion in certain random lattice. Phys. Rev. **109**, 1492–1505 (1955)
39. P.W. Andersen, Solid state physics **2**, 193–243, 1970
40. P. Etchegoin, H.D. Fuchs, J. Weber et al., Phonons in isotopically disordered Ge. Phys. Rev. **B48**, 12661–12671 (1993)
41. J.M. Zhang, M. Giehler, A. Gobel et al., Optical phonons in isotopic Ge studied by Raman scattering. Phys. Rev. **B57**, 1348–1351 (1998)
42. J.M. Zhang, T. Ruf, R. Lauck et al., Raman spectra of isotopic GaN. Phys. Rev. **B56**, 14399–14404 (1997)
43. H. Hanzawa, N. Umemura, Y. Nisida, H. Kanda, Disorder effect of nitrogen impurities, irradiation-induced defects and ^{13}C isotope composition on the Raman spectrum in synthetic I^b diamond, Phys. Rev. **B54**, 3793–3799 (1996)
44. F. Widulle, T. Ruf, M. Konuma et al., Isotope effects in elemental semiconductors: a Raman study of silico. Solid State Commun. **118**, 1–22 (2001)
45. D.T. Wang, A. Gobel, J. Zepenhagen, et al., Raman scattering on α-Sn: dependence on isotopic composition, Phys. Rev. **B56**, 13167–13 171, (1997)
46. F. Widulle, *Raman spectroscopy of semiconductors with controlled isotopic composition* (Ph. D, Stuttgart, Germany, 2002)

47. V.G. Plekhanov, Isotope effects in lattice dynamics. Physics-Uspekhi **46**, 689–715 (2003)
48. K.C. Hass, M.A. Tamor, T.R. Anthony, W.F. Banholzer, Lattice dynamics and Raman spectra of isotopically mixed diamond. Phys. Rev. **B45**, 7171–7182 (1992)
49. J. Spitzer, P. Etchegoin, T.R. Anthony et al., Isotopic—disorder induced Raman scattering in diamond. Solid State Commun. **88**, 509–513 (1983)
50. R.M. Chrenko, ^{13}C-doped diamond: Raman spectra. Appl. Phys. **63**, 5873–5875 (1988)
51. V.G. Plekhanov, *Giant Isotope Effect in Solids* (Stefan University Press, La Jolla, 2004)
52. M. Schwoerer-Bohning, D.A. Arms, A.T. Macrander, Phonon dispersion of diamond measured by inelastic X-ray scattering. Phys. Rev. Lett. **80**, 5572–5575 (1998)
53. S.A. Solin, A.K. Ramdas, Raman spectrum of diamond. Phys. Rev. **B1**, 1687–1699 (1970)
54. V.G. Plekhanov, Experimental evidence of strong scattering in isotopical disordered systems: the case LiH_xD_{1-x}. Phys. Rev. **B51**, 8874–8878 (1995)
55. V.G. Plekhanov, Experimental evidence of strong scattering in isotopical disordered systems, ArXiv: cond-mat/0907.3817
56. V.G. Plekhanov, Lattice dynamics of isotopically mixed systems, Opt. Spectr. (St. Petersburg) **82**, 95–124, 69 (1997)
57. V.G. Plekhanov, Isotopic and disorder effects in large exciton spectroscopy, Uspekhi-Phys. (Moscow) **167**, 577–604, (1997). (in Russian)
58. A.F. Kapustinsky, L.M. Shamovsky, K.S. Bayushkina, Thermochemistry of isotopes. Acta physicochem (USSR) **7**, 799–810 (1937)
59. A.A. Klochikhin, Renormalization of Wannier–Mott exciton spectrum by Fr chlich interaction. Sov. Phys. Solid State **22**, 986–992 (1980)
60. V.G. Plekhanov, Elementary excitations in isotope-mixed crystals. Phys. Reports **410**, 1–235 (2005)
61. Y. Onodera, Y. Toyozawa, Persistence and amalgamation types in the electronic structure of mixed crystals. J. Phys. Soc. Japan **24**, 341–355 (1968)
62. Y. Toyozawa, *Optical Processes in Solids* (Cambridge University Press, Cambridge, 2003)
63. F.I. Kreingol'd, K.F. Lider, K.I. Solov'ev, Isotope shift of exciton line in absorption spectrum Cu_2O, JETP Letters (Moscow) **23**, 679–681, (1976). (in Russian)
64. F.I. Kreingol'd, K.F. Lider, V.F. Sapega, Influence of isotope substitution on the exciton spectrum in Cu_2O crystal, Fiz. Tverd. Tela **19**, 3158–3160, (1977). (in Russian)
65. F.I. Kreingol'd, B.S. Kulinkin, Influence of isotope substitution on the forbidden gap of ZnO crystals, ibid **28**, 3164–3166, (1986). (in Russian)
66. F.I. Kreingol'd, Dependence of band gap ZnO on zero-point energy, ibid **20**, 3138–3140, (1978). (in Russian)
67. F.I. Kreingol'd, K.F. Lider, M.B. Shabaeva, Influence of isotope substitution sulfur on the exciton spectrum in CdS crystal, ibid, **26**, 3940–3941, (1984). (in Russian)
68. J.M. Zhang, T. Ruf, R. Lauck et al., Sulfur isotope effect on the excitonic spectra of CdS. Phys. Rev. **B57**, 9716–9722 (1998)
69. T.A. Meyer, M.L.W. Thewalt, R. Lauck et al., Sulfur isotope effect on the excitonic spectra of CdS. Phys. Rev. **B69**, 115214–5 (2004)
70. D. Karaskaja, M.L.W. Thewalt, T. Ruf, Photoluminescence studies of isotopically-enriched silicon: Isotopic effects on indirect electronic band gap and phonon energies. Solid State Commun. **123**, 87–92 (2003)
71. D. Karaskaja, M.L.W. Thewalt, T. Ruf, Phys. Stat. Sol. (b) **235**, 64–69 (2003)
72. S. Tsoi, H. Alawadhi, X. Lu et al., Electron–phonon renormalization of electronic bandgaps of semiconductors: Isotopically enriched silicon. Phys. Rev. **B70**, 193201–193204 (2004)
73. A.K. Ramdas, S. Rodriguez, S. Tsoi et al., Electronic band gaps of semiconductors as influenced by their isotopic composition. Solid State Commun. **133**, 709–714 (2005)
74. S. Tsoi, S. Rodriguez, A.K. Ramdas et al., Isotopic dependence of the E_0 and E_1 direct gaps in the electronic band structure of Si. Phys. Rev. **B72**, 153203–4 (2005)
75. H. Kim, S. Rodriguez, T.R. Anthony, Electronic transitions of holes bound to boron acceptors in isotopically controlled diamond. Solid State Commun. **102**, 861–865 (1997)

76. A.A. Klochikhin, V.G. Plekhanov, Isotope effect on the Wannier–Mott exciton levels. Sov. Phys. Solid State **22**, 342–344 (1980)
77. V.G. Plekhanov, Direct observation of the effect of isotope-induced-disorder on the exciton binding energy in LiH_xD_{1-x} mixed crystals. J. Phys. Condens. Matter **19**, 086221–9 (2007)
78. V.G. Plekhanov, Isotopetronics-new direction of nanoscience, ArXiv: gen. phys/1007.5386
79. A. Cho (ed.), *Molecular Beam Epitaxy* (Springer, Berlin, 1997)
80. G.B. Stringfellow, *Organometallic Vapor—Phase Epitaxy: Theory and Practice*, 2nd edn. (Academic Press, London, 1999)
81. M.J. Kelly, *Low-Dimensional Semiconductors* (Clarendon Press, Oxford, 1995)
82. J.H. Davis, *The Physics of Low-Dimensional Semiconductors* (Cambridge University Press, Cambridge, 1998)
83. K. Goser, P. Glsektter, J. Dienstuhl, *Nanoelectronics and Nanosystems* (Springer, Berlin, 2004)
84. A.A. Berezin, Isotope superlattices and isotopically ordered structures. Solid State Commun. **65**, 819–821 (1988)
85. E.E. Haller, Isotope heterostructures selectively doped by neutron transmutation. Semicond. Sci. & technol. **5**, 319–321 (1990)
86. M. Cardona, P. Etchegoin, H.D. Fuchs et al., Effect of isotopic disorder and mass on the electronic and vibronic properties of three-, two- and one- dimensional solids. J. Phys. Condens Matter **5**, A61–A72 (1993)
87. J. Spitzer, T. Ruf, W. Dondl et al., Raman scattering by optical phonons in isotopic $^{70}(Ge)_n^{74}(Ge)_n$ superlattices. Phys. Rev. Lett. **72**, 1565–1568 (1994)
88. E. Silveira, W. Dondl, G. Abstreiter et al., Ge self - diffusion in isotopic $^{70}(Ge)_n^{74}(Ge)_m$ superlattices: A Raman study. Phys. Rev. **B56**, 2062–2069 (1997)
89. M. Nakajima, H. Harima, K. Morita, et al., Coherent confined LO phonons in $^{70}Ge/^{74}Ge$ isotope superlattices generated by ultrafast laser pulses, Phys. Rev. **B63**, 161304(R)(1–4) (2001)
90. V.G. Plekhanov, Applications of isotope effects in solids. J. Mater. Science **38**, 3341–3429 (2003)
91. A.V. Kolobov, K. Morita, K.M. Itoh et al., A Raman scattering study of self-assembled pure isotope Ge/Si (100) quantum dots. Appl. Phys. Lett. **81**, 3855–3857 (2002)
92. T. Kojima, R. Nebashi, Y. Shiraki et al., Growth and characterization of $^{28}Si/^{30}Si$ isotope superlattices. Appl. Phys. Lett. **83**, 2318–2320 (2003)
93. L.M. Zhuravleva, V.G. Plekhanov, Nuclear technology in creation of low-dimensional isotope-mixed structures. Nanoind. **4**, 28–30, (2009). (in Russian)
94. http://www.nanoindustry.su
95. L.M. Zhuravleva, V.G. Plekhanov, Isotopetronics and quantum information, Nano microsyst. **N3**, 46–54, (2011). (in Russian)
96. M. Cardona, M.L.W. Thewalt, Isotope effect on the optical spectra of semiconductors. Rev. Mod. Phys. **77**, 1173–1224 (2005)
97. M.A. Herman, W. Richter, H.Sitter, *Epitaxy, Physical Principles and Technical Implementation*, in Springer Series in Materials Science, vol. 62 (Springer, Heidelberg, 2004)
98. V.G.Plekhanov, *Isotope-Mixed Crystals: Fundamentals and Applications* (2011, in press)
99. G. Fasol, M. Tanaka, H. Sakaki et al., Interface roughness and dispersion of confined LO phonons in GaAs/AlAs quantum wells. Phys. Rev. **B38**, 6056–6065 (1988)
100. H. Bilz, W. Kress, *Phonon Dispersion Relations in Insulators* (Springer, Berlin, 1979)
101. P. Michler (ed.), *Single Semiconductor Quantum Dots* (Springer, Berlin, 2009)
102. K. Barnham, D. Vvedensky, *Low-Dimensional Semiconductor Structures* (Cambridge University Press, Cambridge, 2009)
103. P. Harrison, *Quantum Wells, Wires, and Dots* (Wiley, New York, 2001)
104. S.A. Moskalenko, Towards to theory of Mott excitons in alkali halides crystals, Opt. Spectr. **5**, 147–155, (1958) (in Russian)
105. M.A. Lampert, Mobile and immobile effective-mass-particle complexes in nonmetallic solids. Phys. Rev. Lett. **1**, 450–453 (1958)

106. V.G. Plekhanov, Fundamentals and applications of isotope effect in solids. Progr. Mat. Science **51**, 287–426 (2006)
107. B. Hnerlage, R. Levy, J.B. Grun et al., The dispersion of excitons, polaritons and biexcitons in direct-gap semiconductors. Phys. Reports **124**, 163–253 (1985)
108. R.C. Miller, D.A. Kleinman, W.T. Tsang, Observation of the excited level of excitons in GaAs quantum wells. Phys. Rev. **B24**, 1134–1136 (1981)
109. R.C. Miller, D.A. Kleinman, W.T. Tsang, Observation of the excited level of excitons in GaAs quantum wells, ibid **B25**, 6545–6549, (1982)
110. D. Birkedal, J. Singh, V.G. Lyssenko et al., Binding of quasi two-dimensional biexcitons. Phys. Rev. Lett. **76**, 672–675 (1996)
111. G. Bacher, T. Kmmel, Optical properties of epitaxially grown wide bandgap single quantum dots, in [101] pp. 71–121
112. V.G. Plekhanov, Isotope—based quantum information, ArXiv:quant-ph/0909.0820 (2009)
113. G. Chen, T.H. Stievater, E.T. Batteh et al., Biexciton quantum coherence in a single quantum dot. Phys. Rev. Lett. **88**, 117901–117904 (2002)
114. Special issue on high excitation and short pulse phenomena, J. Luminesc. **30**, N1–4 (1985)
115. K. Herz, T. Kmmel, G. Bacher et al., Biexcitons in low-dimensional CdZnSe/ZnSe structures. Phys. Stat. Solidi (a) **164**, 205–208 (1997)

Chapter 3
Classical and Quantum Information

3.1 General Remarks

Before studying the new aspects that quantum mechanics adds to *information theory*, we will have a brief look at the basics of *classical* information theory in the next section. Information theory is a branch of applied mathematics and electrical engineering [1–3] involving the *quantification of information*. This theory related to the mathematical description and estimation of the quality of the *transmission*, *preservation*, *extraction*, and *classification* of *information*. An important feature unifying various branches of science related to information theory is the extensive use of statistical methods (see, e.g. [4, 5]). This is brought about the fact that the process of extraction of information is connected with reducing the indefiniteness in the knowledge of some object, and the natural numerical measure of indefiniteness of an event is its probability. The most important part of information theory in any treatment is the theory of information transmission [1, 6, 7]. The theory of information transmission is concerned with optimum and near-optimum methods of transmission of information over a communication channel under the assumption that the methods of encoding the message into an input signal and of decoding the output into a message may vary within wide ranges. Problems related to the optimal way of preservation of information do not differ, in principle, from problems of optimal transmission of information, since preservation can be regarded as transmission in time rather than in space.

Information theory was developed by *Shannon* to find fundamental limits on signal processing operations such as compressing data and on reliably storing and communicating data [1]. From the mathematical point of view the output and input channel are just applications of mathematical statistics, principally of statistics of stohastic processes. A key measure of information is known as entropy, which is usually by the average number of bits needed for storage or communication (see, also [8]). As is usual, the information is encoded in a sequence of *bits*, i.e., entities that can be in two distinguishable states, which are conventionally labeled with 0 and 1. A bit is the maximal amount of information we can obtain from a yes/no

V. G. Plekhanov, *Isotope-Based Quantum Information*, SpringerBriefs in Physics,
DOI: 10.1007/978-3-642-28750-3_3, © The Author(s) 2012

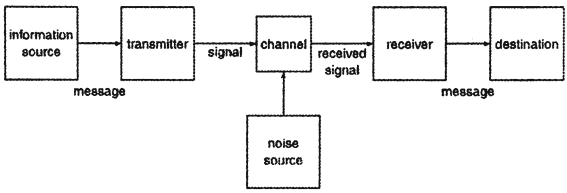

Fig. 3.1 Schematic diagram of a general communication system

question. The definition points to classical logic with reference to "yes/no" (or "1/0" or "true/ false"). *Entropy quantifies* the uncertainty involved in predicting the value of a random variable. The concept of entropy in information theory is closely connected with the concept of entropy in statistical mechanics [3–5].

3.2 Classical Information

The theory of information is based on notions drawn from *probability*. Therefore, some people regard information theory as a branch of applied probability. A simple example on alphabets very bright by characterizes this situation. Possible combinations of the letters a, n, and t are tan, ant, nat. These words may have meaning and significance for different readers but their impact on individuals will vary, depending on the readers' subjective reaction. Subjective information conveyed in this way is impossible to quantify in general. Therefore, the meaning of groups of symbols is excluded from the theory of information; each symbol is treated as an entity in its own right and how any particular grouping is interpreted by an individual is ignored. Information theory is concerned with how *symbols* are affected by various processes but not with information in its most general sense. We should note that information is always information about something. The description of information must be distinguished from this 'something', just as the words used to describe a dog are different from the dog. The description in information theory are called codes.

The fundamental problem of *communication* is that of reproducing at one point either exactly or approximately a message selected at another point. To describe this situation we introduce a *transmitter* and a *receiver* that converts the messages into some physical signal and vice versa. The general layout of such a communication system is illustrated in Fig. 3.1. Given a channel and an information source, the basic problem is to transmit the messages produced by the information source through the channel as efficiently and as reliably as possible. Efficient means that we can send as much information as possible per use of the channel, and reliable means that, despite the disturbance due to the noise added by the channel, the original message is (with high probability) reproduced by the receiver.

An information source is some device or mechanism which generates elements from a certain set. Table 3.1 shows a code book related to a source which generates a vowel of the English alphabet A. The various code words may be taken as a way to

Table 3.1 Code-book for vowels in English language

Vowel	Code-word	Code-word length
a	11	2
e	00	2
i	01	2
o	100	3
u	1010	4
y	1011	4

represent, indeed to code, the vowels. Or we may conceive the *code book* as a strategy for obtaining information about the actual vowel from a knowledgeable 'guru' via series of yes/no questions. In this example, the first question will be 'is the letter one of a, o, u or y?' This corresponds to a '1' as the first binary digit—or bit as we shall say—in the actual code word. Continuing asking questions related to the first bits, we end up knowing the actual vowel. The number of bits required in order to identify a vowel is the code word length, i.e., the number of bits in the corresponding code word. The term 'bit' is used in two ways, as a rather loose reference to 0 or 1 and then, as a more precisely defined unit of information: A *bit* is the maximal amount of information we can obtain from yes/no question.

3.2.1 Shannon Entropy

The concept of information is too broad to be captured completely by a single definition (see, e.g. [3]). But we all know that information may be not only created, elaborated, transmitted through space, and preserved or stored throughout time, but may also be extracted and used for communication. Before introducing some definitions of information theory, it is desirable to remove one possible cause of misapprehension. Possible combinations of the letters a, n, and t are tan, ant, nat. These words may have meaning and significance for readers but their impact on individuals will vary, depending on the reader's subjective reaction. Subjective information conveyed in this way is impossible to quantify in general. Therefore, the meaning of groups of symbols is excluded from the theory of information; each symbol is treated as an entity in its own right and how any particular grouping is interpreted by an individual is ignored. Information theory is concerned with how symbols are affected by various processes but not with information in its most general sense [2].

According to *Shannon* [1] we call I_0 the information value in bits if state $|\ 0\rangle$ is seen, and I_1 the same for the occurrence of $|\ 1\rangle$. We state that in the case of perfect symmetry (see Fig. 3.1), i.e., for $p_0 = p_1 = 0.5$ we should obtain $I_0 = I_1 = 1$b. And it is reasonable to demand that for $p_i = 1$ (i = 0 or 1) we should get $I_i = 0$, whereas for $p_i \longrightarrow 0$, $I_i \longrightarrow \infty$. What is between these limits? In general, the function we are looking for I(p), should be a continuous function (see Fig. 3.1), monotonically decreasing with p so that $I_k > I_i$ if $p_k < p_i$ (naturally the value of the information

gained should be greater for the less probable state. In the above expressions p is *probability* [10]. This function fulfilling such conditions was chosen by Shannon [1] for what is usually called the information content of an outcome that has the probability p_i to occur (see, also [1, 3, 8, 9]):

$$I_i = -K \ln p_i . \tag{3.1}$$

In order to obtain I = 1b for $p_i = 0.5$ we must set $K = 1/\ln 2$. The negative sign is needed so that $I \geq 0$ (p always ≤ 1). Turning to logarithm of base 2 we can write

$$I_i = -\log_2 p_i . \tag{3.2}$$

The base of 2 is therefore especially apposite for dealing with *binary digits* (*bits*) and can therefore be expected to be important in application to computing and coding. Tables of logarithms to base 2 are available but if they are not, hand calculations can be carried out by observing that

$$\log_2 x = \frac{\log_{10} x}{\log_{10} 2} = \frac{\ln x}{\ln 2} = \ln x \log_2 e. \tag{3.3}$$

In general

$$\log_a x = \ln x / \ln a \tag{3.4}$$

and, since the restriction $a > 1$ has been imposed above, $\ln a > 0$ so that the logarithms which arise be always positive multiplies of the natural logarithm.

The most important and useful quantity introduced by *Shannon* [1] is related to the next question: Given the probability values for each alternative, can we find an expression for the amount of information we expect to gain on the average before we actually determine the outcome? A completely equivalent question is: How much prior uncertainty do we have about outcome? It is reasonable to choose the weighted average of I_0 and I_1 for the mathematical definition of the a priory *average information gain* or *uncertainty measure* H:

$$H = p_0 I_0 + p_1 I_1 = -p_0 \log_2 p_0 - p_1 \log_2 p_1 \tag{3.5}$$

in which as usual $p_0 + p_1 = 1$ (for details see [1]). Since H is a quantitative measure of the uncertainty of the state of a system, Shannon called it the *entropy* of the source of information. Since p_i may be zero, some term in H could be undetermined in this definition so, when $p_i = 0$, the value zero is assigned to the corresponding term in (3.5). Let us set, for our case $p = p_0$; then $p_1 = 1 - p$ and:

$$H = -p \log_2 p - (1 - p) \log_2 (1 - p). \tag{3.5a}$$

Figure 3.2 shows a plot of H as a function of p (solid line). It reaches the maximum value of 1b (maximum average information gain in one operation or in one toss

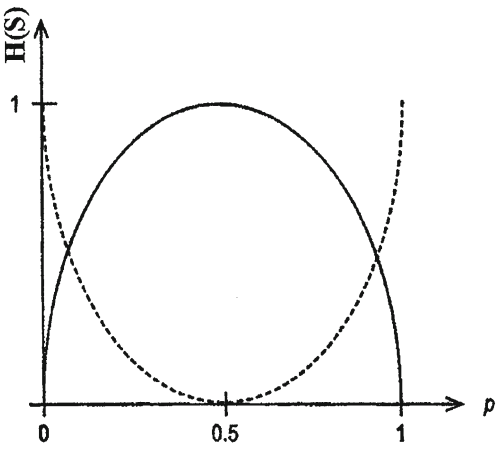

Fig. 3.2 Shannon's average information or entropy H as a function of the probability p of one of the final states of a binary (two state) devices. H is measure of the uncertainty before any final state occurred and expresses the average amount of information to be gained after the determination of the outcome. A maximum uncertainty of one bit (or maximum gain information, once the result is known) exists when the two final states are equiprobable ($p = 0.5$). The dotted curve represents (1-H) (see Eq. (3.8)) an objective measure of the "prior knowledge" before operating the device (after [9])

of a coin) if both *probability* values are the same ($p = 1/2$). If $p = 1$ or 0, we already know the result before we measure, and the expected gain of information will be zero—there is no a priory *uncertainty*. A measure of the average information available before we actually determine the result would be $1 - H$; $p = 1$ or 0 indeed gives 1b of "prior knowledge", and $p = 1/2$ represents zero prior information (broken line in Fig. 3.2), that is, maximum uncertainty.

We can generalize the definition (3.1)–(3.5) for any number N of possible final states, which will then read as:

$$H = -\sum_{i=0}^{N-1} p_i \log_2 p_i \quad \text{with} \sum_i p_i = 1 \tag{3.6}$$

The function H has an absolute maximum when all p_i are equal, i.e., when there is no a priory bias about the possible *outcome*. In that case, by definition of the probability p_i, it is easy to verify that ($p_1 = p_2 = \cdots = p_N = 1/N$)

$$H = \log_2 N. \tag{3.7}$$

When all the events are equally probabe, the most uncertainty prevails as to which event will occur. It is therefore satisfactory that the entropy should be a maximum in such a situation. The fact that H(S) is a maximum when the events are equally uncertain but zero when there is certainty provides some justification for considering

entropy as a measure of uncertainty. To finalize this part we should indicate, as seen from Fig. 3.2, to always fulfill the relation between *information* and *entropy*:

$$\mathrm{I} + \mathrm{H(S)} = 1. \tag{3.8}$$

Below, we briefly show the example of the optimum method of coding (see, also [1, 3, 6, 7]). It can easily be seen from the following example that a message can be compressed when compared to its naive encoding. Let us suppose that we are using four different letters ($\mathrm{b_0}$, $\mathrm{b_1}$, $\mathrm{b_2}$, $\mathrm{b_3}$), which are encoded in the usual manner using two bits $\mathrm{b_0} = 00$, $\mathrm{b_1} = 01$, $\mathrm{b_2} = 10$, $\mathrm{b_3} = 11$. A message n letters long will then be encoded by 2n bits. However, suppose that the letters occur with different probability $\mathrm{b_0}$ with probability 1/2, $\mathrm{b_1}$ with probability 1/4 and $\mathrm{b_2}$ and $\mathrm{b_3}$ with probability 1/8. We can use the following encoding: $\mathrm{b_0} = 0$, $\mathrm{b_1} = 10$, $\mathrm{b_2} = 110$ and $\mathrm{b_3} = 111$. The average length of a message n letters long will then be

$$\mathrm{n}\left(\frac{1}{2}\cdot 1 + \frac{1}{4}\cdot 2 + \frac{1}{4}\cdot 3\right) = \frac{7}{4}\mathrm{n} < 2\mathrm{n}. \tag{3.9}$$

According to *Shannon* [1], this is in fact the best possible compression (see, also [11]). Let us take a set of letters b_x, $0 \leq \mathrm{x} \leq \mathrm{k}$, and a sequence $\{\mathrm{b_1}, \mathrm{b_2}, \ldots, \mathrm{b}_n\}$ of n letters forming a message. Each letter occurs a priory with probability $\mathrm{p}(\mathrm{b}_x)$, $\sum_x \mathrm{p}(\mathrm{b}_x) = 1$. We consider a message n letters long $n \gg 1$. Is it possible to compress the message into a shorter sequence containing essentially the same information? The simplest case is that of two letters, $\mathrm{p(b_0)} = \mathrm{p_1}$, $\mathrm{p(b_1)} = 1 - \mathrm{p}$. The probability of p(q) that an n-letter message contains q letters $\mathrm{b_0}$ is (we neglect the correlation between letters)

$$\mathrm{p(q)} = \mathrm{C}_n^q \mathrm{p}^q (1-\mathrm{p})^{n-\mathrm{q}}. \tag{3.10}$$

And returning to formulae of *Shannon entropy* (3.6) we obtain

$$-\left(\frac{1}{2}\log\frac{1}{2} + \frac{1}{4}\log\frac{1}{4} + \frac{1}{4}\log\frac{1}{8}\right) = \frac{7}{4}. \tag{3.11}$$

The last relation indicates that the proposed encoding is optimal [3].

3.2.2 Von Neumann Entropy

The Shannon entropy measures the uncertainty associated with a classical probability distribution. Quantum states are described in a similar fashion (see, e.g. [8, 10]), with density operators replacing probability distribution. *Von Neumann* defined the entropy of a quantum state $\overrightarrow{\rho}$ by the relation:

$$\mathrm{S}(\overrightarrow{\rho}) = -\mathrm{Tr}(\overrightarrow{\rho}\log\overrightarrow{\rho}). \tag{3.12}$$

In this formula log are taken to base two, as usual. If λ_x are the eigenvalues of $\overrightarrow{\rho}$, then von Neumann's definition can be re-expressed as

$$\mathrm{S}(\overrightarrow{\rho}) = -\sum \lambda_x \log \lambda_x, \tag{3.13}$$

where we define $0 \log 0 \equiv 0$, as for the *Shannon entropy*.

It is instructive to consider a simple example involving a 2D *Hilbert space* spanned by the vectors $\mid \alpha\rangle = \begin{pmatrix} 1 \\ 0 \end{pmatrix}$ and $\mid \gamma\rangle = \begin{pmatrix} 0 \\ 1 \end{pmatrix}$ [8]. Let us define a third vector

$$\mid \beta\rangle \cos\Phi \mid \gamma\rangle + \sin\Phi \mid \alpha\rangle \tag{3.14}$$

and the density matrix

$$\begin{aligned} \overrightarrow{\rho} &= \mathrm{p} \mid \alpha\rangle\langle\alpha \mid + (1-p) \mid \beta\rangle\langle\beta \mid \\ &= \begin{pmatrix} \mathrm{p} + (1-\mathrm{p})\sin^2\Phi & (1-\mathrm{p})\cos\Phi \sin\Phi \\ (1-\mathrm{p})\cos\Phi \sin\Phi & (1-\mathrm{p})\cos^2\Phi \end{pmatrix} \end{aligned} \tag{3.15}$$

The easiest way to calculate the *von Neumann entropy* $\mathrm{S}(\overrightarrow{\rho})$ is via the eigenvalues λ_i of $\overrightarrow{\rho}$

$$\mathrm{S}(\overrightarrow{\rho}) = -\sum \lambda_i \log \lambda_i. \tag{3.13a}$$

The eigenvalues of the above density matrix are

$$\lambda = \frac{1}{2} \pm \sqrt{\frac{1}{4} - \mathrm{p}(1-\mathrm{p})\cos^2\Phi}. \tag{3.16}$$

For $\Phi = 0$ the states of $\mid \alpha\rangle$ and $\mid \beta\rangle$ are distinguishable, the eigenvalues of $\overrightarrow{\rho}$ are $\lambda = \mathrm{p}$ and $\lambda = (1-\mathrm{p})$ and thus $S(\overrightarrow{\rho}) = \mathrm{H(p)}$ (here H(p) is the binary entropy—see Fig. 3.2), whereas for $\Phi \neq 0$ $\mid \alpha\rangle$ and $\mid \beta\rangle$ cannot be distinguished with certainty, and $\mathrm{S}(\overrightarrow{\rho})$ is strictly smaller than H(p), as seen in Fig. 3.3 (see, also [14]).

The quantum entropy has some non-classical properties, whereas classical random variables X, Y always fulfill

$$S(X) \leq S(X, Y), \tag{3.17}$$

that is, the entropy of a subsystem is never greater than that of the total system; this is possible for a quantum system (see, also [12, 13]). Consider two qubits A, B in the pure state

$$\mid \Phi\rangle = \frac{1}{\sqrt{2}} \left(\mid 00\rangle + \mid 11\rangle \right); \tag{3.18}$$

$$\overrightarrow{\rho}_{AB} = \mid \Phi\rangle\langle\Phi \mid \Longrightarrow S(\overrightarrow{\rho}_{AB}) = 0. \tag{3.19}$$

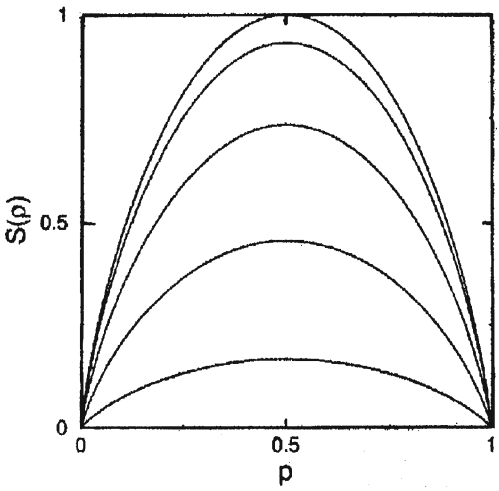

Fig. 3.3 The *von Neumann entropy* for a simple 2D density matrix. Curves are for $\Phi = 0.0; 0.01\pi; 0.2\pi; 0.3\pi$ and 0.4π respectively (top to bottom. For curve $\Phi = 0.0\pi$ the curve is same as in Fig. 3.2

However, the reduced density matrix of subsystem A is $\overrightarrow{\rho}_A = \frac{1}{2}\overrightarrow{1} = S(\overrightarrow{\rho}_A) = 1$. Evidently this is related to the entanglement between A and B [14]. In general, A and B can be considered entangles if and only if

$$S(\overrightarrow{\rho}_{AB}) < S(\overrightarrow{\rho}_A) \quad (\text{or } S(\overrightarrow{\rho}_B), \tag{3.20}$$

where, of course, $\overrightarrow{\rho}_A$ is again the reduced density matrix. The von Neumann entropy can thus be used to define more general measures of entanglement (see, also [15–20]). Most theorems, which are relevant to *quantum information theory*, can be derived from a few fundamental properties which are discussed, proved, and applied in [21, 22].

3.2.3 Introduction in Quantum Information and Quantum Computation

This part is not intended to cover all developments in the quantum information theory and *quantum computation*. Our aim is rather to provide the necessary insights for an understanding of the field so that various non-experts can judge its fundamental and practical importance. *Quantum information theory* and quantum computation are an extremely exciting and rapidly growing field of investigation. Before we discuss some fundamental concepts of quantum information we should remind some of the basic quantum physics for the benefits of readers less familiar with the subject. *Classical information theory* has been around for ever 7 years and there are hundreds of well-tested textbooks not only for physics and mathematics students but also for biologists, engineers, and chemists (see, e.g. [1–3, 10] and references

therein). In contrast, quantum information (QI) theory is in its infancy and involves physics concepts (for more details see below) that are not familiar to everybody. The most fundamental difference between a *classical* and a *quantum system* is that the latter cannot be observed (measured) without being perturbed in a fundamental way [12, 13]. Expressed in more precise terms, there is no process that can reveal any information about the state of a quantum system without disturbing it irrevocably. Thus quantum systems cannot be left undisturbed by measurement, no matter how ideal the instruments are: there are intrinsic limitations to the accuracy with which the values of certain magnitudes or observables [23–25] as they are called in quantum mechanics, can be determined in measurements.

The intrinsic limitation to our potential knowledge of a quantum system is most concisely expressed in the form of the *Heisenberg uncertainty principle*. For a single particle traveling along the x-axis with momentum p_x, this principle states [23–25] that

$$\Delta x \Delta p_x \geq \hbar/2 \tag{3.21}$$

where Δx and Δp_x are the standard deviations of measured values of position and momentum, respectively, obtained for a given type of particle in a series of experiments under strictly identical circumstances of preparation (experimental setup and initial conditions) and measurement (instrumentation and timing). According to the meaning of standard deviation, Δx and Δp_x represent the approximate ranges within which the values of the position and momentum can be expected to be found with reasonable probability (68% for a Gaussian distribution [3]) if measured under the specified conditions.

There are many different kinds of experiments that show a fundamental property of all quantum systems, valid as long as the system is left undisturbed (free from irreversible interactions with the outside *macroscopic world* [8]), namely, the possibility of being in a single state made up of the superposition [26, 27] of two or more basis states. By *superposition* we do not mean that the system is sometimes in one, and sometimes in another state: it is simultaneously in two or more component states. We should underline that there is no classical equivalent to this situation. The principle of superposition tells us that a general state of the photon between vertical and horizontal polarization would be

$$| \Psi \rangle = c_v | \Phi_v \rangle + c_h | \Phi_h \rangle, \tag{3.22}$$

where c_v and c_h are two complex numbers [23–25].

In the *quantum formalism* the values $c_v c_v^* = | c_v |^2$ and $c_h c_h^* = | c_h |^2$ (the star indicating complex conjugate) are the probabilities of finding the system respectively in the state $| \Phi_v \rangle$ or $| \Phi_h \rangle$ after measurement was made to find out which polarization was taken:

$$p_v = | c_v |^2 \quad \text{and} \quad p_h = | c_h |^2 . \tag{3.23}$$

Since their sum must equal one, we require the *normalization condition* [23–25]

$$| c_v |^2 + | c_h |^2 = 1 \tag{3.24}$$

With this normalization, relation (3.24) can also be written in polar form $| \Psi\rangle = cos\alpha \mid \Phi_v\rangle + e^{i\varphi} sin\alpha \mid \Phi_h\rangle$ in which $\cos^2 \alpha = p_v$ and $\sin^2 \alpha = p_h$. The expression brings out explicitly the phase difference φ. We will come back to this form later.

3.2.4 Information is Physical

As is well known, information is not a disembodied abstract entity: it is always tied to physical representation (see, e.g. [28, 29]). It is represented by engraving on a stone tablet, a *spin*, a *charge*, a hole in a punched card, a mark on the sheet of paper, or some other equivalent.[1] This ties the handling of information to all the possibilities and restrictions of our real physical world, its laws of physics and its storehouse of available parts. This view was implicit in *Szilard's discussion* [30, 31] of *Maxwell demon* (see, also [32, 33] and references therein). The laws of physics are essentially algorithms for calculation (see, also [8, 21, 22, 34, 35]).

Thus, information is something that can be encoded in the state of a physical system, and computation (see also below) is a task that can be performed with a physically realizable device. Therefore, since the physical world is fundamentally quantum mechanical, the foundation of information theory and computation science should be sought in quantum physics. In fact, quantum information has weird properties that contrast sharply with the familiar properties of classical information. Be that as it may, information until recently has largely been thought of in classical terms, with quantum mechanics playing a supporting role in the design of the equipment to process it, and setting limits on the rate at which it could be sent through certain channels. Now we know that a fully quantum theory of information and information processing offers (for details see [21, 22]), among other benefits, a brand of cryptography whose security rests on fundamental physics, and a reasonable hope of

[1] As is well known [9], in 1961, Landauer had the important insight that there is a fundamental asymmetry in nature that allows us to process information. Copying classical information can be done reversibly and without wasting any energy, but when information is erased there is always an energy cost of $kT \ln 2$ per classical bit to be paid (for more details see, also [36]). Furthermore, an amount of heat equal to $kT \ln 2$ is damped in the environment at the end of the erasing process. Landauer conjectured that this energy/entropy cost cannot be reduced below this limit irrespective of how the information is encoded and subsequently erased—it is a fundamental limit. Landauer's discovery is important both theoretically and practically, as on the one hand, it relates the concept of information to physical quantities like thermodynamical entropy and free energy, and on the other hand, it may force the future designers of quantum devices to take into account the heat production caused by the erasure of information although this effect is tiny and negligible in today's technology. At the same time, Landauer's profound insight has led to the resolution of the problem of *Maxwell's demon* by Bennett [37, 38]. By the way, for the first time the physical relation between entropy and information was done by Szilard at the investigation of the task of the Maxwell's demon [30, 31]. On the other hand, mathematical definition of the information was introduced by Hartley in 1928 [11] and more elaboration on this definition was done by Shannon [1].

constructing quantum computers (see below) could dramatically speed up the solution of certain mathematical problems (see, e.g. [39, 40]). These benefits depend on distinctively quantum properties such as uncertainty, interference, and entanglement. Thus quantum information theory generalizes the classical notions of source and channel, and the related techniques of source and channel coding, as well as introducing a new resource, entanglement, which interacts with classical and quantum information in a variety of ways that have no classical parallel (for details, see [37, 38, 41] and references therein).

As was shown for the first time by Schrődinger [26, 27] fundamental properties of quantum systems, which might be include to *information processes* are [42–46]:

1. Superposition: a *quantum computer* can exist in an arbitrary complex linear combination of classical Boolean states, which evolve in parallel according to a *unitary transformation*.
2. *Interference*: parallel computation paths in the superposition, like paths of a particle through an interferometer, can reinforce or cancel one another, depending on their relative phase.
3. *Entanglement*: some definite states of complete quantum system do not correspond to definite states of its parts.
4. *Nonlocality* and *uncertainty*: an unknown quantum state cannot be accurately copied (cloned) nor can it be observed without being disturbed (see, also [44, 45].

These four elements are very important in quantum mechanics, and as we will see below in information processing. All (classical) information can be reduced to elementary units, what we call bits. Each bit is a yes or a no, which we may represent as the number 0 or the number 1. Quantum computation and quantum information are built upon an ananalogous concept, the quantum bit [47], or qubit for short. It is a two-dimensional quantum system (for example, a spin 1/2, a photon polarization, an atomic system two relevant states, etc.) with Hilbert space. In mathematical terms, the state of quantum state (which is usually denoted by $\mid \Psi\rangle$ [26, 27]) is a vector in an abstract *Hilbert space* of possible states for the system. The space for a single qubit is spanned by a basis consisting of the two possible classical states, denoted, as above, by $\mid 0\rangle$ and $\mid 1\rangle$. This mean that any state of qubit can be decomposed into the superposition

$$\mid \Psi\rangle = \alpha \mid 0\rangle + \beta \mid 1\rangle \tag{3.25}$$

with suitable choices of the complex coefficients a and b. The value of a *qubit* in state $\mid \Psi\rangle$ is uncertain; if we measure such a qubit, we cannot be sure in advance what result we will get. *Quantum mechanics* just gives the probabilities, from the overlaps between $\mid \Psi\rangle$ and the possible outcomes, rules due originally by Max Born (see, e.g. [8]). Thus the probability of getting 0 is $\mid \langle 0 \mid \Psi\rangle \mid^2 = \mid a \mid^2$ and that for 1 is $\mid \langle 1 \mid \Psi\rangle \mid^2 = \mid b \mid^2$. Quantum states are therefore normalized; $\langle \Psi \mid \Psi\rangle = (b * a*) \cdot \begin{pmatrix} b \\ a \end{pmatrix} = 1$ (where $\mid \Psi\rangle$ is represented by the vector $\begin{pmatrix} b \\ a \end{pmatrix}$) and the probabilities sum to unity (see, also above). Quantum mechanics also tells

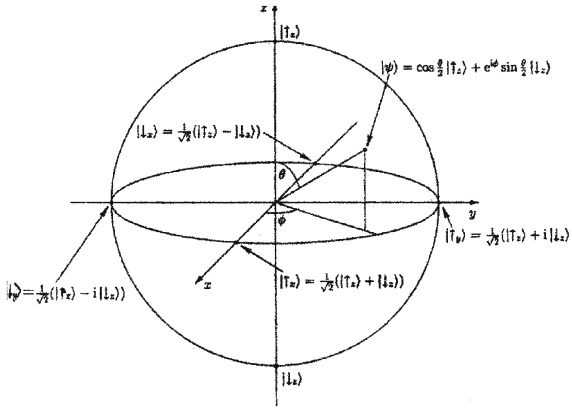

Fig. 3.4 The Bloch sphere of the *Hilbert space* spanned by $|\uparrow_z\rangle$ and $|\downarrow_z\rangle$ (after [9])

us that (assuming the system is not absorbed or totally destroyed by the action of measurement) the qubit state of Eq. (3.25) suffers a projection to $|\,0\rangle$ ($|\,1\rangle$) when we get the result 0(1). Because $|\,\alpha\,|^2 + |\,\beta\,|^2 = 1$ we may rewrite Eq. (3.25) as (see, e.g. [48])

$$|\,\Psi\rangle = \cos\theta\,|\,0\rangle + \mathrm{e}^{i\varphi}\sin\theta\,|\,1\rangle \tag{3.26}$$

where θ, φ are real numbers. Thus we can apparently encode an arbitrarily large amount of classical information into the state of just one qubit (by coding the information into the sequence of digits of θ and φ). However, in contrast to classical physics, *quantum measurement theory* places severe limitations on the amount of information we can obtain about the identity of a given quantum state by performing any conceivable measurement on it. Thus most of the quantum information is "inaccessible" but it is still useful—for example it is necessary in its totality to correctly predict any future evolution of the state and to carry out the process of quantum computation.

The numbers θ and φ define a point on the unit 3D sphere, as shown in Fig. 3.4. This sphere is often called the *Bloch* (*Poinkare*) *sphere* [48–50]; it provides a useful means of visualizing the state of a single qubit. A *classical bit* can only sit at the north or the south pole, whereas a *qubit* is allowed to reside at any point on the surface of the sphere (for details see [34]).

It is easy to represent integers in terms of qubits in the same manner as for ordinary bits. Let us suppose that we wish to write an integer between 0 and 7 in a register of qubits. If this were a classical register, we would need 3 bits (see, also [3, 35]). In a system of base 2, a number between 0 and 7 can be represented in binary notation as a sequence of three digits 0 or 1. A *classical register* will store one of the 8 following configurations:

$$0 = \{000\},\ 1 = \{001\},\ 2 = \{010\},\ 3 = \{011\},\ 4 = \{100\},\ 5 = \{101\},\ 6 = \{110\},$$
$$7 = \{111\}.$$

A system of three qubits will also allow a number from 0 to 7 to be stored, for example, by making these numbers correspond to the following 8 states of three qubits:

$$0 : |\,000\rangle, 1 : |\,001\rangle, 2 : |\,010\rangle, 3 : |\,011\rangle, 4 : |\,100\rangle, 5 : |\,101\rangle, 6 : |\,110\rangle, 7 : |\,111\rangle.$$

Here, we have omitted the tensor product notation; for example, $|\ 101\rangle$ is the abbreviated notation for $|\ \mathrm{I}_A \otimes 0_B \otimes \mathrm{I}_C\rangle$, where the qubits A, B, and C have their state vectors in H_A, H_B, and H_C respectively. Here, we use $|\ \mathrm{x}\rangle, x = 0, \ldots, 7$, to denote one of the eight states above relations, for example, $|\ 5\rangle = |\ 101\rangle$. It is not difficult to generalize to the case of n qubits: representing a number less than $N = 2^n$ requires n qubits, and $|\ \mathrm{x}\rangle$ denotes the state vector with $0 \leq \mathrm{x} \leq 2^n - 1$. The basis of the Hilbert space $\mathrm{H}^{\otimes n}$ formed using orthogonal vectors is called the computational basis. Since we can construct a *linear superposition* of the above eight states, it can be concluded that the state vector of a system of three spin allow to store $2^3 = 8$ numbers at the same time, while if n spins are used we can store 2^n numbers. However, if for example, spins 1/2 are used for the physical support of the *qubits*, a measurement of the three spins along the axis Oz will necessarily give one of the above eight states. We have at our disposal important *virtual information*, but when we try to materialize it in a measurement we can do no better than for a classical system: the measurement gives one of eight numbers, and not all eight at the same time.

3.2.5 Quantum Computation

The theory of *computation* has been long considered a completely theoretical field, detached from physics (see, e.g. [35, 51, 52]). Nevertheless, pioneers such as *Turing*, *Church*, *Post*, *and Gődel* were able [8, 9], by intuition alone, to capture the correct physical picture, but since their work did not refer explicitly to physics, it has been for a long time falsely assumed that the foundations of the theory of classical computation were self-evident and purely abstract. Only in the last three decades were questions about the physics of computation asked and consistently answered [53–57]. Subsequently, in the development of the subject of *quantum computation*—which represents a hybrid of quantum physics and theoretical computer science—it was realized that quantum systems could be harnessed to perform useful computations more efficiently than any classical device.

We should stress that the perspective of *information theory* also provides further new insight into the relationship between entanglement (see above) and non-locality (see, e.g. [58, 59]), beyond the well-studied mediation of non-local correlations between local *measurement outcomes*. The theory of computation and *computational complexity* [10] is normally as an entirely mathematical theory with no references to considerations of physics. However, as we know, any actual computation is a physical process involving the physical evolution of selected properties of a physical system. Consequently, the issues of "what is computable" and "what is the complexity of a

computation" must depend essentially on the laws of physics and cannot be characterized by mathematical alone [28, 29]. This fundamental point was emphasized by Landauer, Deutsch and it is dramatically confirmed by the recent discovers (see, e.g. [21, 22, 34, 35]) that the formalism of quantum physics allows one to transgress some of the boundaries of the classical theory of computational complexity, whose formulation was based on classical intuitions.

As it is well known a fundamental notion of the theory of computational complexity is the distinction between polynomial and exponential use of resources in a computation (see, also [60]). This will provide a quantitative measure of our essential distinction between quantum and classical computation. Consider a computational task as follows: given an integer N, decide whether N is a prime number or not. We wish to assess the resources required for this task as a function of the size of the input which is measured by $n = \log_2 N$, the numbers of bits needed to store N. If T(n) denotes the number of steps (on a standard universal computer) needed to solve the problem, we ask whether T(n) can be bounded by some polynomial function in n or whether T(n) grows faster than any polynomial (e.g. exponential). More generally it may consider any language L—a language being a subset of the set of all finite strings of 0's and 1's—and consider the computational task of recognizing the language, i.e., given a string σ of length n the computations outputs 0 if $\sigma \in$ L and outputs 1 if $\sigma \notin$ L. The language L is said to be in complexity class P (it is mean "*polynomial time*") if there exists an algorithm which recognizes L and runs in time T(n) bounded by polynomial function. Otherwise, the recognition of L is said to require *exponential time*.

Thus, the standard mathematical theory of computational complexity assesses the complexity of a computation in terms of the resources of time (number of steps needed) and space (amount of memory required). In the quantum computation we have been led to consider the accounting of other physical resources such as energy and precision (for details see [61, 62]). The algorithm of quantum computation such as Shor's algorithm [61, 62] depends critically for efficiency and validity on effects of increasingly large-scale entanglements with increasing input size (see, also [63]).

Further evidence for the power of *quantum powers* came in 1995 when Grover [64, 65] showed that another important problem—the problem of conducting a search through some unstructured search space—could also be speeded up on a *quantum computer*. While Grover's algorithms did not provide as spectacular a speed up as Shor's algorithms, the widespread applicability of search-based methodologies has excited considerable interest in Grover's algorithm (for details see also [66]).

3.2.6 Quantum Teleportation

The role of entanglement in quantum information processing is fundamental. Motivated by paper [58] Schrődinger in his famous paper [26, 27] wrote "Maximal knowledge of a total system does not necessary include total knowledge of all its parts, not even when these are fully separated from each other and at the momentary not

influencing each other at all" and he coined the term "entanglement of our knowledge" to describe this situation [48].

A composite system is a system which consists of two or more parts and the simplest one is a system consisting of two qubits (carried by two particles of the same kind, or other appropriate *quantum registers* (see [9]). We call the two systems A (Alice) and B (Bob). Any states of each of the systems can be written as

$$| \Psi\rangle_A = \alpha \mid 0\rangle_A + \beta \mid 1\rangle_A \text{ and } | \Phi\rangle_B = \gamma \mid 0\rangle_B + \delta \mid 1\rangle_B \tag{3.27}$$

with $| \alpha |^2 + | \beta |^2 = 1$ and $| \gamma |^2 + | \delta |^2 = 1$. The subindices A and B refer to two physical entities (the qubits) and the vectors $| 0\rangle$ and $| 1\rangle$ refer to their basis states (in the case of a pair particles, to some binary internal variable like spin, polarization, pair of energy levels, etc.). Each pair of coefficients in (3.27) satisfies the normalization condition [23–25]. (The composite state of the two systems is then simply the *tensor product* (or direct product) of the two states.

$$| \Psi_{\text{prod}}\rangle = | \Psi\rangle_A \otimes | \Phi\rangle_B \tag{3.28}$$

Such a state is called a product state, but product states are not only physically realizable states. If we let the two systems interact with each other, any superposition of product states is realizable. Hence a general composite state can be written as

$$| \Psi\rangle = \sum_{i,j} \alpha_{ij} \mid \Psi_i\rangle_A \otimes | \Phi_j\rangle_B \tag{3.29}$$

where $\sum | \alpha_{ij} |^2 = 1$ and the sets $\{| \Psi_i\rangle\}$ and $\{| \Phi_j\rangle\}$ are orthonormal bases for the two subsystems. *Any composite state that is not a product state is called an entangled state*. A composite quantum state consisting of two parts only, is called a bipartite state [77], as opposed to multipartite states which consist of more than two parts. For bipartite qubit states, four entangled states play a major role [59], namely the singlet state

$$| \Psi^-\rangle \equiv \frac{1}{\sqrt{2}}(| 01\rangle - | 10\rangle) \tag{3.30a}$$

and three triplet states

$$| \Psi^+\rangle \equiv \frac{1}{\sqrt{2}}(| 01\rangle + | 10\rangle) \tag{3.30b}$$

$$| \Phi^-\rangle \equiv \frac{1}{\sqrt{2}}(| 00\rangle - | 11\rangle) \tag{3.30c}$$

$$| \Phi^+\rangle \equiv \frac{1}{\sqrt{2}}(| 00\rangle + | 11\rangle) \tag{3.30d}$$

where we have used $|ij\rangle$ as a shorthand notation for $|i\rangle\otimes|j\rangle$. They are called *Bell states* [59] or *EPR* [58] *pairs*. Together, they form an orthogonal basis for the state space of two qubits, called the Bell basis. The Bell states are maximally entangled and one can be converted into another by applying a *unitary transform* locally on any one of the subsystems. Note that if we measure the state of one qubit in a Bell state (that is, measure the Z operator which has eigenvalues ± 1), we immediately know the state of the other particle. In the singlet Bell state, a measurement of qubit A will yield one of the eigenstates $|0\rangle$ and $|1\rangle$, each with probability of 1/2. These results leave *qubit* B in state $|1\rangle$ or $|0\rangle$, respectively. For a single qubit we could always change to another basis where the outcome of a Z measurement would be given. For a spin $-1/2$ particle this means that the spin is always pointing in some direction, even though the state will show up as a superposition in a basis where the state is not one of the basis states. If the particle is entangled with another particle, though, the direction of the spin of that particle alone is not well-defined. Actually, for particles in one of the Bell states, the probability for measuring the spin of the particle to "up" (while ignoring the other particle) is 1/2 for any direction (for details see [66]).

Further, we briefly describe *entangled states* of two polarized exciton states in a single dot created and detected optically. As was noted above *quantum information*, *quantum computation*, *quantum cryptography*, *and quantum teleportation* intrinsic *quantum mechanical correlations* (see [49, 50] and references therein). A fundamental requirement for the experimental realization of such a proposal is the successful generation of highly entangled quantum states. In particular, as will be shown below, coherent evolution of two qubits in an entangled state of the Bell type is fundamental to both quantum cryptography and quantum teleportation. Maximally *entangled states* of three qubits, such as the so-called Greenberger–Horne–Zeilinger (GHZ) states [67, 68], are not only of intrinsic interest but also of great practical importance in such proposals [69]. New systems and methods for the preparation and measurement of such maximally entangled states are therefore being sought intensively (see, e.g. [9, 70–72]). We should add in this connection that recent experimental work of Gammon et al. (see, e.g. reviews [73, 74] and references therein) suggests that optically generated *excitons* in QDs represent ideal candidates for achieving coherent wavefunction control on the *nanometer* and *femtosecond* scales.

When two *quantum dots* are sufficiently close, there is a resonant energy transfer process originating from the Coulomb interaction whereby an exciton can hop between dots [75]. The *Coulomb exchange interaction* in QD molecules give rise to a non radiative resonant energy transfer (i.e., *Főrster process* [76]) which correspond to the exchange of a virtual photon, thereby destroying an exciton in a dot and then recreating it in a close by dot. It is well known that the presence and absence of an exciton in a dot, for example in isotope-mixed crystals serve as a qubit). The basic quantum operations can be performed on a sequence of pairs of physically distinguishable quantum bits and, therefore, can be illustrated by a simple four-level system shown in Fig. 3.5. In an optically driven system where the $|01\rangle$ and $|10\rangle$ states can be directly excited, direct excitation of the upper $|11\rangle$ level from the ground state $|00\rangle$ is usually forbidden (see, e.g. [77] and references therein) and

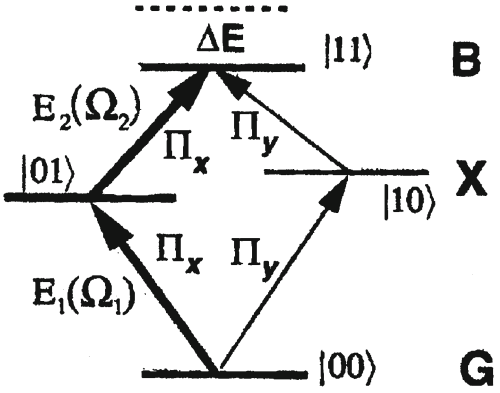

Fig. 3.5 Model for a single QD. | 11⟩, | 01⟩, | 10⟩ and | 00⟩ denote the biexciton, the exciton and the ground states, respectively. ΔE is the biexciton binding energy. The optical rules for various transition are indicated

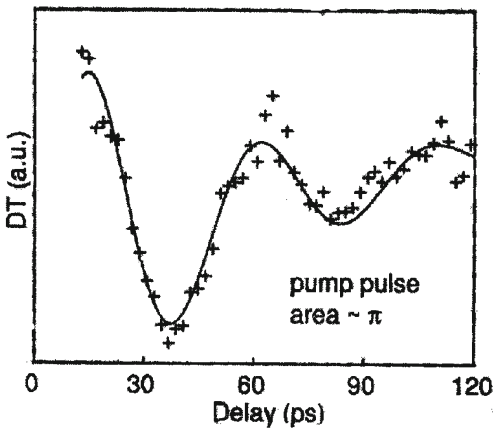

Fig. 3.6 An *entangled state* involving two polarized excitons confined in a single dot was created and detected optically as evidenced by quantum beats between states | 01⟩ and | 10⟩ shown. The quantum coherence time ($\simeq$ 40 psec.) between these two states is directly extracted from the decay of the envelope (after [73])

the most efficient alternative is coherent nondegenerate two-photon excitation, using | 01⟩ and | 10⟩ as an intermediate states. The temporal evolution of the non-radiative Raman coherence between states | 01⟩ and | 10⟩ was directly resolved in quantum beats measured in *differential transmission* (DT) geometry as shown in Fig. 3.6. In order to increase the quantum operations beyond one dot, interdot exciton interaction is required. One proposal is to use an electric field to increase the dipole–dipole interaction between two excitons in separate dots [9, 75]. The procedure we will analyze below is called *quantum teleportation* and can be understood as follows. The naive idea of teleportation involves a protocol [12, 13, 70] whereby an object positioned at a place A and time t first "dematerializes" and then reappears at a distant place B at some later time $t + T$. Quantum teleportation implies that we wish to apply this procedure to a quantum object. However, a genuine quantum teleportation

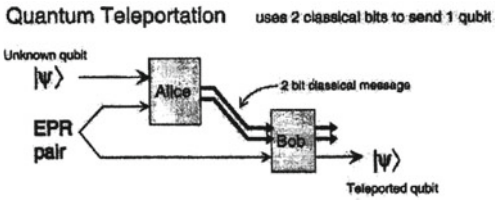

Fig. 3.7 Quantum teleportation requires quantum entanglement as a resource. In this case, Alice receives a qubit in an unknown state, and destroys it by performing a Bell measurement on that qubit and a member of an entangled pair of qubits that she shares with Bob. She sends a two-bit classical message (her measurement outcome) to Bob, who then performs a unitary transformation on his member of the pair to reconstruct a perfect replica of the unknown state. We could see one qubit suffices to carry two classical bits of information

differs from this idea, because we are not teleporting the *whole object* but just its state from particle A to particle B. As quantum particles are indistinguishable anyway, this amounts to 'real' teleportation. One way of performing teleportation is first to learn all the properties of that object (thereby possibly destroying it). We then send this information as a classical string of data to B where another object with the same properties is recreated (see Fig. 3.7). One problem with this picture is that, if we have a single quantum system in an unknown state, we cannot determine its state completely because of the *uncertainty principle* [26, 27, 44]. More precisely, we need an infinite ensemble of identically prepared quantum systems to be able completely to determine its quantum states. So it would seem that the laws of quantum mechanics prohibit teleportation of single quantum systems. However, as we can see above, the very feature of quantum mechanics that leads to the uncertainty principle (the superposition principle [23–25]) also allow the existence of entangled states [26, 27]. These *entangled states* will provide a form of quantum channel to conduct a teleportation protocol. We should remind once more, after the teleportation is completed, the original state of the particle at A is destroyed (although the particle itself remains intact) and it is the entanglement in the quantum channel.

As will be shown below, coherent evolution of two *qubits* in entangled states of the Bell type [59] is fundamental to both *cryptography* and *teleportation*.

Consider a system consisting of two subsystems. Quantum mechanics associates to each subsystem a Hilbert space. Let H_A and H_B denote these two *Hilbert spaces*: let $|\, i\rangle_A$ (where $i = 1, 2, 3, \ldots\ldots$) represent a complete orthogonal basis for H_A, and $|\, j\rangle_B$ (where $j = 1, 2, 3, \ldots\ldots$) a complete orthogonal basis for H_B. Quantum mechanics associates to the system, i.e. the two subsystems taken together, the Hilbert space $H_A \otimes H_B$, namely the Hilbert space spanned by the states $|\, i\rangle_A \otimes |\, j\rangle$. Further, we will drop the tensor product symbol $\otimes$ and write $|\, i\rangle_A \otimes |\, j\rangle$ as $|\, i\rangle_A \,|\, j\rangle_B$ and so on.

Any linear combination of the basis states $|\, i\rangle_A \,|\, j\rangle_B$ is a state of the system, and any state $|\, \Psi\rangle_{AB}$ of the system can be written as

$$| \Psi\rangle_{AB} = \sum_{i,j} \mathrm{C}_{ij} \mid i\rangle_A \mid j\rangle_B, \tag{3.31}$$

where the C_{ij} are complex coefficients; below we take $| \Psi\rangle_{AB}$ to be normalized, hence

$$\sum_{i,j} \mid \mathrm{C}_{ij} \mid^2 = 1. \tag{3.32}$$

1. A special case of Eq. (3.31) is a direct product in which $| \Psi\rangle_{AB}$ factors into (a tensor product of) a normalized $| \Psi^{(A)}\rangle_A = \sum_i C_i^{(A)} \mid i\rangle_A$ in H_A and a *normalized state*

$$| \Psi^{(B)}\rangle_B = \sum_j \mathrm{C}_j^{(B)} \mid j\rangle_B \text{in } \mathrm{H}_B:$$

$$| \Psi\rangle_{AB} = | \Psi^{(A)}\rangle_A \mid \Psi^{(B)}\rangle_B = \left(\sum_i C_i^{(A)} \mid i\rangle_A\right) \times \left(\sum_j C_j^{(B)} \mid j\rangle_B\right). \tag{3.33}$$

   Note every state in $\mathrm{H}_A \otimes \mathrm{H}_B$ is a product state. Take, for example, the state $\frac{(|1\rangle_A|1\rangle_B + |2\rangle_A|2\rangle_B)}{\sqrt{2}}$; if we try to write it as a direct product of states of H_A and H_B, we will find that they cannot.
2. If $| \Psi\rangle_{AB}$ is not a product state, we say that it is entangled (for details see [71, 72]).

Quantum teleportation is a method for moving quantum states from one location to another (Fig. 3.8) which suffers from none of these problems. Suppose Alice and Bob share a pair of qubits which are initially in the entangled state $(| 00\rangle + | 11\rangle)/\sqrt{2}$. In addition, Alice has a system which is in some potentially unknown state $| \Psi\rangle$. The total state of the system is therefore

$$| \Psi\rangle \left(\frac{(| 00\rangle + | 11\rangle)}{\sqrt{2}}\right). \tag{3.34}$$

By writing the state $| \Psi\rangle$ as $\alpha \mid 0\rangle + \beta \mid 1\rangle$ and doing some *simple algebra*, we see that the initial state can be rewritten as

$$\begin{aligned}(| 00\rangle + | 11\rangle) \mid \Psi\rangle + (| 00\rangle - | 11\rangle) Z \mid \Psi\rangle \\ + (| 01\rangle + | 10\rangle) X \mid \Psi\rangle + (| 01\rangle - | 10\rangle) XZ \mid \Psi\rangle.\end{aligned} \tag{3.35}$$

Here, and below we omit normalization factors from the description of quantum states. Suppose Alice performs a measurement on the two qubits in her possession, in

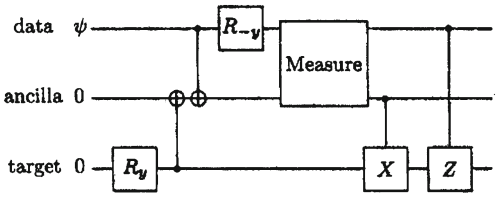

Fig. 3.8 Circuit for quantum teleportation. The measurement is in the computational basis, leaving the measurement result stored in the data and ancila qubits. R_y and R_{-y} denote rotations of 90° about the y and −y axes on the *Bloch sphere* (after [77])

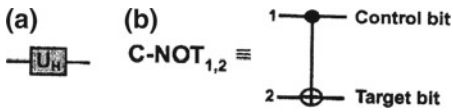

Fig. 3.9 Schematic representation of **a** the Hadamard gate, and **b** the C-NOT gate

the Bell basis consisting of the four *orthogonal vectors*: $|\,00\rangle + |\,11\rangle$; $|\,00\rangle - |\,11\rangle$; $|\,01\rangle + |\,10\rangle$; $|\,01\rangle - |\,10\rangle$, with corresponding measurement outcomes which we label 00, 01, 10 and 11 [187]. From the previous equation, we see that Bob's state, conditioned on the respective *measurement outcomes*, is given by

$$00 :|\,\Psi\rangle; 01 : X\,|\,\Psi\rangle; 10 : Z\,|\,\Psi\rangle; 11 : XZ\,|\,\Psi\rangle. \tag{3.36}$$

Therefore, if Alice transmits the two classical bits of information, she obtains from the measurement to Bob, it is possible for Bob to recover the original state $|\,\Psi\rangle$ by applying unitary operators inverse to the identity X, Z and XZ, respectively. More explicitly, if Bob receives 00, he knows his state is $|\,\Psi\rangle$, if he receives 01 then applying an X gate (see below) will cause him to recover $|\,\Psi\rangle$, if he receives 10 then applying a Z gate causes him to recover $|\,\Psi\rangle$, and if he receives 11 then applying an X gate followed by a Z gate will enable him to recover $|\,\Psi\rangle$ (see Fig. 3.9). This completes the *teleportation process.*

Further, we describe a practical scheme capable of demonstrating quantum teleportation which exploits *entangled states of excitons* in coupled QDs [75]. As we saw above, the general scheme of teleportation [26, 27], which is based on EPR pairs [58] and Bell measurements [59] using classical and purely non-classical correlations, enables the transportation of an arbitrary quantum state from one location to another without knowledge [45] or movement of the state itself through space. In order to implement the quantum operations for the description of the teleportation scheme, we employ two elements: the *Hadamard transformation* and the *quantum controlled NOT gate* (C-NOT gate). In the orthonormal computation basis of single qubits $\{|\,0\rangle, |\,1\rangle\}$, the C-NOT gate acts on two qubits $|\,\varphi_i\rangle$ and $|\,\varphi_j\rangle$ simultaneously as follows $\text{C-NOT}_{ij}(|\,\varphi_i\rangle\,|\,\varphi_j\rangle) \longrightarrow |\,\varphi_i\rangle\,|\,\varphi_i \oplus |\,\varphi_j\rangle\rangle$. Here, $\oplus$ denotes addition modulo 2. The indices i and j refer to the *control bit* and the *target bit* respectively (see Fig. 3.10). The Hadamard gate U_H acts only on single *qubits* by performing

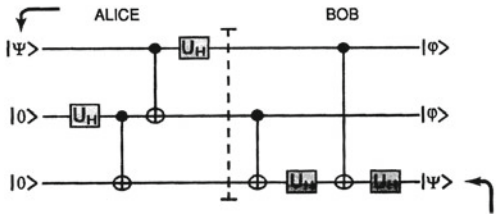

Fig. 3.10 Circuit scheme to teleport unknown quantum state of exciton from Alice to Bob using arrangement of 3 qubits (coupled quantum dots)

the rotations $U_H(|\,0\rangle) \longrightarrow \frac{1}{\sqrt{2}}(|\,0\rangle + |\,1\rangle)$ and $U_H(|\,1\rangle) \longrightarrow \frac{1}{\sqrt{2}}(|\,0\rangle - |\,1\rangle)$. The above transformation can be written as

$$U_H = \begin{pmatrix} 1 & 1 \\ 1 & -1 \end{pmatrix}, \qquad C\text{-}NOT = \begin{pmatrix} 1\,0\,0\,0 \\ 0\,1\,0\,0 \\ 0\,0\,0\,1 \\ 0\,0\,1\,0 \end{pmatrix} \tag{3.37}$$

and represented of quantum circuits as in Fig. 3.10. We also introduce a pure state $|\,\Psi\rangle$ (see Eq. (3.10)).

As discussed above, $|\,0\rangle$ represents the vacuum state for exciton while $|\,1\rangle$ represents a *single exciton*. As usual, we refer to two parties, Alice and Bob. Alice wants to teleport an arbitrary, unknown qubit state $|\,\Psi\rangle$ to Bob. Alice prepares two QDs (b and c) in the state $|\,0\rangle$ and then gives the state $|\,\Psi 00\rangle$ as input to the system. By performing the series of transformation, Bob receives as the output of the circuit the state $\frac{1}{\sqrt{2}}(|\,0\rangle + |\,1\rangle)_a \frac{1}{\sqrt{2}}(|\,0\rangle + |\,1\rangle)_b\,|\,\Psi\rangle_c$. Consider a system of three identical and equispaced QDs containing no net charge, which initially prepared in the state $|\,\Psi\rangle_a\,|\,0\rangle_b\,|\,0\rangle_c$. Following this initialization, we illuminate QDs b and c with the radiation pulse $\xi(t) = A\exp(-i\omega t)$ with defining τ. For a 0 or $2\pi-$ pulse, the density of probability for finding the QDs b and c in the Bell state $\frac{1}{\sqrt{2}}(|\,0\rangle + |\,1\rangle)$ requires indicated τ (see e.g. [73]). Hence, this time τ_{Bell} corresponds to the realization of the first two gates of the circuit in Fig. 3.10, i.e., the Hadamard transformation over QD b followed by the C-NOT gate between QDs b and c. After this, the information in qubit c is sent to Bob and Alice keeps in her memory the state of QS b. Next, we need to perform a C-Not operation between QDs a and b and, following that, a *Hadamard transform* over the QD a: this procedure then leaves the system in the state

$$\frac{1}{\sqrt{2}}\{|\,00\rangle(\alpha\,|\,0\rangle + |\,1\rangle) + |\,01\rangle(\beta\,|\,0\rangle + \alpha\,|\,1\rangle + |\,10\rangle(\alpha\,|\,0\rangle - |\,1\rangle) + |\,11\rangle(-\beta\,|\,0\rangle + |\,1\rangle)\}. \tag{3.38}$$

As we can seen from Eq. (3.40), we are proposing the realization of the *Bell basis* measurement in two steps: first we have rotated the Bell basis into the computational basis $(|\,00\rangle, |\,01\rangle, |\,10\rangle, |\,11\rangle$ by performing the unitary operations shown before the dashed line in Fig. 3.11. Hence, the second step is to perform a measurement in this

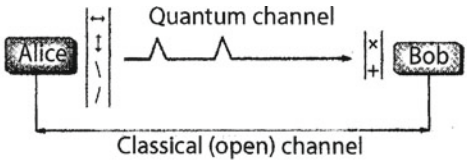

№	Actions								Secrecy
1	A → B	1	0	0	1	0	0	1	1	secret
		↕	/	↔	\	↔	↔	↕	↕	quantum channel
2	B measures	+	+	×	×	+	×	×	+	open channel
		↕	↕	/	\	↔	/	/	↕	secret
3	A → B: meas. type A → B: rightly	√			√	√			√	open channel
4	A and B create the code	↕			\	↔			↕	secret
		1			1	0			1	

Fig. 3.11 One example of the sequence actions for *quantum cryptography* using different polarized states of photons (after [12, 13])

computational basis. The result of this measurement provides us with two classical bits of information, conditional the states measured by nanoprobing on QDs a and b. These classical bits are essential for completing the teleportation process: rewriting Eq. (3.40) as

$$\frac{1}{2}\{|\,00\rangle\,|\,\Psi\rangle+|\,01\rangle\sigma_x\,|\,\Psi\rangle+|\,10\rangle\sigma_z\,|\,\Psi\rangle+|\,11\rangle(-i\sigma_y\,|\,\Psi\rangle \tag{3.39}$$

we see that if, instead of performing the set of operations shown after the dashed line in Fig. 3.10. Bob performs one of the conditional unitary operations I, σ_x, σ_z or $(-i\sigma_y)$ over the QD c, the *teleportation process* is finished since the excitonic state $|\,\Psi\rangle$ has been teleported from dot a to dot c. For this reason only two unitary exclusive-or transformations are needed in order to teleport the state $|\,\Psi\rangle$. This final step can be verified by measuring directly the *excitonic luminescence* from dot c, which must correspond to the initial state of dot a. For instance, if the state to be teleported is $|\,\Psi\rangle \equiv|\,1\rangle$, the final measurement of the near-field luminescence spectrum of dot c must give an *excitonic emission line* of the same wavelength and intensity as the initial one for dot a.

3.2.7 Quantum Cryptography

Cryptology, the mathematical science of *secret communications*, has a long and distinguished history of military and diplomatic uses dating back to the ancient Greeks (see, e.g. [78–82]). It consists of *cryptography*, the art of *codemaking* and *cryptoanalysis*, the art of code-breaking. With the proliferation of the Internet and electronic mail, the importance of achieving secrecy in communication by cryptography [80–83]—the art of using coded messages—is growing each day.

The two main goals of cryptography are for a sender and intended recipient to be able to communicate in a form that is unintelligible to third parties, and—second—

for the *authentication* [79, 84, 85] of messages to prove that they were not altered in transit. Both these goals can be accomplished with provable security if sender and recipient are in possession of shared, secret "key" material. Thus key material, which is trust random number sequence, is a very valuable commodity even though it conveys no useful information itself. One of the principal problems of cryptography is therefore the so-called "*key distribution problem*". How do the sender and intended recipient come into possession of secret key material while being sure that third parties ("*eavesdroppers*") cannot acquire even partial information about it? It is provably impossible to establish a secret key with conventional communications, and so key distribution has relied on the establishment of a physically secure channel or the conditional security of "difficult" mathematical problems (see, e.g. [71, 83]) in public key cryptography. Amazingly, quantum mechanics has now provided the foundation [72, 80–82] stone to a new approach to cryptography—quantum cryptography. Namely, the *quantum cryptography* (QC) can solve many problems that are impossible from the perspective of conventional cryptography (for details see [84]).

QC was born in the late 1960s when Wiesner [198] wrote "*Conjugate Coding*". Unfortunately, this highly innovative paper was unpublished at the time and it went mostly unnoticed. There, Wiesner explained how quantum physics could be used in principle to produce bank notes that would be impossible to counterfeit and how to implement what he called a "multiplexing channel" a notion strikingly similar to what Rabin [87] was to put forward more than 10 years later under the name of "oblivious transfer" [88].

Later, Bennett and Brassard [89, 90] realized that instead of using single quanta for information storage they could be used for *information transmission*. In 1984, they published the first *quantum cryptography protocol* now known as "BB84" [89]. A further advance in theoretical quantum cryptography took place in 1991 when Ekert [91, 92] proposed that EPR [58] entangled two-particle states could be used to implement a quantum cryptography protocol whose security was based on *Bell's inequalities* [59]. Also in 1991, Bennett and coauthors demonstrated the *quantum key distribution* (QKD) was potentially practical by constructing a working prototype system for the BB84 protocol, using *polarized photons* [83, 93–95].

In 1992, Bennett published a "minimal" QKD scheme ("B92") and proposed that it could be implemented using single-photon interference with photons propagating for long distances over *optical fibers* [96]. After that, other QKD protocols have been published [77] and experiments were done in different countries (for details see [195, 204–207]).

QKD is a method in which quantum states are used to establish a random secret key for *cryptography*. The essential ideas are as follows: Alice and Bob are, as usual widely separated and wish to communicate (see also Fig. 3.11). Alice sends to Bob 2n qubits, each prepared in one of the states $|0\rangle, |1\rangle, |+\rangle, |-\rangle$, randomly chosen. As is well known, many other methods are possible (see, e.g. [44, 72, 83]); we consider here this one merely to illustrate the concept of QC. Bob measures his received bits, choosing the measurement basis randomly between $[|0\rangle, |1\rangle]$ and $[|+\rangle, |-\rangle]$. Next, Alice and Bob inform each other publicly (i.e. anyone can listen in) of the base they used to prepare or measure each *qubit*. They find out on which occasions they

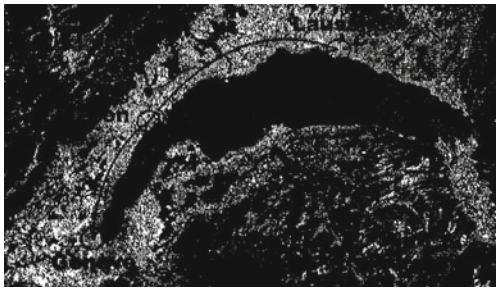

Fig. 3.12 Sattelite view of Lake Geneva with the cities of Geneva and Nyon and Lausanne (after [95])

by chance used the same basis, which happens on average half the time, and retain just those results. In the absence of errors or *interference*, they now share the same random string of n *classical bits* (they agree for example to associate $|\,0\rangle$ and $|\,+\rangle$ with 0; $|\,1\rangle$ and $|\,-\rangle$ with 1. This classical bit string is often called the raw quantum transmission, RQT (for details see [72]).

So far nothing has been gained by using *qubits*. The important feature is, however, that it is impossible for anyone to learn Bob's measurement results by observing the qubits during performance, without leaving evidence of their presence [83]. The crudest way for an *eavesdropper* Eve to attempt to discover the key would be for her to intercept the qubits and measure them, then pass them on to Bob. On average half the time Eve guesses Alice's basis correctly and thus does not disturb the qubit. However, Eve's correct guesses do not coincide with Bob's, so Eve learns the state of half of the n qubits which Alice and Bob are later to trust, and disturb the other half, for example sending to Bob $|\,+\rangle$ for Alice's $|\,0\rangle$. Half of those disturbances will be projected by Bob's measurement back onto the original state sent by Alice, so overall Eve corrupts n/4 bits of the RQT. Alice and Bob can now detect Eve's presence simply by randomly choosing n/2 bits of the RQT and announcing publicly the values they have. If they agree on all these bits, then they can trust no eavesdropper was present, since the probability that Eve was present and they happened to choose n/2 uncorrupted bits is $(3/4)^{n/2} \simeq 10^{-125}$ for $n = 1000$. The n/2 bits form the secret key. From this picture, we see that Alice and Bob do not use the *quantum channel* (Fig. 3.10) to *transmit information*, but only to transmit a random sequence of bits, i.e. key. Now if the key is unperturbed, then quantum physics guarantees that no one has received any information about this key by *eavesdropping*, i.e., measuring, the *quantum communication channel*. In this case, Alice and Bob can safely use this key to encode messages. In conclusion, we note that the authors of paper [95] performed successfully quantum key exchange over different installed cables, the longest connecting the cities of Lausanne and Geneva (see Fig. 3.12).

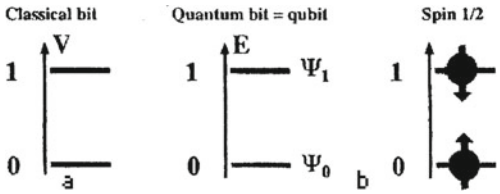

Fig. 3.13 Representation of information in a classical computer (**a**) versus quantum computer (**b**). The spin 1/2 (**b**) is a prototypical example of a qubit

3.3 Quantum Communication

One of the most active areas of *quantum information processing* (QIP) is *quantum communication*, i.e., the transfer of information encoded in quantum mechanical degrees of freedom. This is typically done by encoding the information in photons (*electrons*, *excitons* see this chapter). Semiclassically, a photon can carry a *bit*: it can be transmitted or not, thus corresponding to a logical 0 or 1 (yes or no). Other encoding schemes include the *polarization of the photon*, which may be vertical or horizontal (see, e.g. [83, 84]).

Quantum communication has evolved into a very active field. Besides its fundamental interest, it promises a number of possible applications: taking quantum mechanics into account may improve the information content of *communication channels*. As is known a photon *qubit* can transmit up to two *classical bits of information* [21, 22]. In addition, it has been shown that communication with individual photons may be made secure, i.e., it is impossible to tap into such communication without the users of the communication line noticing it. This is a sequence of no-cloning theorem [45, 46]: while it is conceivable that an *eavesdropper* intercepts a photon, thus detecting that information is being transferred, and that she subsequently reemits a similar photon to the original receiver, she cannot send an exact copy of the original photon. This necessarily allows the two partners who are trying to establish a secure communication to realize that their communication is being monitored—not for individual photons but from a statistical analysis of the successfully transmitted photons (for details see [80–83]).

As we saw above the *classical information* is encoded in a sequence of bits, i.e., entities that can be in two distinguishable states, which are conventionally labeled with 0 and 1. In electronic devices, these states are encoded by voltage (e.g. $0 \sim$ low is represented by voltage < 0.8V and $1 \sim$ high by voltages > 2.4V) (see, e.g. [99]). The main difference between quantum mechanical and classical information is that [100], in the quantum mechanical case, the system is not necessarily in the states 0 and 1. Instead, it can be in arbitrary *superposition* (linear combination) of these states (see [33]). To emphasize this difference between quantum and classical bits, the term "qubit" (short for quantum bit [47]) has been adopted for the quantum mechanical unit of information (see, Fig. 3.13).

Like any change in a quantum mechanical system, logical operations are driven by a suitable *Hamiltonian* acting on the state than represents the quantum register. It is in most cases difficult to find a Hamiltonian [54–57] that directly performs the

Table 3.2 Truth table of CNOT gate

Control-qubit	Target qubit	Result
0	0	00
0	1	01
1	0	11
1	1	10

desired transformation, such as the decomposition of an integer into its prime factors. Instead, the total transformation is usually split into elementary logical operations that transform a single *bit* of information or connect two bits by operating on one bit in a way that depends om the state of the other bit. It turns out that every possible logical operation can be constructed concatenating *elementary gate* operations that belong to one of two groups:

(1) Single qubit operations, corresponding to arbitrary rotations of the spinor representing the qubit, and,
(2) One type of two-qubit operations, e.g. the "controlled NOT" or CNOT [101].

As will be shown below, a *quantum computer* implementation that can perform arbitrary calculations must therefore implement these two types of operations. Particularly critical are the two-qubit operations, since they require interactions between the qubits. A typical operation is CNOT gate, whose truth table is shown in Table 3.2: this particular gate has two *inputs* and two *outputs*. If the control qubit is zero, it simply passes both qubits to the output. If the control qubit is one, it passes the control qubit through unchanged, but inverts the *target qubit*.

Dense coding is the simplest example of the application of *quantum entanglement* [26, 27] to communication. It allows Alice to send two bits of classical information to Bob by sending only a single qubit. The dense coding protocol works as follows (see schematic picture in Fig. 3.14 and the quantum circuit implementing the protocol in Fig. 3.15) (for details see [21, 22]). Consider a source emits an *EPR pair* of particles (Fig. 3.14) shared by Alice and Bob. The source is such that particles are emitted with opposite momenta. The scheme for quantum dense coding utilizes entanglement [26, 27] between two qubits, each of which individually has two orthogonal states, $|0\rangle$ and $|1\rangle$. Classically, there are four possible polarizations for a pair of such particles: 00, 01, 10, and 11 (see, e.g. [52]). Identifying each combination with different information implies that we can encode two bits of information by manipulating both particles. Quantum mechanics also allows one to encode the information in *superpositions* (linear combinations) of the classical combinations. As we already know such superpositions of states of two (or more) particles are called *entangled states* [26, 27] and a convenient basis in which to represent such states for two particles, labeled 1 and 2, is formed by the maximally entangled *Bell states* [3] (see, also [44]):

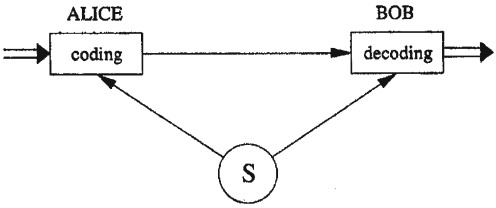

Fig. 3.14 A schematic picture of the *dense coding protocol*. The double lines denote two classical bits and the single lines a quantum bit. S is source which created the *EPR pairs* and then sends on member of the pair to Alice, and the other to Bob

Fig. 3.15 A quantum circuit implementing the dense coding protocol. U = I, σ_x, σ_z or $i\sigma_y$ are the identity and Pauli matrix, H is is Hadamard gate

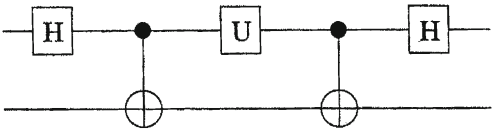

$$|\,\Psi^+\rangle = \frac{1}{\sqrt{2}}\,(|\,0\rangle_1\,|\,1\rangle_2 + |\,1\rangle_1\,|\,0\rangle_2)\,, \tag{3.40}$$

$$|\,\Psi^-\rangle = \frac{1}{\sqrt{2}}\,(|\,0\rangle_1\,|\,1\rangle_2 - |\,1\rangle_1\,|\,0\rangle_2)\,, \tag{3.41}$$

$$|\,\Phi^+\rangle = \frac{1}{\sqrt{2}}\,(|\,0\rangle_1\,|\,0\rangle_2 + |\,1\rangle_1\,|\,1\rangle_2)\,, \tag{3.42}$$

$$|\,\Phi^-\rangle = \frac{1}{\sqrt{2}}\,(|\,0\rangle_1\,|\,0\rangle_2 - |\,1\rangle_1\,|\,1\rangle_2) \tag{3.43}$$

identifying each *Bell state* with different information, yet, now by manipulating only one of the two particles. This is achieved in the following quantum communication scheme (see, also Fig. 3.15). Initially, Alice and Bob each obtain one particle of an entangled pair, say, in the state $|\,\Psi^+\rangle_{12}$ given in Eq. (3.40). Bob then performs one out of possible unitary transformations on his particle (particle 2) alone. The four such transformations are:

1. Identity operation (not changing the original two-particle state $|\,\Psi^+\rangle_{12}$.
2. State exchange ($|\,0\rangle_2 \longrightarrow |\,1\rangle_2$ and $|\,1\rangle_2 \longrightarrow |\,0\rangle_2$, changing the two-particle state to $|\,\Phi^+\rangle_{12}$).
3. State exchange and phase shift (see (3.24)) together (giving the state $|\,\Phi^-\rangle_{12}$).

Since the four manipulations result in the four *orthogonal Bell states* (see, also [44]), four distinguishable messages, i.e., 2 bits of information, can be sent via Bob's two-state particle to Alice, who finally reads the encoded information by determing the Bell state of the two-particle system. This scheme enhances the information capacity of the transmission channel to two bits compared to the classical maximum of one bit (for details see [100]).

References

1. C.E. Shannon, A mathematical theory of communications. Bell Syst. Techn. J. **27**(379–423), 623–656 (1948)
2. L. Brillouin, *Science and Information Theory* (Academic Press, New York, 1962)
3. T.M. Cover, J.A. Thomas, *Elements of Information Theory (Chichester* (J. Wiley & Sons, New York, 1991)
4. E.T. Jaynes, Information Theory and statistical mechanics. Phys. Rev. **106**, 620–630 (1957)
5. E.T. Jaynes, Information Theory and statistical mechanics. II. Phys. Rev. **108**, 171–190 (1957)
6. A.N. Kolomogorov, The theory of information transmission. Izv. Akad. Nauk (Moscow) (1957), pp. 66–99 (in Russian)
7. A.N. Kolomogorov, Three approaches to the quantitative definition of information. Probl. Inform. Transmission **1**, 4–7 (1965)
8. B.B. Kadomtsev, *Dynamics and information* (UFN, Moscow, 1999). (in Russian)
9. V.G. Plekhanov, Isotope-based quantum information, ArXiv: quant-ph/0909.0820 (2009)
10. V.G. Plekhanov, Quantum information and quantum computation. Trans. Computer Sci. College (N 1), Tallinn 2004, pp. 161–284. (in Russian)
11. R.V.L. Hartley, Transmission of Information. Bell Syst. Techn. J. **7**, 535–563 (1928)
12. V.G. Plekhanov, Fundamentals and applications of isotope effect in solids. Prog. Mat. Sci. **51**, 287–426 (2006)
13. V.G. Plekhanov, L.M. Zhuravleva, Isotoptronics in medicine, geology and quantum information. Nanoindustry (Moscow) 1, 52–54 (2010) (in Russian)
14. C.H. Bennett, H.J. Bernstein, S. Popescu et al., Concentrating partial entanglement by local operations. Phys. Rev. **A53**, 2046–2052 (1996)
15. C. Witte, M. Trucks, A new entanglement measure induced by the Hilbert-Schmidt norm, ArXiv: quant-ph/9811027 (1998)
16. J.P. Paz, A.J. Roncaglia, Entanglement dynamics during decoherence, ArXiv:quant-ph/0909.0423 (2009)
17. C. Brukner, M. Zukowski, A. Zeilinger, The essence of entanglement, ArXiv: quant-ph/0106119 (2001)
18. T.E. Tessier, Complementarity and entanglement in quantum information theory. The University of New Mexico, Ph. D.Thesis in Physics, (2004)
19. M. Avellino, Entanglement and quantum information transfer in arrays of interacting systems, Ph. D. Thesis, University of London (2009)
20. K.-A.B. Soderberg, C. Monroe, Phonon-mediated entanglement for trapped ion quantum computing. Rep. Prog. Phys. **73**, 036401–24 (2010)
21. M.A. Nielsen, I.L. Chuang, *Quantum Computation and Quantum Information* (Cambridge University Press, Cambridge, 2000)
22. O. Morsch, *Quantum Bits and Quantum Secrets: How Quantum Physics Revolutionizing Codes and Computers* (Wiley-VCH, Weinham, 2008)
23. P.A.M. Dirac, *The Principles of Quantum Mechanics* (Oxford University Press, Oxford, 1958)
24. R.P. Feynman, R.P. Leighton, M. Sands, *The Feynman Lecture in Physics*, vol. 3 (Addison-Wesley, Reading, MA, 1965)
25. L.D. Landau, E.M. Lifshitz, *Quantum Mechanics (Nonrelativistic Theory)* (Pergamon Press, New York, 1977)
26. E. Schrödinger, Die gegenwartige Situation in der Quanenmechanik. Naturwissenschaften **23**, S. 807–812, 823–843, 844–849 (1935)
27. E. Schrödinger, The present situation in quantum mechanics, in *Quantum Theory and Measurement*, ed. by J.A. Wheeler, W.H. Zurek (Princeton University Press, Princeton, 1983), pp. 152–168
28. R. Landauer, The physical nature of information. Phys. Lett. **A217**, 188–193 (1996)
29. R. Landauer, Minimal energy requirements in communication. Science **272**, 1914–1918 (1996)
30. L. Szilard, Über die Entropieverminderung in einen thermodynamischen System bei Eingriffen intelligenter Wesen. Zs. Phys. **53**, 840 (1929)

31. L. Szilard, On the decrease of entropy in a thermodynamic system by the intervention of intelligent beings, in *Quantum Theory and Measurement*, ed. by J.A. Wheeler, W.H. Zurek (Princeton University Press, Princeton, 1983), pp. 539–549
32. C.M. Caves, W.G. Unruh, W.H. Zurek, Comment on quantitative limits on the ability of a Maxwell demon to extract work from heat. Phys. Rev. Lett. **65**, 1387–1390 (1990)
33. W.H. Zurek, Maxwell's demon. Szillard's engine and quantum measurement, ArXiv: quant-ph/0301076
34. N.D. Mermin, *Quantum Computer Science* (Cambridge University Press, Cambridge, 2007)
35. D. McMahon, *Quantum Computing Explained* (Wiley Interscience, Hoboken, NJ, 2008)
36. R. Landauer, Irreversibility and heat generation in the computation proces. IBM J. Res. Develop. **3**, 183–204 (1961)
37. C. Bennett, The thermodynamics of computation. Int. J. Theor. Phys. **21**, 905–940 (1982)
38. C. Bennett, Quantum information: qubits and quantum error correction. Int. J. Theor. Phys. **42**, 153–176 (2003)
39. A. Barenco, Quantum physics and computers. Contemporary Phys. **37**, 375–389 (1996)
40. A. Barenco, Quantum computation: an introduction, in [173] pp. 143–184
41. C. Bennett, Quantum information and computation. Phys. Today **48**, 24–30 (1995)
42. D. Deutsch, Quantum theory, the Church-Turing principle and the universal quantum computer. Proc. Roy. Soc. (London) **400**, 97–117 (1985)
43. D. Deutsch, *The Fabric of Reality* (Penguin Press, Allen Line, 1998)
44. S. Ya, Kilin. Quantum information. Phys.-Uspekhi **42**, 435–456 (1999)
45. W.K. Wooters, W.H. Zurek, A single quantum state cannot be cloned. Nature **299**, 802–803 (1982)
46. D. Dieks, Communications by EPR-devices. Phys. Lett. **A92**, 271–272 (1982)
47. B. Schumacher, Quantum coding. Phys. Rev. **A51**, 2738–2747 (1995)
48. R. Josza, Quantum information and its properties, in [51], pp. 49–75
49. T. Spiller, Quantum information processing: cryptography, computation, and teleportation. Proc. IEEE **84**, 1719–1746 (1996)
50. T. Spiller, Basic elements of quantum information technology, in [51], pp. 1–28
51. H.-K. Lo, T. Spiller, S. Popescu (eds.), *Introduction to Quantum Computation and Quantum Information* (World Scientific, London, 1998)
52. D. Bouwmesater, A.K. Ekert, A. Zeilinger (eds.), *The Physics of Quantum Information: Quantum Cryptography, Teleportation, Computation* (Springer, New York, 2000)
53. YuI Manin, *Countable and Uncountable* (Soviet Radio, Moscow, 1980). (in Russian)
54. P. Benioff, The computer as a physical system: A microscopic quantum mechanical Hamiltonian model of computers as represented by Turing machine. J. Stat. Phys. **22**, 563–591 (1980)
55. P. Benioff, Quantum mechanical Hamiltonian models of Turing machine. J. Stat. Phys. **29**, 515–546 (1982)
56. P. Benioff, Quantum mechanical models of Turing machines that dissipate no energy. Phys. Rev. Lett. **48**, 1681–1684 (1982)
57. R. Feinman, Quantum computers. Found. Phys. **16**, 507–532 (1986)
58. A. Einstein, B. Podolsky, B.N. Rosen, Can quantum mechanical description of physical reality considered complete? Phys. Rev. **47**, 777–780 (1935)
59. J.S. Bell, *Speakable and Unspeakable in Quantum Mechanics* (Cambridge University Press, Cambridge, 1987)
60. D.P. DiVincenzo, Physical implementation of quantum computation. Fortsch. Physik (Prog. Phys.) **48**, 771–780 (2000); ArXiv: quant-ph/0002077
61. P.W. Shor, Polynomial-time algorithms for prime factorization and discrete logarithms on a quantum computers. SIAM J. Comput. **26**, 1494–1509 (1997); ArXiv: quant-ph/ 9508027
62. P.W. Shor, Introduction to quantum algorithm. AMS PSARM **58**, 143–159 (2002); ArXiv, quant-ph/ 0005003
63. J. Eisert, M.M. Wolf, Quantum computing. in Handbook Innovative Computing (Springer, Berlin, Heidelberg, 2004)

64. L.K. Grover, Quantum mechanics helps in searching for a needle a haytack. Phys. Rev. Lett. **79**, 325–328 (1997)
65. L.K. Grover, Tradeoffs in the quantum search algorithm. ArXiv, quant-ph/ 0201152
66. N. Yanofsky, M. Manucci, *Quantum Computing for Computer Scientists* (Camdridge University Press, Cambridge, 2008)
67. J.F. Clauser, A. Shimony, Bell's theorem: experimental tests and implications. Rep. Prog. Phys. **41**, 1881–1927 (1978)
68. D.M. Greenberger, M.A. Horne, A. Shimony, A. Zeilinger, Am. J. Phys. **58**, 1131–1139 (1990)
69. A. Olaya-Castro, N.F. Johnson, Quantum information processing in nanostructures, ArXiv:quant-ph/0406133
70. C.H. Bennett, G. Brassard, C. Crepeau et al., Teleporting an unknown quantum state. Phys. Rev. Lett. **70**, 1895–1899 (1995)
71. I.V. Bagratin, B.A. Grishanin, N.V. Zadkov, Entanglement quantum states of atomic systems. Phys. Uspekhi (Moscow) **171**, 625–648 (2001). (in Russian)
72. A. Galindo, M.A. Martin-Delgado, Information and computation: classical and quantum aspects. Rev. Mod. Phys. **74**, 347–423 (2002)
73. D. Gammon, D.G. Steel, Optical studies of single quantum dots. Phys. Today (October 2002), pp. 36–41
74. M. Scheiber, A.S. Bracker, D.D. Gammon, Essential concepts in the optical properties of quantum dot molecules. Solid State Commun. **149**, 1427–1435 (2009)
75. S. Kiravittaya, A. Rastelli, O.G. Schmidt, Advanced quantum dot configurations. Rep. Prog. Phys. **72**, 046502–34 (2009)
76. V.M. Agranovich, D.M. Galanin, *Transfer the Energy of the Electronic Excitation in Condensed Matter* (Science, Moscow, 1978). (in Russian)
77. V.G. Plekhanov, Elementary excitations in isotope-mixed crystals. Phys. Rep. **410**, 1–235 (2005)
78. S. Singh, *The Code Book: The Science of Secrecy from Ancient Egypt to Quantum Cryptography* (Fourth Estate, London, 1999)
79. W. Diffie, M.E. Hellman, Privacy and authentication: an introduction to cryptography. IEEE Trans. Inf. Theory **67**, 71–109 (1976)
80. G. Gilbert, M. Hamric, Practical Quantum Cryptography: A Comprehensive Analysis, ArXiv: quant-ph/0009027; 0106043
81. D. Mayers, Unconditional security in quantum cryptography, Arxiv quant-ph/0003004
82. E. Wolf, Quantum cryptography. in Progress in Optics, vol 49 (Elsevier, Amsterdam, 2006)
83. N. Gisin, G. Ribordy, W. Tittel, H. Zbinden, Quantum cryptography. Rev. Mod. Phys. **74**, 145–195 (2002)
84. H.-K. Lo, Quantum cryptology, in [51] pp. 76–119
85. See the articles in the issue IEEE 76 (1988)
86. S. Wiesner, Conjugate coding. SIGAST News **15**, 78–88 (1983)
87. M.O. Rabin, How to exchange secrets by oblivious transfer. Techn. Memo, TR-81 (Aiken Computation Laboratory, Harvard University, 1981)
88. C.H. Bennett, G. Brassard, C. Crepeau, Practical quantum oblivious tranfer. Advances in Cryptology, Crypto'91, Lecture Notes in Computer Science, vol 576, (Springer-Verlag, Berlin, 1992), pp. 351–366
89. C.H. Bennett, G. Brassard, Quantum cryptography. in Proceedings of IEEE International Conference on Computers, Systems, and Signal Processing (Bangalore, India, 1984), pp. 175–179
90. C.H. Bennet, F. Bessette, G. Brassard et al., Experimental quantum cryptography. J. Cryptology **5**, 3–28 (1992)
91. A.K. Ekert, Quantum cryptography based on Bell's theorem. Phys. Rev. Letters **67**, 661–665 (1991)
92. A. Ekert, R. Jozsa, Quantum computation and Shor's factoring algorithm. Rev. Mod. Phys. **68**, 733–753 (1996)
93. H. Zbinden, Experimental quantum cryptography, in [51] pp. 120–143

94. R. Renner, Security quantum key distribution. Ph.D. of Natural Science (Swiss Federal Institute of Technology, Zurich, 2005)
95. D. Stucki, N. Gisin, O. Guinnard, R. Ribordy, H. Zbinden, Quantum key distribution over 67 km a plug&play system. New J. Phys. **4**, 41–8 (2002)
96. C.H. Bennett, Quantum cryptography using any two nonorthogonal states. Phys. Rev. Let. **68**, 3121–3124 (1992)
97. C.H. Bennett, G. Brassard, N.D. Mermin, Quantum cryptography without Bell's theorem. Phys. Rev. Letters **68**, 557–559 (1992)
98. R.J. Hughes, D.M. Adle, P. Duer et al., Quantum cryptography. Contemp. Phys. **36**, 149–163 (1995)
99. K. Goser, P. Glösekötter, J. Dienstuhl, *Nanoelectronics and Nanosystems* (Springer, Berlin, 2004)
100. T.A. Walker, Relationships between Quantum and Classical Information, Ph. D. Thesis (University of York, 2008)
101. S.L. Braunstein, *Quantum Computations* (Encyclopedia of Applied Physics, Wiley-VCH, New York, 1999), pp. 239–256

Chapter 4
Concepts of Quantum Computers

4.1 Introduction

Information is quantized in classical digital information processing as well as in quantum information processing. As is well known [1, 2] in analogy to the *classical bit*, the elementary quantum information processing is called a *qubit* [3]. Any two distinct states of a quantum system can be used as qubit (see Fig. 3.4 in Chap. 3). The two main concepts in *quantum computing* are the qubit and the *unitary logic gate* (see, also [4]). The main insight into quantum computing is to represent numbers in a register consisting of a row of cells where each cell, instead of strong a 0 or 1 as in a classical computer, is represented by a two-level quantum system in a superposition state. We will see how in this way a quantum register can hold a superposition of all numbers from $0...2^n - 1$ where n is the number of cells in the register.

A register consisting of n qubits can store numbers from 0 to $2^n - 1$. To specify this state requires 2^n complex numbers or 2^{n+1} real numbers. To store them with a precision of one byte on a classical computer would require the same number of bytes. So the state of a 50-bit quantum computer would require $2^{51} = 2.25 \times 10^{15}$ bits ($\sim$2 million GB) of memory on a classical computer. Since the evolution of quantum systems is determined by unitary transformation [1, 2] any set of operations carried out on a *quantum computer* will have to be reversible (see, e.g. [5]). That means we will have to redesign many *classical logic gates* to perform the logical operations reversibly. For example a classical AND gate is irreversible (it is in general impossible to reconstruct the input from the output) so one needs to find a reversible system that is logically equivalent. What is called a logic gate in quantum computing is just a series of rotations of the spin 1/2 system representing a qubit [4].

V. G. Plekhanov, *Isotope-Based Quantum Information*, SpringerBriefs in Physics,
DOI: 10.1007/978-3-642-28750-3_4, © The Author(s) 2012

4.2 Current Status: The Di Vincenzo Criteria

In this part we consider the *five criteria of Di Vincenzo* [6] checklist, which must all be satisfied for any physical implementation of a quantum computer:

1. A scalable physical system with well-characterized qubits. That means a well-defined *Hilbert space* [1, 2] within which to represent quantum information.
2. Initialization of the qubits to a known (pure) state.
3. Qubit read out. It means a performing arbitrary unitary transformation on the state of the qubits(typically by implementing arbitrary single-qubit operations and at least one non-trivial two qubit operation).
4. Long coherence time, in another words, avoiding decoherence for long enough to compute.
5. Some means of reading out the state of the qubits at the end of the calculation.

1. To start with, a scalable physical system with well-characterized qubits is needed. In order to build a quantum computer with many qubits, we need some physical system that:
    a. Allows us to implement such qubits, and
    b. Accommodates a sufficiently large number of them.

Actually, point (a) is not quite that obvious. After all, we know that quantum computers rely on quantum effects, and in everyday life such effects are almost always negligible. So we already know that the system we are looking for must allow us to tap into the quantum world, and that means our candidates for qubits presumably have to be very small, possibly on the scale of individual particles that obey the rules of quantum physics, such as photons, electrons, excitons, atoms (ions) and so forth.

As for point (b) we will see that in some cases one can find systems that can very successfully hold a handful of qubits but cannot be extended to accommodate tens or even hundreds of them. *Scalability* is therefore, one of the major obstacles in many realizations of quantum computation.

2. The second of the Di Vincenzo criteria looks even more obvious, but in fact is very subtle. Clearly, in order to perform a calculation, we must first have a "blank state" to write our input on, such as a number we want to factorize. In classical computers, this simply means flushing the memory and writing a "0" in each memory element. In the quantum world, however, things are not quite that simple, and we really have to make sure that each qubit is in the quantum state $|0\rangle$, which can involve rather complicated manipulations [1].
3. One way to classify the range of systems involved is to consider the range of time scales available for manipulation of *quantum computation*, corresponding to the range of excitation energies ΔE and corresponding time-scales $\hbar/\Delta E$. So what exactly is a long decoherence time? Seconds, minutes, or might millisecond already be enough? The answer is it depends. And what it depends on is, not surprisingly, the times it takes to complete a calculation,

or a part of it. Since quantum calculations are made up of lots of quantum logic gates, it all boils down to a simple equation. If we call $t_{\text{decoherence}}$ the time in which a quantum state is destroyed due to decoherence and t_{gate} the time it takes to run the state through a quantum logic gate, then quantum computation is possible if

$$t_{\text{decoherence}} > t_{\text{gate}}. \tag{4.1}$$

It is a bit like in a battle: nobody will ever be strong enough to fight forever-it is enough to last just a little longer than the enemy. As will be shown below the long decoherence time (of the order of a second) of liquid state NMR is one of its biggest advantages. However, typical gate times are at least several milliseconds, so the number of gates that can be applied is limited to approximately 100 (for details see [1, 2] and below).

4 and 5. The fourth and last of Di Vincenzo's criteria states that it is necessary to be able to perform high quantum efficiency, qubit-specific measurements. "High quantum efficiency" means that when one makes a measurement, one is very likely to actually get an answer. Similar requirements apply, for instance, to *quantum cryptography* (see, above). There, it is necessary to have photodetectors that register an arriving photon with a high probability. Likewise, in quantum computing the end result is read out from the qubit by a quantum measurement, and if such a measurement fails to give a result, thats bad news. Finally, qubit-specific means that if one has a quantum computer with, say, ten qubits and one wants to read out the state of qubit number 5 then one should actually read out the state of that specific qubit and not of qubit number 4 or 6. Again, this may sound pretty obvious, but practicing this can be a big obstacle.

According to the modern definition of quantum computer it is a device if it obeys the following criteria: any quantum computer must consist of a quantum memory, with an additional structure that

1. Facilitates a controlled quantum evolution of the *quantum memory*;
2. Includes a method for information theoretic cooling of the memory; and
3. Provides a readout mechanism for subsets of the quantum memory. The criteria are met when the device is scalable and operates fault tolerantly (for details see [7]).

4.3 Elementary Gates for Quantum Computation

The evolution of nano- and *optoelectronic devices* [8] and the associated digitization of information has relied on improvements in the fabrication of materials that have led to ever smaller and faster components. Then in size, in particular, has allowed more components to be packed onto a chip, thus making them more powerful by

integrating more functions. Simultaneously, the decrease in size is a prerequisite for making faster devices, as long as they rely on a fixed, system—wide clock. As early as 1965, Moore [9] noticed that the number of components that could be placed on a chip had grown *exponentially* over many years, while the feature size had shrunk at a similar rate. This trend continued over the next 40 years and is expected to do so for the foreseeable future.

Figure 4.1 shows the current expectation: it represents the projections that the *semiconducting industry* association makes for the coming decade. As shown in Fig. 4.1 the feature size of electronic devices is now less than 100 nm and decreasing at a rate of some 12% per year [8]. This trend could in principle continue for another 40 years before the ultimate limit is reached, which corresponds to the size of the atom. Much before this ultimate limit, however, the feature size will become smaller than some less well-defined limit, where the electrons that do the work in the modern devices, will start to show that their behavior is governed by quantum mechanics, rather than the classical physical laws that are currently to describe their behavior (see, also [10]).

In quantum mechanics there are some basic principles, such as the correspondence principle, *Heisenberg's uncertainty principle*, or *Pauli's principle*, that encode the fundamentals of that theory. The knowledge of those principles provides us with the essential understanding of a quantum mechanics at a glance, without going into the complete formalism of that subject (see, e.g. [11]). A similar thing happens in other areas in physics. In*computer science* there are guiding principles for the architecture of a computer (hardware) and the programs to be run (software) [1, 2]. Likewise, in quantum computing we have seen that there are basic principles associated with the ideas of quantum parallelism (superposition principle) and quantum programming (constructive interference). By principles of quantum computation we mean those rules that are specific to the act of computing according to the laws of quantum mechanics. As mentioned above, the quantum version of parallelism is realized through the superposition principle of *quantum mechanical amplitudes*, likewise the act of programming a quantum computer should be closely related to a *constructive interference* of those amplitudes involved in the superposition of quantum states in the register of the computer (for details see [1, 2]).

A key step towards the realization of the practical quantum computer is to decompose its functioning into the simplest possible *primitive operations* or *gates* (see, also [12, 13]). A universal gate such as NAND (in classical computers) operates locally on a very reduced number of bits (actually two). However, by combining NAND gates in the appropriate number a sequence we can carry out arbitrary computations on arbitrary many bits. This was very useful in practice for it allowed device, leaving the rest to the circuit designer. The same rationale applies to quantum circuits. When a quantum computer is working it is a unitary evolution operator that is effecting a predetermined action on a series of qubits. These qubits form the memory register of the machine, or a quantum register. A quantum register is a string of qubits with a predetermined finite length. The space of all the possible register states makes up the *Hilbert space* of states associates with the quantum computer. A quantum memory register can store multiple sequences of classical bits in *superposition*. This is a

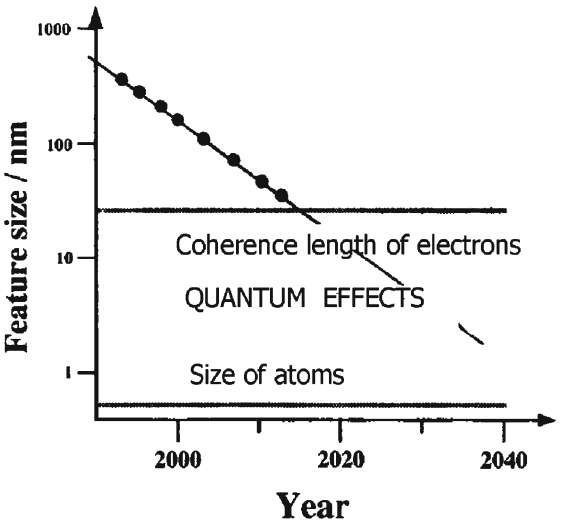

Fig. 4.1 Prospective evolution of feature size in microelectronic (nanoelectronic) circuits (after international semiconductor association roadmap)

manifestation of quantum parallelism. A quantum logic gate is a unitary operator acting on the states of a certain set of qubits (see, also Fig. 4.2a). If the number of such qubits is n, the quantum gate is represented by a $2^n \times 2^n$ matrix in the unitary group $U(2^n)$. It is thus a reversible gate: we can reverse the action, thereby receiving the initial quantum state from final one. One-qubits are the simplest possible gates because they take one input qubit and transform it into one output qubit. The quantum NOT gate is a *one-qubit gate* (Fig. 4.2a). Its unitary evolution operator U_{NOT} is [14]

$$U_{\text{NOT}} = \begin{bmatrix} 0 & 1 \\ 1 & 0 \end{bmatrix}. \tag{4.2}$$

The action of a unitary operator U_{NOT} on a quantum state $|\Psi\rangle = a|0\rangle + b|1\rangle$ or written in matrix notation as $|\Psi\rangle = \begin{bmatrix} a \\ b \end{bmatrix}$ (see, also [15])

$$|\Psi\rangle_{\text{final}} = U|\Psi\rangle_{\text{initial}} \tag{4.3}$$

can be calculated by standard matrix multiplication. For example, the output state obtained after applying U_{NOT} to $|\Psi\rangle = \begin{bmatrix} a \\ b \end{bmatrix}$ is

$$U_{\text{NOT}}|\Psi\rangle = \begin{bmatrix} 0 & 1 \\ 1 & 0 \end{bmatrix} \times \begin{bmatrix} a \\ b \end{bmatrix} = \begin{bmatrix} b \\ a \end{bmatrix}, \tag{4.4}$$

which is state vector corresponding to the state $a|1\rangle + b|0\rangle$ (for details see [15]).

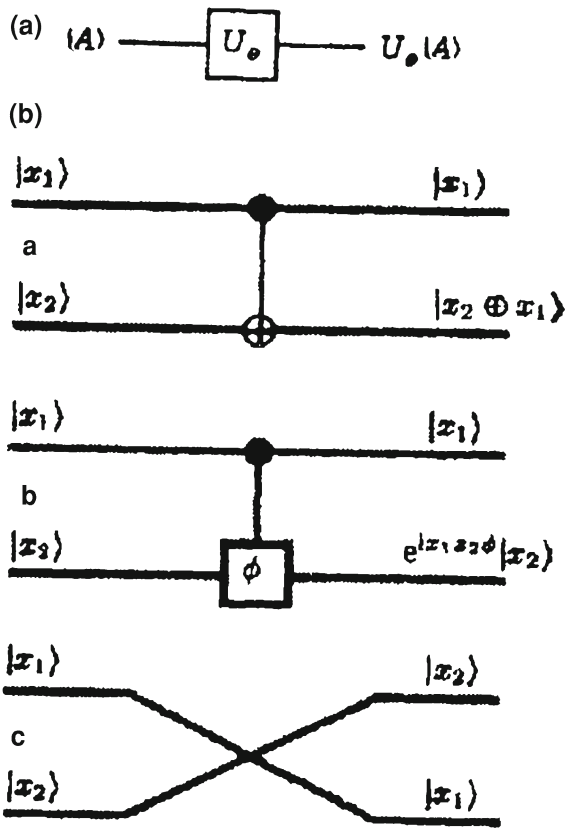

Fig. 4.2 **a** Example of a unitary gate. **b** Quantum binary gates. **a** CNOT gate. **b** CPHASE gate, **c** SWAP gate (after [4])

Another one-qubit gate without analog in classical circuity and heavily used in *quantum computers* is the so-called *Hadamard* (*H*) *gate* [12–14]. This gate is defined as:

$$\mathrm{U}_H = \frac{1}{\sqrt{2}} \begin{bmatrix} 1 & 1 \\ 1 & -1 \end{bmatrix}. \tag{4.5}$$

This gate transforms the computational basis states into the equal superposition states, and back

$$|0\rangle \leftrightarrow^H \leftrightarrow \frac{|0\rangle + |1\rangle}{\sqrt{2}} \text{and} |1\rangle \leftrightarrow^H \leftrightarrow \frac{|0\rangle - |1\rangle}{\sqrt{2}} \tag{4.5a}$$

The Hadamard gate corresponds to a rotation over 180° about an axis halfway between the $\widehat{x}$ and the $\widehat{z}$ axes. The NOT corresponds to a 180° rotation about the $\widehat{x}$ axis, up to an overall phase factor, which is irrelevant (see, also Figs. 4.3, 4.4, 4.5, 4.6, 4.7, 4.8).

Fig. 4.3 The truth table and circuit representation for the identity gate

a	$\overline{a}$
0	1
1	0

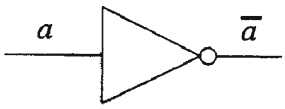

Fig. 4.4 The truth table and circuit representation for the NOT gate

a	b	$a \wedge b$
0	0	0
0	1	0
1	0	0
1	1	1

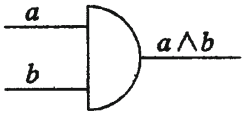

Fig. 4.5 The truth table and circuit representation for the AND gate

a	b	$a \vee b$
0	0	0
0	1	1
1	0	1
1	1	1

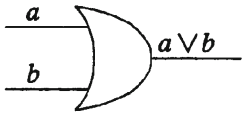

Fig. 4.6 The truth table and circuit representation for the OR gate

a	b	$a \oplus b$
0	0	0
0	1	1
1	0	1
1	1	0

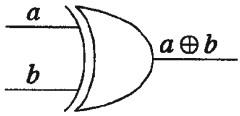

The XOR (exclusive-OR), or CNOT (controlled-NOT) gate is an example of a quantum logic gate on two qubits (see, also [16–21]). It is instructive to give the unitary action $U_{\text{XOR, CNOT}}$ of this gate in several forms [22]. Its action on the two-qubit basis states is

$$\begin{aligned} U_{\text{CNOT}}|00\rangle &= |00\rangle; \quad U_{\text{CNOT}}|10\rangle = |11\rangle \\ U_{\text{CNOT}}|01\rangle &= |01\rangle; \quad U_{\text{CNOT}}|11\rangle = |10\rangle \end{aligned} \tag{4.6}$$

From this definition we can see that the name of this gate is quite apparent, as it means that it executes a NOT operation on the second qubit conditioned to have the first qubit in the state $|1\rangle$. Its matrix representation is

Fig. 4.7 The truth table and circuit representation for the XOR gate

a	b	$a \uparrow b$
0	0	1
0	1	1
1	0	1
1	1	0

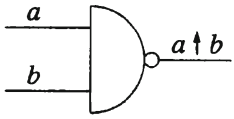

a	b	$a \downarrow b$
0	0	1
0	1	0
1	0	0
1	1	0

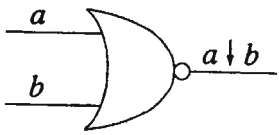

Fig. 4.8 The truth table and circuit representation for the NAND gate

$$U_{\text{CNOT}} = U_{\text{XOR}} = \begin{vmatrix} 1\,0\,0\,0 \\ 0\,1\,0\,0 \\ 0\,0\,0\,1 \\ 0\,0\,1\,0 \end{vmatrix} = \begin{vmatrix} \text{I} & 0 \\ 0 & \sigma_x \end{vmatrix}. \tag{4.7}$$

The action of the CNOT operator (4.6) immediately translates into a corresponding truth table. The diagrammatic representation of the CNOT gate is shown in Fig. 4.2b. We shall see how this quantum CNOT gate plays a paramount role in both the theory and experimental realization of *quantum computers*. It allows the implementation of conditional logic at a quantum level. The generalization of the CNOT gate is the control—U (CU) gate, where the *Pauli matrix* σ_x is replaced by a 2×2 unitary matrix U:

$$\text{CU} = \begin{vmatrix} I & 0 \\ 0 & U \end{vmatrix}. \tag{4.8}$$

The CU gate leaves the target bit unchanged if $x = 0$ and modify it as $|y\rangle \longrightarrow |y\rangle$ if $x = 1$. The CU gate can be constructed starting from the CNOT gate. It is necessary to find three unitary operators A, B, and C such that

$$\text{CBA} = I, \quad C\sigma_x B\sigma_x A = U. \tag{4.9}$$

In quantum physics, the *Toffoli gate* may be constructed from CU gates and CNOT gates (with $U = \sqrt{\sigma_x}$) and the equation

$$\sqrt{\sigma_x} = \frac{1}{1+i}\begin{vmatrix} 1 & i \\ i & 1 \end{vmatrix}, \tag{4.10}$$

which is not possible in classical physics where the operation $\sqrt{\sigma_x}$ does not exist. In contrast to the classical case, it is not necessary to introduce the Toffoli gate explicitly to construct the ensemble of reversible logic circuit (for details see [1, 2, 24, 25]).

Unlike the CNOT gate, their two-qubit gates are with no classical analog (see, also [23]). One example is the controlled-phase gate or CPHASE:

$$U_{\text{CPHASE}} = \begin{bmatrix} 1 & 0 & 0 & 0 \\ 0 & 1 & 0 & 0 \\ 0 & 0 & 1 & 0 \\ 0 & 0 & 0 & e^{i\Phi} \end{bmatrix}. \tag{4.11}$$

It implements a conditional phase shift on the second qubit [14]. Other interesting *two-qubit gates* are the SWAP gate, which interchanges the states of the two-qubits, and the $\sqrt{\text{SWAP}}$ gate, whose matrix representations are

$$U_{\text{SWAP}} = \begin{bmatrix} 1 & 0 & 0 & 0 \\ 0 & 1 & 0 & 0 \\ 0 & 0 & 1 & 0 \\ 0 & 0 & 0 & 1 \end{bmatrix}, \tag{4.12}$$

$$U_{\sqrt{SWAP}} = \begin{bmatrix} 1 & 0 & 0 & 0 \\ 0 & \frac{1+i}{2} & \frac{1-i}{2} & 0 \\ 0 & \frac{1-i}{2} & \frac{1+i}{2} & 0 \\ 0 & 0 & 0 & 0 \end{bmatrix}. \tag{4.13}$$

An immediate extension of the CNOT construction to three qubits yields the CCNOT gate (or C^2 NOT—controlled-controlled-not gate) which is also called Toffoli gate [24, 25] (see, also [26]). The Deutsch gate $D(\theta)$ is also an important three-qubit gate [27]. It is a controlled- -controlled-S or C^2S operation, where

$$U_{D(\theta)} = ie^{-\frac{\theta\sigma_x}{2}} = i\cos\frac{\theta}{2} + \sigma_x \sin\frac{\theta}{2} \tag{4.14}$$

is a unitary operation that rotates a qubit about the X axis by an angle θ and then multiplies it by a factor i and σ_x. Here σ_x is the *Pauli matrix*

$$\sigma_x = \begin{bmatrix} 0 & 1 \\ 1 & 0 \end{bmatrix}. \tag{4.15}$$

and other Pauli matrixes are

$$\sigma_y = \begin{bmatrix} 0 & -i \\ i & 0 \end{bmatrix}, \sigma_z = \begin{bmatrix} 1 & 0 \\ 0 & -1 \end{bmatrix}, \tag{4.16}$$

which obey the relations

$$\sigma_x \sigma_y = i\sigma_z, \sigma_x \sigma_z = -i\sigma_y, \sigma_y \sigma_z = i\sigma_x \tag{4.17}$$

$$\sigma_x^2 = \sigma_y^2 = \sigma_z^2 = \sigma_I, \tag{4.18}$$

where

$$\sigma_I = \begin{bmatrix} 1 & 0 \\ 0 & 1 \end{bmatrix}. \tag{4.19}$$

The rest of the discussion of one-qubit gates expands on the following notion: any one-qubit unitary operation can be written in the form (see, e.g. [1, 2])

$$U = e^{i\alpha} R_{\widehat{n}}(\theta), \tag{4.20}$$

where $R_{\widehat{n}}(\theta)$ corresponds to a rotation in the *Bloch sphere* (see, Chap. 3, Fig. 3.14) about the $\widehat{n} = (n_x, n_y, n_z)$ axis and over an angle θ. With $\overrightarrow{\sigma} = (\sigma_x, \sigma_y, \sigma_z)$ we can construct $\mathrm{R}_{\widehat{n}}(\theta)$ by exponentiating the *Pauli operators* as follows:

$$R_{\widehat{n}}(\theta) \equiv \exp\left(-i\frac{\theta \widehat{n}\,\overrightarrow{\sigma}}{2}\right) = \cos(\theta/2)\,\sigma_I - i\sin(\theta/2)\left[n_x\sigma_x + n_y\sigma_y + n_z\sigma_z\right]. \tag{4.21}$$

Rotations about $\widehat{x}$, $\widehat{y}$ and $\widehat{z}$ axis respectively, are thus given by

$$R_x(\theta) = \exp\left(\frac{-i\theta\sigma_x}{2}\right) = \cos(\theta/2)\,\sigma_I - i\sin(\theta/2)\,\sigma_x = \begin{bmatrix} \cos\frac{\theta}{2} & -i\sin\frac{\theta}{2} \\ -i\sin\frac{\theta}{2} & \cos\frac{\theta}{2} \end{bmatrix}, \tag{4.22}$$

$$R_y(\theta) = \exp\left(\frac{-i\theta\sigma_y}{2}\right) = \cos(\theta/2)\,\sigma_I - i\sin(\theta/2)\,\sigma_y = \begin{bmatrix} \cos\frac{\theta}{2} & -\sin\frac{\theta}{2} \\ -\sin\frac{\theta}{2} & \cos\frac{\theta}{2} \end{bmatrix}, \tag{4.23}$$

$$R_z(\theta) = \exp\left(\frac{-i\theta\sigma_z}{2}\right) = \cos(\theta/2)\,\sigma_I - i\sin(\theta/2)\,\sigma_z = \begin{bmatrix} e^{-i\theta/2} & 0 \\ 0 & -i\theta/2 \end{bmatrix}, \tag{4.24}$$

Examples of multi-qubit gates can be found in the references [22–27].

4.4 Spintronics

Portable communication systems demand the miniaturization and integration of low-power electronic devices. At the same time, faster devices are needed to process information [32–39]. *Moore's Law* [9], the prediction that the number of transistors per square inch on integrated circuits will be double every 18 months, has been held remarkably accurate in the electronics industry since the 1970s (see, also [9–15]). Now the scientific community faces great challenges as the scale of electronic devices has been reduced to the level where quantum effects become significant factors in device operations (see, also above). Electron spin (and more generally nuclear) is one such effect that offers the opportunity to continue the gains predicted by Moore's Law (see Fig. 4.1), by taking advantage of the confluence of magnetics and semiconductor electronics in the newly emerging discipline of *spin electronics (spintronics)*. From a fundamental view point [40, 41] *spin-polarization transport* in a material occurs when there is an imbalance of spin populations at the *Fermi energy* (see Fig. 4.9). In ferromagnetic metals this imbalance results from a shift in the energy states available to spin up and spin down electrons.[1] In practical applications, a ferromagnetic metal may be used as a source of spin-polarized electronics to be injected into semiconductor, a superconductor or a normal metal, or to tunnel through an insulating barrier. Then, depending on the magnetization direction of a material, relative to the spin polarization of the electrons, a material can function either as a conductor or an insulator for electrons of a specific polarization. The use of both charge and spin degrees of freedom in semiconductors is expected to enable a revolutionary class of electronics whose functionality will surpass that of the existing semiconductor technology. Spin electronics combines semiconductor microelectronics with spin-dependent effects that arise from the interaction between electrons and a magnetic field. Since the characteristic length of spin-dependent effects is of the order of 1 nm compared to 10 nm for semiconductor electronics, spin-electronic devices have the potential to achieve much higher integration densities. Conventional electronics are based on the number of charges and their energies, and device performance is limited in speed due to energy dissipation, whereas spintronics is based on the direction of spin and spin coupling, and is capable of much higher speeds at low power consumption. The advantages of *spin-electronic devices* would include

[1] Spin-polarizable transport will occur naturally in any material for which there is an imbalance of the spin populations at the Fermi level. This imbalance commonly occurs in ferromagnetic metals because the density of states available to spin-up and spin-down electrons is often nearly identical, but the states are shifted in energy with respect to each other (see Fig. 4.9). This shift results in an unequal filling of the energy bands, which is the source of the net magnetic moment for the materials, but it can also cause the spin-up and spin-down carriers at the *Fermi level* to be unequal in number, character, and mobility. This inequality can produce a net spin polarization in a transport measurement, but the sign and magnitude of that polarization depends on the specific measurement being made. For example, a ferromagnetic metal may be used as a source of spin-polarized carriers injected into a semiconductor, a superconductor, or a normal metal or can be used to tunnel through an insulating barrier. The nature of the specific spin-polarized carriers and the electronic energy states associated with each material must be identified in each case (for details see [33–35, 38, 39, 41–43]).

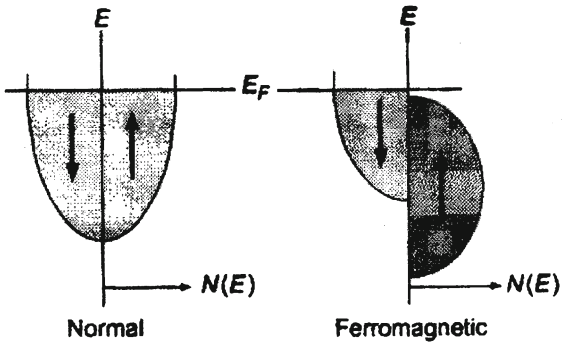

Fig. 4.9 A schematic representation of density of electronic states that are available to electrons in a normal metal and in a ferromagnetic metal whose majority spin states are completely filled. E is the electron energy, E_F is the*Fermi level* and N(E) is a density of states

non-volatility permitting data retention in non-powered conditions, increased integration densities, higher data processing speeds, low electrical energy demands, and fabrication process compatible with those currently used in semiconductor microelectronics. There is strong evidence that the technology shift taking place from *semiconductor electronics* to *spin-dependent devices* will help to meet the sensing and storage demands of *information technology* in the twenty-first century (for details see [33–35, 38, 39, 41].

The next part discusses the basic approach of *spintronics technology*. We begin by describing the operation of an integrated *magnetoelectronic device cell* [33–35, 38–40]. The device cell is composed of a paramagnetic metal film P sandwiched between two ferromagnetic films F1 and F2 (Fig. 4.10a). Each ferromagnetic film is a single domain, and the axis of magnetization of each film, $\widehat{M}_1$ and $\widehat{M}_2$, lies in the plane of film. For simplicity, we consider the case in which $\widehat{M}_1$ points down and $\widehat{M}_2$ points either down or up. A battery is connected with one terminal to F1 and the other to the bottom of P. When the switch is closed, a current flows through F1 into P and is drained from back to the battery. A third wire is attached to F2 and leads to a gedanken voltmeter, which can read the voltage V_{F2} of F2 with a single input and does not aground (Fig. 4.10b). The details of the current transport and of the effect of current transport on V_{F2} can be understood with the use of a microscopic model and density-of-state diagrams (Fig. 4.10c). For the sake of simplicity, this model neglects the resistance of the films and of the interface between the films and assumes there is no spin scattering at the interface itself (see, also [44–46]). The diagrams have been drawn out of proportion to demonstrate the nonequilibrium effects. In reality [33–35], typical *Fermi energies*, E_F, are 5–10 V, the nonequilibrium effects, $E_{F,\mathrm{F2}} - E_{F,0}$, are less than millivolt, and thermal smearing (neglected in Fig. 4.10) is order 10 mV. The ferromagnets are depicted in a band model in which the majority-spin subband (that of downspins and that which determines the direction of $\widehat{M}_1$) lies entirely below the Fermi level. This would be appropriate, though, oversimplified, for the 3d band or a hybridized sd band of transition ferromagnets, like Ni, Fe, Co, or an alloy, such as permalloy $\mathrm{Ni}_x\mathrm{Fe}_{1-x}$. The paramagnet is represented with a free-electron model. With the switch open (Fig. 4.10c, shadow diagrams), the *Fermi levels* of

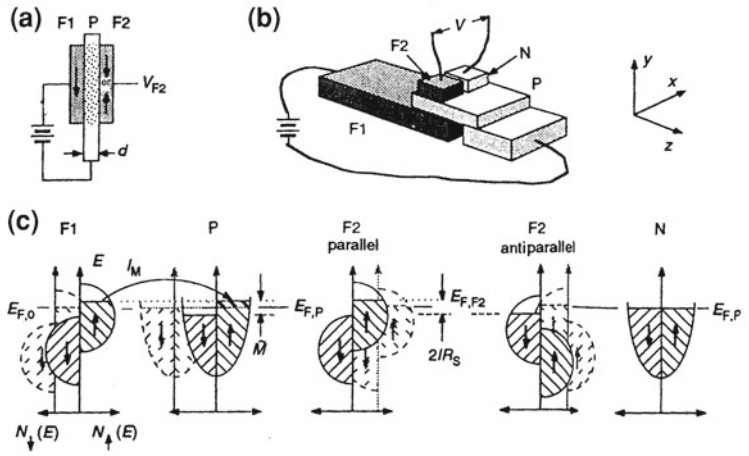

Fig. 4.10 **a** Scheme model of three-terminal device in cross-section. *Arrows* in the ferromagnetic films F1 and F2, which sandwich the paramagnetic film P, refer to magnetization orientation as determined by majority-spin subband. **b** Geometry of s spin switch device. N-nonmagnetic metal counter electrode. **c** Diagrams of the densities of state N(E), as function of energy, of the F1–F2 system depicted in a (after [33–35]

the contiguous metals align with value $E_{F,0}$. When the switch is closed, an electric current, I_e, is driven from F1 to P. However, current transport involves only electrons of energy within a thermal range $E_F \pm k_B T$, where k_B is *Boltzmann's constant* T is temperature. Because the down spin subband is well below E_F, only the up spin subband is available to carry the current. Thus, the electric current is also a current of magnetic dipole; it is a spin-polarized electric current of magnetization [38, 39]

$$I_M = g\beta I_e/e, \tag{4.25}$$

where β, the *Bohr magneton*, is the magnetic moment of each electron and e is the electron charge. Here, g is a phenomenological parameter,

$$g = \frac{J_\uparrow - J_\downarrow}{J_\uparrow + J_\downarrow}, \tag{4.26}$$

where $J_{\uparrow,\downarrow}$ are the current densities of each subband, which describes the efficiency of spin transport. In the simplified model of Fig. 4.10c, $g = 1$, but more generally the magnitude of g is diminished by current contributions from the other spin subband, and $|g| \leq 1$. Conceptually, F1 acts as a spin polarizer in a manner loosely analogous to a polarizing film for light but with the important difference that *conduction electrons* move diffusively, in contrast to photons (for details see [40, 41]).

While there are clear advantages for introducing semiconductors in novel spintronics applications, many basic questions pertaining to combining semiconductors

with other materials to produce a viable spintronics technology remain open [43]. For example, whether placing a semiconductor in contact with another material would impede spin transport across the interface is far from well-understood. In addition to the near-term studies of various spin transistors and spin transport properties of *semiconductors*, a long-term and ambitious subfield of *spintronics* is the application of electron and nuclear spins to quantum information processing and quantum computation (see, e.g. [41, 47, 48] and references therein). Obviously, the spins of electrons and spin-1/2 nuclei provide as was shown above perfect candidates for quantum bits (qubits) as their Hilbert spaces are generally well-defined and their decoherence relatively slow [36, 38, 39, 42].

The first scheme for a spintronics device based on a *field effect transistor* (FET)-like geometry is the Datta and Das [32] high mobility by field effect spin transistor shown in Fig. 4.11a. The *heterostructures* (here InAlAs/InGaAs) provide an inversion layer channel for 2D electron transport between two ferromagnetic electrodes. One acts as an *emitter*, the other is a *collector*. The emitters emit electrons with their spins oriented along the direction of the electrode's magnetization (along the transport direction in Fig. 4.11a), while the collector (with the same electrode magnetization) acts as a spin filter and accepts electrons with the same spin only. In the absence of spin relaxation and spin-dependent processes during transport, every emitted electron enters the collector. Depending on the amount of the electron spin (when entering into the collector) in the direction of the collector magnetization, the electron current is modulated: an electron passes through if its spin is parallel and does not if it is antiparallel to the magnetization [37, 42].

The Johnson *spin transistor* [33] is a trilayer structure consisting of a nonmagnetic metallic layer sandwiched between two ferromagnets (see also [49, 50]). It is an all-metal transistor using the same philosophy as giant-magnetoresistive (GMR) devices [38, 39]: the current flowing through the structure is modified by the relative orientation of the magnetic layers, which, in turn, can be controlled by an applied magnetic field. In this scheme, demonstrated in Fig. 4.11b, the battery is applied in the control circuit (emitter-base), while the direction of the current in the working circuit (base-collector) is effectively switched by changing the magnetization of the collector. The current is drained from the base in order to allow for the working current to flow under the "reverse" base-collector bias (antiparallel magnetization). Neither current nor voltage is amplified, but the device acts as an effective switch or spin valve to sense changes in an external magnetic field (for details see [36, 51, 52]).

One application of Das Sarma et al. proposed that spin-polarized *p–n* junction is the *spin-polarized sole cell* (see [41] and references therein), described in Fig. 4.11c. As in ordinary solar cell batteries, light illuminates the depletion layer of a semiconductor (like GaAs), generating electron-hole pairs. The huge built-in electric field in the layer (typically 10^4 V/cm [41]) swiftly sweeps electrons into the *n* and holes into the *p* regions. If a wire connects the edges of the junction, a current flows. If the light is circularly polarized (filtered solar photons), the generated electrons are spin polarized. As the spin-polarized electrons created in the depletion layer pump the spin into n region, the resulting current is spin polarized.

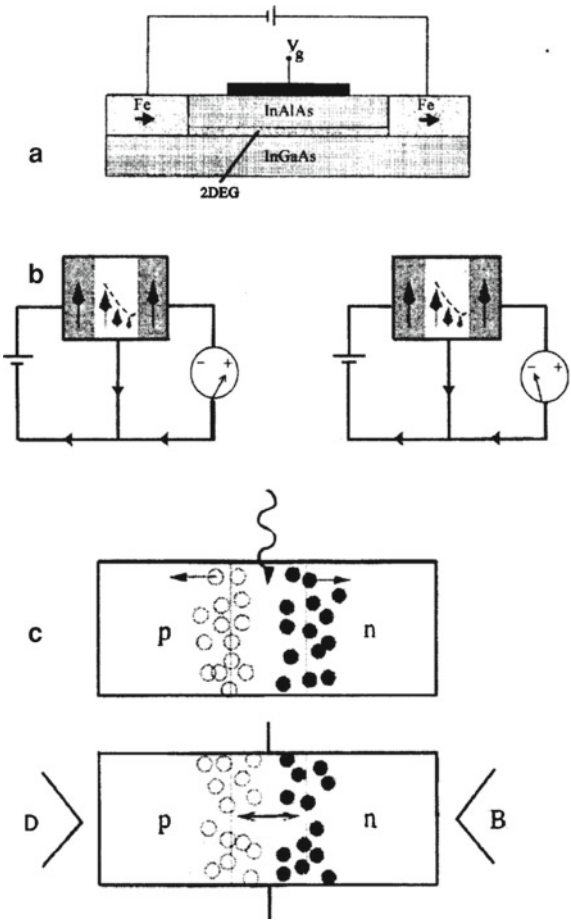

Fig. 4.11 Schemes of selected spintronics devices. **a** The Datta and Das [32] *spin transistor*. Electrons travel in the 2D inverted region channel (filled region) between two ferromagnetic electrodes. Electron spins pieces in the Rashba field which can be controlled by the gate voltage, modulating the current. **b** The Johnson spin transistor [33–35]. Depending on the orientation of the magnetizations in the two ferromagnetic layers, the current in the collector circuit flows either from the base into the emitter (*left*) or from the emitter into the base (*right*). **c** *Spin-polarized solar battery*. Filtered solar light (circularly polarized) generates electron-hole pairs in the depletion region. The polarization is carried only by electrons if the semiconductor is IIIi-V, like GaAs. The resulting current flowing in an external circuit that connects the n and p regions is spin-polarized. **d** *Magnetic field effect transistor* (MFET). Magnetic field B is applied along the *p–n* junction. The current in the circuit connecting the junction in the transverse direction depends critically on the size of the depletion layer (it is small for a larger layer and large for a smaller layer). If the g-factors of the electrons or holes are large, a change in B can lead to a large change in the width of the depletion layer and in the magnitude of the transverse current (after [37])

Finally, Fig. 4.11d shows recent proposal by Das Sarma and coauthors [37] of a *magnetic field effect transistor* (MFET). Electrodes of an external circuit are placed perpendicular to the *p–n* junction. The current is determined by the amount of available electrons in the region of the junction around the electrodes. If the depletion layer is wider than the electrodes, no (or very small) current flows. As the width decreases, more and more electrons come into contact with the electrodes and the current rapidly increases. As was shown in [41] such device could find use in magnetic sensor technology like magnetic read heads or magnetic memory cells.

One of the most ambitious *spintronics devices* (see, also above) is the *spin-based quantum computer* in solid-state structures (see, e.g. [15]). Using electron (or nuclear) spin for quantum computer purposes is a manifestly obvious idea since a fermion with spin 1/2 is a natural and intrinsic qubit [36, 51]. *Quantum computation*, as we know, requires both long quantum coherence time and precise external control [4]. Thus, one needs to be able to precisely manipulate the dynamics of spins, in particular, to rotate single spins and entangle two and more spins (for details see below).

4.5 An Introduction to Quantum Algorithms

4.5.1 Background

In the same scientific paper in which Deutsch introduced the notion of the *universal quantum computer,* he also presented the first *quantum algorithm* [53, 54]. We should note, however, that *quantum Turing machines* were first considered by Benioff [55, 56] and developed by Deutsch in [53]. The problem that this algorithm addresses, later referred to as Deutsch's problem, is a very simple one. Yet the *Deutsch algorithm* already exemplifies the advantages of a quantum computer through skillfully exploiting quantum parallelism. Like the Deutsch algorithm, all other elementary quantum algorithms in this part amount to deciding which black box out of finitely many alternatives one has at hand. Such a black box is often also referred to as oracle. An input may be given to the oracle, one may read out or use the outcome in later steps of the quantum algorithm, and the objective is to find out the functioning of the black box. It is assumed that this oracle operation can be implemented with some sequence of quantum logic gates. The complexity of the quantum algorithm is then quantified in terms of the number of queries to the oracle.

4.5.2 The Deutsch–Jozsa Algorithm

In 1992, Deutsch and Jozsa [57] invented the first ever quantum algorithm. The *Deutsch–Jozsa algorithm* achieves an exponential advantage over classical

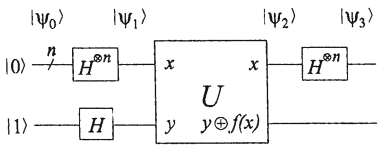

Fig. 4.12 Quantum circuit for the *Deutsch–Jozsa algorithm*

algorithms in solving Deutsch's problem [53, 54] with certainty. Deutsch's problem may be solved as follows: you are given a black box or *oracle* f which takes n input bits and returns one output bit. Furthermore, you are told that the black box either outputs the same value (0 or 1) for all possible input strings x, or outputs 0 for exactly half the possible input values and 1 for the other input values. Deutsch's problem is a thus a promise problem, and the promise is that f is either constant or balanced.

How many oracle queries do you need classically to solve Deutsch's problem with certainty? As soon as you find the oracle returns 0 for some inputs and 1 for other inputs, you know for certain that f is balanced. However, if the output is still the same after trying $2^n/2$ different input values, the function f might still be balanced, even though most likely it is constant. Only when $2^n/2+1$ input values produce the same output, you can be sure the function is really constant. Thus, in the worst case, you need $2^n/2+1$ queries.

Using a *quantum computer*, the input of the oracle can be put in a superposition of all possible input values, and a single oracle query suffices to determine with certainty whether f is constant or balanced. We note that rather to compute individual $f(x)$, which we know a quantum computer cannot do in fewer steps than a classical computer, the task is to determine a global property of the function, namely whether f constant or balanced. This is a type of problem for which quantum computers may offer an advantage.

The procedure of the *Deutsch–Jozsa algorithm*, as improved by Cleve et al. [58] are outlined in Fig. 4.12. The initial state is

$$|\Psi_0\rangle = |0\rangle^{\otimes n}|1\rangle \tag{4.27}$$

where $^{\otimes n}$ indicates that the first register, the input register, is of size n (below we will often leave this implicit). The second register, the output register, contains only one*qubit*. First we apply a *Hadamard gate* on each of the n + 1 qubits, resulting in the state

$$|\Psi_1\rangle = \sum_{x=0}^{2^n-1} \frac{|x\rangle}{\sqrt{2^n}} \left[\frac{|0\rangle - |1\rangle}{\sqrt{2}}\right]. \tag{4.28}$$

The input register is now in an equal superposition of all possible x. The reason why the *output register* is placed in $\frac{|0\rangle-|1\rangle}{\sqrt{2}}$ will become clear below. Next, we query the oracle f which effects the unitary transformation

$$U_f = |x\rangle|y\rangle \longrightarrow^{f} \longrightarrow |x\rangle|y \oplus f(x)\rangle, \tag{4.29}$$

where $\oplus$ stands for addition modulo 2. The oracle thus transforms $|\Psi_1\rangle$ into

$$|\Psi_2\rangle = \sum_x \frac{|x\rangle}{\sqrt{2^n}} \left[\frac{|0 \oplus f(x)\rangle - |1 \oplus f(x)\rangle}{\sqrt{2}} \right]. \tag{4.30}$$

This is an instance of quantum parallelism. Now, we see that whenever f(x) = 0, the output register does not change, and whenever f(x) = 1, the output register is changed to $\frac{|1\rangle - |0\rangle}{\sqrt{2}} = -\frac{|0\rangle - |1\rangle}{\sqrt{2}}$. Thus the oracle query has no net effect other than a sign flip whenever $f(x) = 1$ and we can rewrite $|\Psi_2\rangle$ as

$$|\Psi_2\rangle = \sum_x \frac{(-1)^{f(x)}\,|x\rangle}{\sqrt{2^n}} \left[\frac{|0\rangle - |1\rangle}{\sqrt{2}} \right]. \tag{4.31}$$

The value of $f(x)$ is thus encoded in the coefficient of $|x\rangle$, by virtue of initializing the output qubit to $\frac{|0\rangle - |1\rangle}{\sqrt{2}}$. Since the state of the output qubit never changes, we could in fact leave this qubit out altogether and implement f via the unitary transformation $|\Psi\rangle \longrightarrow^{f} \longrightarrow (-1)^{f(x)}\,|x\rangle$ [58].

We already see that if f is constant, the phase factor $(-1)^{f(x)}$ is constant as well, so it becomes a physically irrelevant overall phase (see, also [4]). In this case, the subsequent $H^{\otimes n}$ operation restores the first register to the state $|0\rangle$. For the case of balanced f, let us first calculate $H|x_i\rangle$ and then $H^{\otimes n}|x\rangle$. From (4.5a), we see that

$$H|x_i\rangle = \frac{|0\rangle + (-1)^{x_i}\,|1\rangle}{\sqrt{2}} \sum_{z=0,1} \frac{(-1)^{x_i z}\,|z\rangle}{\sqrt{2}} \tag{4.32}$$

Therefore,

$$H^{\otimes n}|x_1, \ldots, x_n\rangle = \frac{\sum\limits_{z_1,\ldots z_n} (-1)^{x_1 z_1 + \cdots + x_n z_n}\,|z_1 \ldots z_n\rangle}{\sqrt{2^n}} = \frac{\sum\limits_z (-1)^{x \cdot z}\,|z\rangle}{\sqrt{2^n}}, \tag{4.33}$$

where $x \times z$ is the bitwise inner product of x and z, modulo 2. Using this result, we find that

$$|\Psi_3\rangle = H^{\otimes n}|\Psi_2\rangle = \sum_z \sum_x \frac{(-1)^{\mathrm{x}\cdot\mathrm{z}+\mathrm{f(x)}}\,|z\rangle}{\sqrt{2^n}} \left[\frac{|0\rangle - |1\rangle}{\sqrt{2}} \right]. \tag{4.34}$$

We now measure the first register. For constant f, the amplitude of the $|0\rangle^{\otimes n}$ term, $\sum\limits_x (-1)^{f(\mathrm{x})}$, is either +1 or −1, depending on the constant value f takes. Given the normalization condition of Eq. (4.34)

$$\sum_k |c_k|^2 = 1 \tag{4.35}$$

the amplitude of the remaining terms must thus be zero, as we anticipated. For balanced f, we always have that $\sum_x (-1)^{f(x)} = 0$ as there are as many positive and negative $f(x)$. The amplitude of the $|0\rangle^{\otimes n}$ term is thus zero in this case. In summary, if the measurement of the first register gives all 0's we know f is constant, and otherwise f is balanced.

Thus, we have shown that the*Deutsch–Jozsa algorithm* solves Deutsch's problem exponentially faster than any classical machine. While this is truly remarkable in itself, the practical importance of this algorithm is limited. First, Deutsch's problem is an artificial mathematical problem which has no known applications. Second, classical computers can solve this problem quickly and with high probability of success by asking the oracle what $f(x)$ is for a few random x: the probability for obtaining k times the same answer (either 0 or 1) is f balanced decreases as $(1/2)^{k-1}$. Only if absolute certainty is required, exponentially many oracle queries may be required classically. The significance of this algorithm therefore lies mostly in that it inspired later, more useful algorithms, is relatively easily understood, and can be used as a simple test for implementations of quantum computer.

4.5.3 Simon's Algorithm

Simon's problem is an instance of an oracle problem which is classically hard, even for probabilistic algorithms, but tractable for *quantum computers* [59, 60]. The task is to find period p of a certain function f : $\{0, 1\}^N \longrightarrow \{0, 1\}^N$, which is promised to be 2-to-1 with $f(x) = f(y)$ if and only if $y = x \oplus$ p. Here, x and y denote binary words of length N, where $\oplus$ now means bitwise addition modulo 2. The problem can be stated as a decision problem as well and the goal would then be to decide whether or not there is a period, i.e. whether f is 2-to-1 or 1-to-1.

Classically, the problem is hard, since the probability of having found two identical elements x and y after $2^{N/4}$ queries is still less than $2^{-N/2}$. *Simon's quantum solution* is now the following: start with a state vector $(\mathrm{H}|0\rangle)^{\otimes N}|0\rangle^{\otimes N}$ and run the oracle once yielding the state vector $2^{-N/2}\sum_x |x\rangle|f(x)\rangle$. Then measure the second register. If the measurement outcome is (f_0), then the state vector of the first register will be

$$\frac{1}{\sqrt{2}}\left(|x_0\rangle + |x_0 \oplus p\rangle\right). \tag{4.36}$$

Applying a *Hadamard gate* to each of the N remaining qubits leads to

$$\frac{1}{2^{(N-1)/2}}\sum_{y}((-1)^{x_0\times y}+(-1)^{(x_0\oplus p)\times y})|y\rangle=\frac{1}{2^{(N-1)/2}}\sum_{p\times y=0}(-1)^{x_0\times y}\,|y\rangle. \tag{4.37}$$

If we finally measure the first register in computational basis, we obtain a value y which is such that $y \times p = 0$ modulo 2. Repeating this procedure in order to get $N - 1$ linearly independent vectors $y_1, \ldots, y_{N-1}$ we can determine p from the set of equations $\left[y_i \times \mathrm{p} = 0\right]$. To this end we have to query the oracle O(N) times. Hence, we get an exponential speed up compared to any classical algorithm. And in contrast to the *Deutsch–Jozsa algorithm* this exponential gap remains if we allow for probabilistic classical algorithms. *Simon's algorithm* has much in common with *Shor's algorithm* [61–64]: they both try to find the period of function, both yield an exponential speed-up, and both make use of classical algorithms in a post processing step (for detail see [1, 2, 65].

4.5.4 Grover's Algorithm

In 1996, Lov Grover invented a quantum algorithm for *unstructured searches* [66–68]. An example of a structured search is finding the phone number matching with a certain name using a phone book with N alphabetically listed names. An example of an unstructured search is to find the name matching with a certain phone number using the same phone book. The time this takes goes up linearly with N: on average you will have to try $[N\,(N+1)\,/2-1]\,N \approx N/2$ different names before you find the one with the desired number. In contrast, using Grover's algorithm, such a search can be accomplished in $\sqrt{\mathrm{N}}$ attempts.

Mathematically, we can describe this as the following promise problem. Given an *oracle* which returns $f(x) = 0$ for all values of x except for a unique entry $x = x_0$ for which $f(x) = 1$ (there is a unique name x_0 in the phone book which has the desired phone number), find the special element x_0 in the least number of oracle queries. As in the Deutsch–Jozsa algorithm, the oracle query takes the form of the transformation (see, also [1, 2])

$$U_f = |x\rangle|y\rangle \longrightarrow^{f} \longrightarrow |x\rangle|y \oplus f(x)\rangle, \tag{4.38}$$

where we will initialize the state of the output qubit $|\mathrm{y}\rangle$ to $\frac{|0\rangle-|1\rangle}{\sqrt{2}}$. As we have seen early, the content of the output register in fact does not change, and $f(x)$ is encoded in the sign of $|\mathrm{x}\rangle$. We will therefore leave out the second register and from now on only consider the effect of the oracle call on $|\mathrm{x}\rangle$.

The steps in *Grover's algorithm* for search space of size $\mathrm{N} = 2^n$ are:

a. Initialize to $|0\rangle^{\otimes n}$.
b. Apply $\mathrm{H}^{\otimes n}$ to obtain $\frac{1}{\sqrt{N}}\sum_{x=0}^{N-1}|\mathrm{x}\rangle$.

c. Repeat the following subroutine, known as the *Grover iteration*, $\left[\pi\sqrt{N}/4\right]$ times:

1. Query the oracle U_f: $|x\rangle \longrightarrow {}^{f} \longrightarrow (-1)^{f(x)}|x\rangle$. This flips the phase of the $|x\rangle$ term.
2. Apply $H^{\otimes n}$.
3. Flip the phase of all terms except the $|0\rangle$ term. Thus: $|x\rangle \longrightarrow -|x\rangle$; $|0\rangle \longrightarrow |0\rangle$.
4. Apply $H^{\otimes n}$.

Steps 2, 3, and 4 together are often referred to as inversion about the average, because their combined effect is to invert the amplitude of each term $|x\rangle$ about the average amplitude of all 2^n terms.

Figure 4.13 graphically illustrates the operation of *Grover's algorithm*. The amplitude of all terms $|x\rangle$ are equal after step b in the algorithm. The amplitude of $|x_0\rangle$ builds up after each Grover iteration, at the expense of the amplitude of the remaining terms, until it reaches a maximum and decreases again. For increasing numbers of Grover iterations, the amplitude of the special element $|x_0\rangle$ oscillates sinusoidally. The first maximum occurs after $[\pi\sqrt{N}/4]$ iterations. If we measure the n qubits at this point, the measurement result will be x_0 with high probability and the search far succeeded. And after that we can ask: How does the number of elementary operations required for a Grover search scale with the size N of the search space? Steps b and d take $n = \log_2 N$ Hadamard gates each. Step c, the conditional phase flip, can be done in $O(n) = O(\log_2 N)$ operations, as noted early (see, also [1, 2]). The cost of the oracle depends on f and we will come back to it shortly, but in any case the oracle is called only once per iteration. The *Grover iteration* must be repeated $(O\sqrt{N})$ times, so the entire algorithm requires $(O\sqrt{N}\log_2 N)$ operations and $O(\sqrt{N})$ oracle calls, as opposed to over classical search algorithms (for details see [1, 2, 66–69]).

4.5.5 Shor's Factorization Algorithm

Shor's algorithm [61–64] is without doubt not only one of the *cornerstones of quantum information theory* but also one of the most surprising advances in the theory of computation itself: a problem, which is widely believed to be hard becomes tractable by referring to (quantum) physics—an approach completely atypical for the theory of computation, which usually abstracts away from any physical realization. The problem of Shor's algorithm deals with factorization, a typical *NP problem* [70–75]. In other words, currently one of the most important quantum algorithm is that of finding the period of function. Below we are following very close to above cited papers.

We suppose a function $f(x)$ is periodic with period r, i.e., $f(x) = f(x + r)$. Further, we suppose that $f(x)$ can be efficient computed from x, and all we know initially is that $N/2 < r < N$ for some N. Assuming there is no analytic technique to

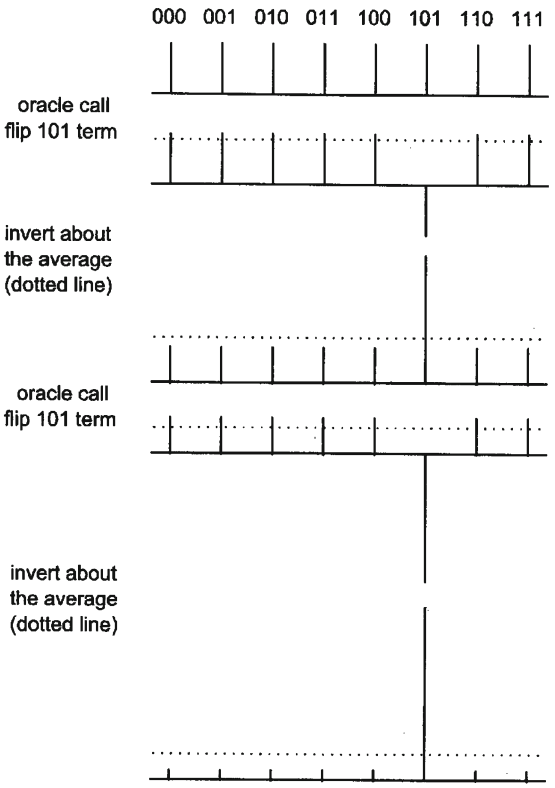

Fig. 4.13 Illustration of amplitude amplification in *Grover's algorithm* for $N = 8(n = 3)$ and $|x_0\rangle = |101\rangle$. The diagram shows the (real) amplitude of the eight terms $|000\rangle$ through $|111\rangle$. The starting point is an equal superposition of all terms. After each *Grover iteration* (an oracle call followed by inversion about the average), the amplitude of the special element is amplified. For the case $N = 8$, the amplitude of the $|x_0\rangle$ reaches almost 1 after two Grover iterations

deduce the period of $f(x)$, the best we can do on a classical computer is to calculate $f(x)$ of order $N/2$ values of x, and find out when the function repeats itself (for well-behaved functions only $O(\sqrt{N})$ values may be needed on average. This is inefficient since the number of operations is exponential in the input size logN (for details see [73, 76, 77]).

The indicated task can be solved efficiently on a quantum computer by the elegant method shown in Fig. 4.14, due to Shor [61–64], building on Simon [59, 60, 75]. The *quantum computer* requires $2n$ qubits, plus a further $0(n)$ for workspace, where $n = \lceil 2\log N \rceil$, where the notation $\lceil x \rceil$ means the nearest integer greater than x. These are divided into two registers, each of n qubits. These registers will be referred to as the x and y registers: both are initially prepared in the state $|\,0\,\rangle$ [1, 2, 75]. Next, the *Hadamard gate* H is applied to each qubit in the x register, making the total state

$$\frac{1}{\sqrt{w}} \sum_{x=0}^{w-1} |x\rangle|0\rangle, \tag{4.39}$$

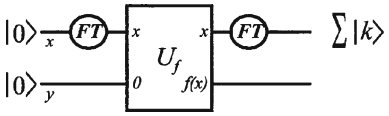

Fig. 4.14 Quantum network for *Shor's period finding algorithm*. Here, each *horizontal line* is a quantum register rather than a single qubit. The circles on the *left* represent the preparation of the input state $|0\rangle$. The encircled FT represents the Fourier transform, and the box connecting the two register represents a network to perform unitary transformation U_f (for details see text)

where $w = 2^n$. This operation is referred to as a *Fourier transform* (see also [1, 2, 76, 77]) in Fig. 4.14. The notation $|\,\mathrm{x}\,\rangle$ means a state as $|0011010\rangle$, where 0011010 is the integer x in binary notation. In this context the basis $\{|0\rangle, |1\rangle\}$ is referred to as the computational basis. It is convenient to use this basis when describing the computer [71, 72].

Next, a network of *logic gates* is applied to both x and y registers, to perform the transformation $U_f|x\rangle|0\rangle = |x\rangle|f(x)\rangle$. Note that this transformation can be unitary because the input state $|\mathrm{x}\rangle|\,0\rangle$ is in one-to-one correspondence with the output state $|\mathrm{x}\rangle|\mathrm{f(x)}\rangle$, so the process is reversible. Further, applying U_f to the state given in Eq. (4.38), we obtain

$$\frac{1}{\sqrt{w}} \sum_{\mathrm{x}=0}^{\mathrm{w}-1} |\mathrm{x}\rangle|\mathrm{f(x)}\rangle. \tag{4.40}$$

This state is presented in Fig. 4.15a. At this point something rather wonderful has taken place: the value of f(x) has been calculated for $w = 2^n$ values of x, all in one go. This feature is referred to as quantum parallelism and represents a huge parallelism because of the exponential dependence on n (imaging having 2^{100}, i.e., a million times *Avogadro's number*, of *classical processors* [74]).

Although the 2^n evaluations of f(x) are in some sense present in the quantum state in Eq. (4.39), unfortunately we cannot gain direct access to them [73, 75]. A measurement of the y register, which is the next step in the algorithm, will only reveal one value of $f(x)$ (see, also [65]). Further, we suppose the value obtained is $f(x) = u$. The y register state collapses [5] onto $|u\rangle$, and the total state becomes

$$\frac{1}{\sqrt{M}} \sum_{j=0}^{M-1} |d_u + jr\rangle|u\rangle, \tag{4.41}$$

where $d_u + \mathrm{jr}$, for $j = 0, 1, 2, \ldots M-1$, are all the values of x for which $f(x) = u$. In other words the periodicity of $f(x)$ means that the x register remains in superposition of $M \simeq w/r$ states, at values of x separated by the period r. Note that the offset d_u of the set of x values depends on the value u obtained in the measurement of the y register.

Now it remains to extract the periodicity of the state in the x register. This is done by applying a Fourier transform (for details see e.g. [73]), and then measuring the

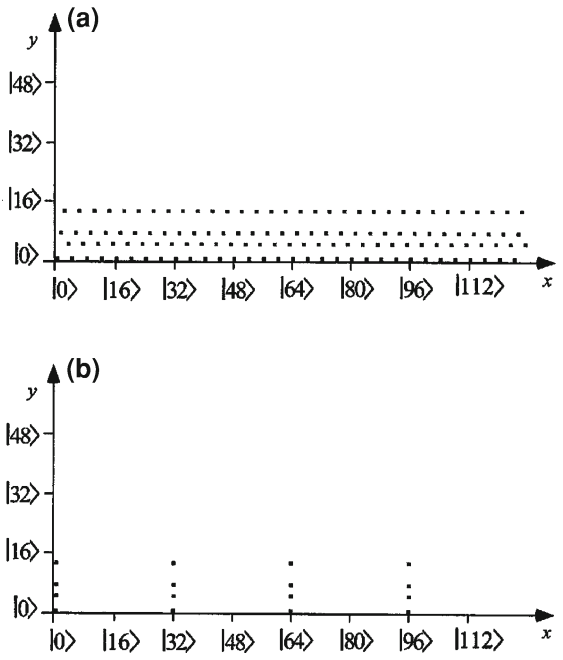

Fig. 4.15 Evolution of the quantum state in Shor's algorithm. The quantum state is indicated schematically by identifying the non-zero contributions to the superposition. Thus a general state $\sum c_{x,y}|x\rangle|y\rangle$ is indicated by placing a filled square at all those coordinates (x, y) on the diagram for which **a** Eq. (4.39), **b** Eq. (4.42) (after [74])

state. The discrete *Fourier transform* (FT) employed is the following unitary process

$$U_{\mathrm{FT}}|x\rangle = \frac{1}{\sqrt{w}} \sum_{x=0}^{w-1} e^{2\pi \mathrm{ikx/w}}|k\rangle. \tag{4.42}$$

We note that Eq. (4.38) is an example of this, operating on the initial state $|0\rangle$. The quantum network to apply U_{FT} is based on the fast FT algorithm (see, e.g. [78]). The quantum version was worked out by Coppersmith [79] and Deutsch [57] and a clear presentation may also be found in [70, 73] (for details see, also [74]).

Further analysis shows that the y register no longer concerns us, so we will just consider the x state from Eq. (4.40):

$$U_{\mathrm{FT}} \frac{1}{\sqrt{\mathrm{w/r}}} \sum_{j=0}^{w/r-1} |\mathrm{d}_u + \mathrm{jr}\rangle = \frac{1}{\sqrt{r}} \sum_k \widetilde{f}(k)|k\rangle, \tag{4.43}$$

where

$$\left|\widetilde{f}(k)\right| = \left\{ \begin{array}{l} 1, \text{ if } k \text{ is a multple of w/r} \\ 0 \text{ otherwise} \end{array} \right\}. \tag{4.44}$$

This state is illustrated in Fig. 4.15b. The final state of the x register is now measured, and we see that the value obtained must be a multiple of w/r. It remains to deduce r from last conclusion. We have $x = \lambda w/r$, where λ is an unknown parameter. If λ and r have no common factors, then we cancel x/w down to an irreducible fraction and thus obtain λ and r. If λ and r have common factors, which is unlikely for larger r, then the algorithm fails. In this case, the whole algorithm must be repeated from the start. After a number of repetitions no greater than ~log r, and usually much less than this, the probability of success can be shown to be arbitrary close to unity (see, also [45]).

To conclude, examining Fig. 4.15 and Eqs. (4.39–4.42) we would say that the most important features are contained in Eq. (4.39). They are not only the quantum parallelism already mentioned, but also quantum entanglement, and finally, quantum interference (for details see [61–64, 71]).

The search for new quantum algorithm is undoubtedly one of the most important challenges in quantum computer today. Following Shor's [61–64] discovery of quantum algorithms for factoring and discrete log in 1994 and Grover's [66–68] quantum search algorithm in 1995, there was a period of over 5 years with no substantially new quantum algorithms. During this period, the mathematical structure of *Shor's algorithm* was clarified via the formalism of the hidden subgroup problem (HSP) polynomial-time quantum algorithms were known for every finitely generated abelian group. Over the last couple of years, we are starting to see some progress toward the discovery of new algorithms. In 2002, Hallgren [80] gave polynomial-time quantum algorithms for Pell's equation and the class group problem, thus breaking the Buchman–Williams cryptosystem. This extended the framework to nonfinitely generated abelian groups. The two most important open questions in quantum algorithms are graph isomorphism and the (gap) shortest-lattice vector problem. The first of these corresponds to the HSP in the symmetric group, and Regev [81] showed that the second can be reduced to the HSP in the dihedral group. The dihedral group is a particularly simple nonabelian group, because it has a cyclic subgroup of index two. The *standard quantum algorithm* for abelian HSP can be generalized in a natural way to nonabelian groups. It was shown by Gridni and coauthors [82] that for sufficiently nonabelian groups the standard algorithm yields only an exponentially small amount of information about the hidden subgroup. On the other hand, authors [83] showed that the quantum query complexity of the problem is polynomial. This suggests that novel algorithmic ideas are necessary to tackle the nonabelian HSP. Recently, Kuperberg [84] gave an $O(2^{\sqrt{n}})$ algorithm for the dihedral HSP. The algorithm was an interesting modification of the standard algorithm. Other computational problems that are potential targets for quantum algorithms are the nonsolvable group membership, McElise cryptosystem, and the learning *Adiabatic computation* AC circuits.

A different approach to designing quantum optimization algorithms via adiabatic evolution was proposed by Farhi et al., [85]. Initial efforts in this direction concentrated on the question about whether adiabatic optimization could solve *NP-complete problems* such as variants on SAT in polynomial time. Surprisingly, query

lower bounds do not rule out this possibility [86]. However, van Dam and Vazirani [87] and more recently Reichardt [88] gave classes of SAT instances for which the spectral gap is exponentially small. Nevertheless, Farhi et al., [85] showed that adiabatic quantum optimization algorithms can tunnel through local optima and give an exponential speedup over local search. Aharonov and Ta-Shma [89] suggested that rather than optimization problems,*adiabatic algorithms* might be better suited for quantum-state generation. They also showed that every problem in the complexity class statistical zero knowledge (SZK) can be reduced to the problem of generating an appropriate quantum state. Aharonov et al., [90, 91] showed that a slightly more general formulation of adiabatic algorithms, when used for quantum-state generation, is in fact universal for quantum computer. Designing quantum algorithms via quantum-state generation is a novel and potentially important direction, because it ties into classical algorithm-design techniques using *Markov chains* and techniques such as bounds on conductance and spectral gaps. As a first step, it would be interesting to even give such an algorithm for solved problems such as quadratic residuosity or discrete logarithms (for details see also [1, 2, 92]).

4.6 A Physical Models for a Quantum Computer

4.6.1 Liquid State NMR Quantum Computer

In the field of *nuclear magnetic resonance* (NMR) over the last few decades sophisticated techniques have been developed to manipulate and detect nuclear spin states using both static and oscillating magnetic fields simultaneously. These techniques have been used, for instance to study structural properties of molecules and even biological samples [93–96]. The *qubits* in NMR *quantum computing* are given by the *spins* of suitable atomic nuclei [99], placed in a static magnetic field $\vec{\mathrm{B}}_0$. Therefore, we shall here be exclusively interested in spin—1/2 nuclei, such as ^{1}H, ^{13}C, ^{15}N, ^{19}F as well as ^{31}P, as they have two discrete eigenstates (see, Fig. 4.16). Spin—0 nuclei, for example ^{12}C and ^{16}O, are not magnetic and therefore not detectable with NMR. Nuclei with spin quantum number greater than 1/2, such as ^{2}H, ^{14}N, ^{35}Cl, ^{79}Br, do not make for good qubits, either, mapping the larger number of states (e.g. the spin quantum number of a spin—3/2 particle can be $-3/2$, $-1/2$, 1/2 or 3/2) onto qubit states, and performing quantum logic gates on them, introduces additional complications. More significantly, nuclear spins with spin $>1/2$ tend to have very short coherence time.

The *Hamiltonian* of a spin—1/2 particle in a magnetic field of strength B_0 along the $\vec{z}$ axis is [93, 94]

$$H_0 = -\hbar\gamma B_0 I_z = -\hbar\omega_0 I_z = \begin{bmatrix} -\hbar\omega_0/2 & 0 \\ 0 & \hbar\omega_0/2 \end{bmatrix}, \tag{4.45}$$

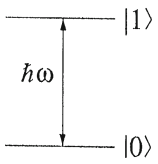

Fig. 4.16 Energy diagram for a single spin—1/2

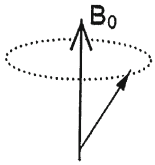

Fig. 4.17 Precession of a spin about the axis of a static magnetic field

where γ is the gyromagnetic ratio of the nucleus and $\omega_0/2\pi$ is the Larmor frequency of the spin (often call ω_0 simply the *Larmor frequency*). I_z is the angular momentum operator in the $\overrightarrow{z}$ direction, which relates to the well known *Pauli matrix* as $2\mathrm{I}_z = \sigma_z$ ($2\mathrm{I}_x = \sigma_x$ and $2\mathrm{I}_y = \sigma_y$). The interpretation of Eq. 4.16 is that the energy of the $|0\rangle$ or $|\uparrow\rangle$ state (given by $\langle 0|\mathrm{H}|0\rangle$ the upper left element of H) is lower than the energy of $|1\rangle$ or $|\downarrow\rangle$ ($\langle 1|\mathrm{H}|1\rangle$) by an amount $\hbar\omega_0$, as illustrated in the energy diagram of Fig. 4.16. The energy splitting is known as the *Zeeman splitting*. The time evolution $e^{-iHt/\hbar}$ of the spin state under the Hamiltonian of Eq. 4.16 corresponds to a precession motion in the *Bloch sphere* (see above) about the axis of the static magnetic field, similar to the precession of a spinning top about the ais of gravitation, as shown in Fig. 4.17. The B_0 field is typically of the order of 10 Tesla, resulting in precession frequencies ω_0 of a few hundred MHz, which is in the radio-frequency range.

The magnetic signal of a single nuclear spin is too weak to be directly detected.. Therefore, NMR experiments are done using a large ensemble of identical molecules, typically of the order of 10^{18}, dissolved in a liquid solvent. The same operations are applied to all the molecules in the ensemble, so the final state of the spins is the same in all molecules (for details see [76, 77])

NMR quantum computation is based on the same principle as used in magnetic resonance imaging for medical diagnosis (see above). As the name suggests, this technique involves atomic nuclei, or more precisely, their spins. Nuclear spins give rise to magnetic moment (see Eq. 4.16), meaning that the nuclei behave like little compass needles when exposed to magnetic fields. *Spins* are quantized and can only take on specific values (contrary to compass needles, which can point in any direction, i.e., take any desired value. One can switch between these values (see Fig. 4.16) by irradiating the nucleus with microwave at a particular frequency, the so-called resonance frequency of the*nuclear spin*. Since inside a molecule a particular atomic nucleus has a couple of neighbors that slightly change the resonance frequency of its spin, one can address a specific nucleus by tuning to its precise resonance frequency. The switching between spin states and the coupling between neighboring nuclear spins are good starting points for *quantum computatio*n. The spins can act as qubits, and the coupling makes it possible to realize two-qubit gates [72]. In 1998, Chuang

and his colleagues managed [97, 98] to run *Deutsch's algorithm* on a chloroform molecule (see, also [1, 2]). By sending carefully tailored microwave pulses to the molecules, they could perform the quantum logic gates necessary to implement the algorithm and read out the final answer. In 2001, a more complex molecule was used to realize *Shor's algorithm* [100] on the number 15.

That *NMR quantum computation* will one day lead to a commercially available quantum computer is rather unlikely. Although the demonstration of Shor's algorithm using NMR was an important step and stimulated research efforts in quantum computation, there are obvious reasons why this approach is not the way in the future. The most obvious of those reasons is the lack of scalability. In Chuang's experiment, Shor's algorithm was essentially carried out on billions of identical copies of the same computer, a molecule containing a handful of atoms. Therefore, the power of an NMR quantum computer is fundamentally limited by what a single molecule can do. That, in turn, will depend on the number and kind of atoms the molecule contains, how they are arranged in the molecule, and so forth.

4.6.2 Trapped Ions and Atoms

On the experimental side, implementing quantum processors is a formidable task, and no realistic scalable design presently exists. The activity have been focused on the operation of simple systems, with at most a few qubits [101]. First, microscopic quantum systems like atoms [101–103] and ions [104] has been considered (see, also [105]). Their main advantage is their excellent quantumness, but their scalability is questionable. The most advanced qubit implementation is based on ions in linear traps, coupled to their longitudinal motion [104] and addressed optically. Although the trend is to develop atom-chips, these implementations based on microscopic quantum objects still lack the flexibility of microfabricated electronic circuits, which constitute the second main road investigated. Here, quantumness is limited by the complexity of the circuits that always involve a macroscopic number of atoms and electrons.

The *ion trap method* is illustrated in Fig. 4.18, and described in detail in the literature [104, 105]. A string of ions is confined by a combination of oscillating and static electric fields in a linear "*Paul trap*" [61–64] in high vacuum (10^{-8} Pa). A single laser beam is split by beam splitters and acousto-optic modulators into many beam pairs, one pair illuminating each ion. Each ion has two long-lived states, for example different levels of the ground state hyperfine structure (the lifetime of such states against spontaneous decay can exceed thousands of years). Following [105] let us refer to these two states as $|g\rangle$ and $|e\rangle$; they are orthogonal and so together represent one*qubit*. Each laser beam pair can drive coherent Raman transitions between the internal states of the relevant ion. This allows any single-qubit quantum gate to be applied to any ion, but not two-qubit gates. The latter requires an interaction between ions, and this is provided by their *Coulomb repulsion*. However, exactly how to use

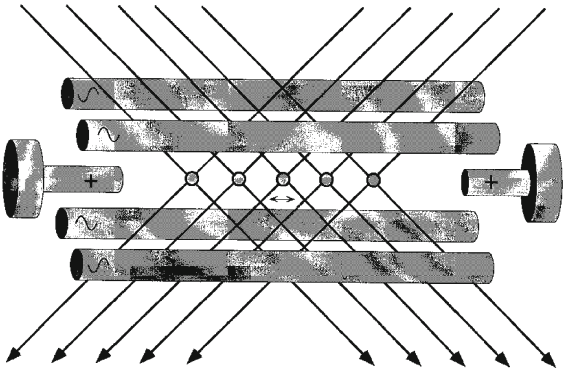

Fig. 4.18 Ion trap quantum information processor. A string of singly charged atoms is stored in a linear ion trap. The ions are separated by $\sim 20\mu$m by their mutual repulsion. Each ion is addressed by a pair of laser beams which coherently drive both Raman transitions in the ions, and also transitions in the state of motion of the string. The motional degree of freedom serves as a single-qubit "bus" to transport quantum information among the ions. State preparation is by optical pumping and laser cooling; readout is by electron shelving and resonance fluorescence, which enables the state of each ion to be measured with high signal to noise ratio

this interaction is far from obvious; it required the important insight by the authors of the *ion trap quantum processor* [106, 107].

Light carries not only energy but also momentum, so whenever a laser beam pair interacts with an ion, it exchanges momentum with the ion. In fact, the mutual repulsion of the ions means that the whole string of ions moves en masse when the motion is quantized (analog *Mössbauer effect)* [76, 77]. The motion of the ion string is quantized because the ion string is confined in the potential provided by the Paul trap [1, 2]. The quantum states of motion correspond to the different degrees of excitation (phonons) of the normal modes of *vibration* of the string. In particular we focus on the ground state of motion $|n = 0\rangle$ and the lowest *excited state* $|n = 1\rangle$ of the fundamental mode. To achieve, for example, CNOT between ion x and ion y, we start with the motion in the ground state $|n = 0\rangle$. A pulse of the laser beams on ion x drives the transitions $|n = 0\rangle|g\rangle_{\mathrm{x}} \longrightarrow |n = 0\rangle|g\rangle_{\mathrm{x}}$, $|n = 0\rangle|e\rangle_{\mathrm{x}} \longrightarrow |n = 1\rangle|g\rangle_{\mathrm{x}}$, so the ion finishes in the ground state, and the motion finishes in the initial state of the ion: this is a SWAP operation. Next, a pulse of the laser beams on ion y drives the transitions

$$\begin{aligned}
|n = 0\rangle|\mathrm{g}\rangle_{\mathrm{y}} &\longrightarrow |\mathrm{n} = 0\rangle|\mathrm{g}\rangle_{\mathrm{y}} \\
|\mathrm{n} = 0\rangle|\mathrm{e}\rangle_{\mathrm{y}} &\longrightarrow |\mathrm{n} = 0\rangle|\mathrm{e}\rangle_{\mathrm{y}} \\
|\mathrm{n} = 1\rangle|\mathrm{g}\rangle_{\mathrm{y}} &\longrightarrow |\mathrm{n} = 1\rangle|\mathrm{g}\rangle_{\mathrm{y}} \\
|\mathrm{n} = 1\rangle|\mathrm{e}\rangle_{\mathrm{y}} &\longrightarrow -|\mathrm{n} = 1\rangle|\mathrm{e}\rangle_{\mathrm{y}}.
\end{aligned} \tag{4.46}$$

Finally, we repeat the initial pulse on ion x. The overall effect of three pulses is

$$
\begin{aligned}
|\mathrm{n}=0\rangle|\mathrm{g}\rangle_x|\mathrm{g}\rangle_\mathrm{y} &\longrightarrow |\mathrm{n}=0\rangle|\mathrm{g}\rangle_x|\mathrm{g}\rangle_\mathrm{y}\\
|\mathrm{n}=0\rangle|\mathrm{g}\rangle_x|\mathrm{e}\rangle_\mathrm{y} &\longrightarrow |\mathrm{n}=0\rangle|\mathrm{g}\rangle_x|\mathrm{e}\rangle_\mathrm{y}\\
|\mathrm{n}=0\rangle|\mathrm{e}\rangle_x|\mathrm{g}\rangle_\mathrm{y} &\longrightarrow |\mathrm{n}=0\rangle|\mathrm{e}\rangle_x|\mathrm{g}\rangle_\mathrm{y}\\
|\mathrm{n}=0\rangle|\mathrm{e}\rangle_x|\mathrm{e}\rangle_\mathrm{y} &\longrightarrow -|n=0\rangle|\mathrm{e}\rangle_x|\mathrm{e}\rangle_\mathrm{y},
\end{aligned}
\tag{4.47}
$$

which is exactly a CNOT between x and y. Each laser pulse must have a precisely controlled frequency and duration (see, e.g. [76, 77]). The CNOT gate and the single-qubit gates together provide a universal set, so we can perform arbitrary transformations of the joint state of all the ions. To complete the description of this method, we must be able to prepare the initial state and measure the final states. The first is possible through the methods of optical pumping and laser cooling, the second through the quantum jump or electron shelving measurement technique. All these are powerful techniques developed in the atomic physics community over the last three decades. To conclude, the basic requirements for a general-purpose quantum computing device with trapped ions have been demonstrated and no fundamental road block is in sight. However, building such a device is extremely challenging. Especially, the stringet requirements for fault tolerance and for *scalability* to many thousands of qubits pose huge difficulties (for details see [105] and references therein).

4.6.3 Solid State Quantum Computers

At first sight it might appear crazy for solid-state physicists to enter the field of *quantum information processing*. After all, the entities with which they deal are typically much more strongly interacting than the atomic components used in atom-trap or ion-trap approaches (see, also [108]), and this would seem to make them much less suitable for the coherent manipulation of quantum information. But this has not prevented the appearance of a number of very imaginative proposals for using the numerous excitations in condensed matter for quantum information processing. At the moment these are just proposals. But very significant progress is being made toward surmounting the technological challenges required to turn the proposals into reality. Our brief consideration will by no means be comprehensive, but it will serve to illustrate something of the tremendous range of possible condensed -matter approaches to quantum information processing including *isotope-mixed crystals processors.*

4.6.3.1 Superconducting Qubits

In two preceding examples the qubits were carried by individual quantum objects, nuclear spins in the NMR case and ions (atoms) in the case of trapped ions. We now turn to a system where the *qubits* are carried by a *macroscopic degree of freedom*, the current in a superconducting circuit containing one or several Josephson junction

(Fig. 4.19). As we all know, low temperatures of the order of tens of millikelvins are required for these circuits to exhibit quantum behavior. These circuits are small by everyday standards (a few micrometers), but very large compared to atomic sizes. Still more remarkable is the fact that the parameters of these quantum systems are fixed by fabrication, and not by *Nature* as is the case for individual quantum system like electrons or ions. (see, also [109]). They are engineered quantities which can be modified by changing the dimensions of the circuits, and in this sense they are unambiguously macroscopic quantities. It has been known for about a century that at low temperatures the electrical resistance of most metals and alloys drops abruptly to zero below a transition temperature T_C of order 1K, and the metal becomes a *superconductor*. Superconductors also exhibit a remarkable feature called *Meissner effect*: magnetic fields are expelled from the bulk of a superconductor: they cannot penetrate deeper than a distance known as the *London penetration length*, which is of order of 0.1 μm (for details, see, e.g. [110]).

Although the currents that flow in superconductors consist of millions of electrons, they can be viewed as a single huge quantum state. Consequently, it is also possible for the current to exist in a superposition of two or more quantum states; for example, in a superposition of flowing at the same time clockwise and counterclockwise inside a metal ring. Also, a current swinging back and forth in an oscillator circuit can exist in a superposition of several harmonic oscillator states (which are very familiar to those of ions oscillating in a trap). It is tempting, therefore, to use such states of superconductors as qubits for *quantum computation* [111].

There are several advantages of such an approach compared to ion traps and optical lattices. First, superconducting circuits are man-made objects, and hence it is possible to adjust the properties of the circuit (almost) at will. Ions and atoms, by contrast are provided by *Nature* and can only be taken as they come. Second, superconducting circuits can be fabricated using the well-known techniques that are also used for making integrated circuits and microchips. And finally, we know a lot about controlling currents and electrons in circuits, so it will be easy to control qubits in superconductors.

In spite of these advantages, using superconductors for quantum computation is not quite as straighforward as it may seem at first sight. One fundamental reason for why one cannot simply use the quantized states of a superconducting oscillator circuit is that these quantum states are all at the same distance from each other. This makes it impossible to single out exactly two states that will be $|0\rangle$ and$|1\rangle$ of potential qubit. But there is a remedy, the so-called *Josephson-junction*. Such a junction consists, basically, of a tiny slab of insulating material between two superconductor wires (see Fig. 4.19). Classically, no current flow through an insulator, but in quantum mechanics the Cooper pairs in the superconductors can bridge the gap by tunneling. In a Josephson-junction, it is possible to single out two quantized states that can be used as $|0\rangle$ and$|1\rangle$ states of a qubit [11]. The first realization of CNOT gate in superconductor was recently described in [112].

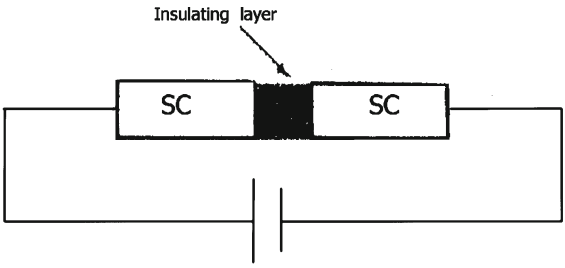

Fig. 4.19 Schematic depiction of a *Josephon junction*: a thin insulating layer is sandwiched between two superconducting (SC) wires

4.6.3.2 Kane's Model

The development of efficient quantum algorithms for classically hard problems has generated interest in the construction of a quantum computer. A quantum computer uses superpositions of all possible input states. By exploiting this*quantum parallelism*, certain algorithms allow one to factorize [61–64] large integers with astounding speed, and rapidly search through large databases [66–68], and efficiently simulate quantum systems [55, 56, 113]. In the nearer term such devices could facilitate secure communication and distributed computing. In any physical system, bit errors will occur during the computation. In *quantum computing* this is particularly catastrophic, because the errors cause decoherence [4] and can destroy the delicate *superposition* that needs to be preserved throughout the computation. With the discovery of quantum error correction [61–64, 114] and fualt-tolerant computing, in which these errors are continuously corrected without destroying the *quantum information*, the construction of a real computer has become a distinct possibility. The tasks that lie ahead to create an actual quantum computer are formidable: Preskill [115] has estimated that a quantum computer operating on 10^6 qubits with a 10^{-6} probability of error in each operation would exceed the capabilities of contemporary conventional computers on the prime factorization problem. To make use of *error-correcting codes*, logical operations and measurement must be able to proceed in parallel on qubits throughout the computer.

Phosphorous donors in silicon present a unique opportunity for solid - state quantum computation [116–118]. Electrons spins on isolated Si:P donors have very long decoherence times of ~ 60 ms in isotopically purified ^{28}Si at 7 K [119]. By contrast, electron spin dephasing times in GaAs (for example) are orders of magnitude shorter due spin-orbit interaction; and the background nuclear spins of the III–V host lattice cannot be eliminated by isotope selection. Finally, the Si:P donor is a self-confined, perfectly uniform single-electron quantum dot with a non-degenerate ground state. A strong *Coulomb potential breaks* the 6-valley degeneracy of the silicon conduction band near donor site, yielding a substantial energy gap of $\sim$ 15 meV to the lowest excited [120] as needed for quantum computation. As we all know, the Si:^{31}P system was exhaustively studied more than 40 years ago in the first electron-nuclear double-resonance experiments. At sufficiently low ^{31}P concentrations at temperature $T = 1.5$ K, the electron spin relaxation time is thousands of seconds and the ^{31}P

nuclear spin relaxation time exceeds 10 hours. It is likely that at millikelvin temperatures the phonon limited ^{31}P relaxation time is of the order of 10^{18} seconds [121], making, as we said above, this system ideal for quantum computation.

Kane's original proposal [116–118] envisions encoding quantum information onto the *nuclear spin* 1/2 states of ^{31}P qubits in a spinless I = 0 ^{28}Si lattice. The Kane architecture employs an array of top-gates (see Fig. 4.20). to manipulate the ground state wavefunctions of the spin-polarized electrons at each donor site in a high magnetic field B $\sim$ 2 T, at very low temperature (T $\simeq$ 100 mK). "A -gates" above each donor turn single-qubit NMR rotations via the contact hyperfine interaction; and "J-gates" between them induce an indirect two-qubit nuclear exchange interaction via overlap of the spin-polarized electron wavefunctions (see, also [122]). In other words, spin—1/2 ^{31}P donor nuclei are qubits, while donor electrons together with external A-gates provide single-qubit (using external magnetic field) and two-qubit operations (using hyperfine and electron exchange interactions). Specifically, the single. donor nuclear spin splitting is given by [116–118]

$$\hbar\omega_A = 2\mathrm{g}_n\mu_\mathrm{n}\mathrm{B} + 2\mathrm{A} + \frac{2\mathrm{A}^2}{\mu_B\mathrm{B}}, \tag{4.48}$$

where $\mathrm{g_n}$ is the nuclear spin g-factor (= 1.13 for ^{31}P [115]), μ_n is the nuclear magneton, A is the strength of the hyperfine coupling between the ^{31}P nucleus and the donor electron spin, and B is the applied magnetic field. It is clear that by changing A one can effectively change the nuclear spin splitting, and thus allow resonant manipulations of individual nuclear spins (Fig. 4.21). If the donor electrons of two nearby donors are allowed to overlap, the interaction part of the spin Hamiltonian for the two electrons and the two *nuclei* include electron–nuclear hyperfine coupling and electron–electron exchange coupling [116–118] (see also [123, 124])

$$\mathrm{H} = \mathrm{H_{Zeeman}} + \mathrm{H}_{int} = \mathrm{H_{Zeeman}} + \mathrm{A}_1\vec{\mathrm{S}_1}\cdot\vec{\mathrm{I}_1} + \mathrm{A}_2\vec{\mathrm{S}_2}\cdot\vec{\mathrm{I}_2} + \mathrm{J}\vec{\mathrm{S}_1}\vec{\mathrm{S}_2}, \tag{4.49}$$

where $\vec{\mathrm{S}_1}$ and $\vec{\mathrm{S}_2}$ represent the two electron spins, $\vec{\mathrm{I}_1}$ and $\vec{\mathrm{I}_2}$ are the two *nuclear spins*, A_1 and A_2 represent the hyperfine coupling strength at the two donor sites, and J is the exchange coupling strength between the two donor electrons, which is determined by the overlap of the donor electron wavefunctions. The lowest order perturbation calculation (assuming $\mathrm{A}_1 = \mathrm{A}_2 = \mathrm{A}$ and J is much smaller than the electron Zeeman splitting) results in an effective exchange coupling between the two nuclei and the coupling strength is (see [116–118])

$$\mathrm{J}_{nn} = \frac{4\mathrm{A}^2\mathrm{J}}{\mu_B\mathrm{B}\,(\mu_B\mathrm{B} - 2\mathrm{J})}. \tag{4.50}$$

Now the two donor electrons essentially shuttle different nuclear spin qubits and are controlled by external gate voltages. The final measurement is done by first transferring nuclear spin information into electron spins using hyperfine interaction, then

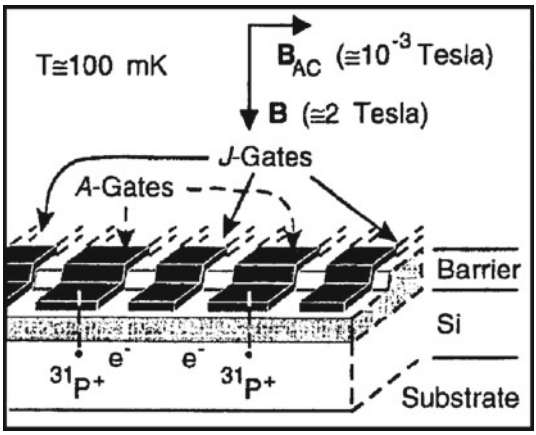

Fig. 4.20 Illustration of two cells in a 1D array containing ^{31}P donors and electrons in a Si host, separated by a barrier from metal gates on the surface. "A gates" control the resonance frequency of the nuclear spin qubits; "J gates" control the electron-mediated coupling between adjacent nuclear spins. The ledge over which the gates cross localizes the gate electric field in the vicinity of the donors (after [116–118])

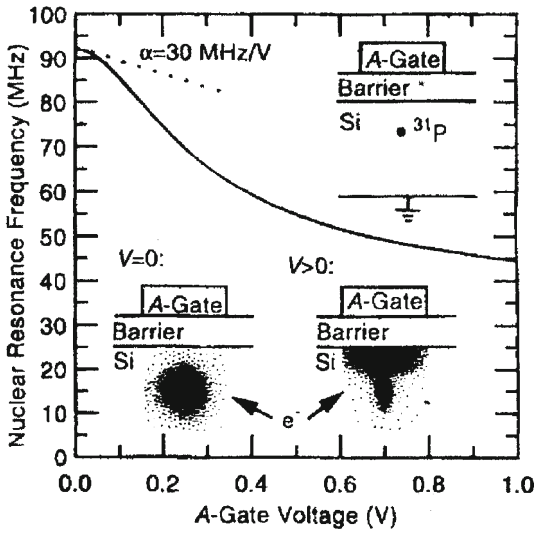

Fig. 4.21 Dependence of the hyperfine coupling constant on the gate voltage (after [116–118])

converting electron spin information into charge states such as charge locations [123]. A significant advantage of silicon is that its most abundant isotope ^{28} Si is spinless, thus providing a "quiet" environment for the donor nuclear spin qubits. In addition, Si has also smaller intrinsic spin-orbit coupling than other popular semiconductors such as GaAs. In general, nuclear spins have very long coherence times because they do not strongly couple with their environment, and are thus good candidates for qubits (see, also [15, 121, 124]).

Although the nuclear spin offers unlimited decoherence times for quantum information processing, the technical problems of dealing with nuclear spins through the electrons are exceedingly difficult. A modified versions of the *Kane architecture* was soon proposed using the spin of the donor electron as the qubit [125–128].

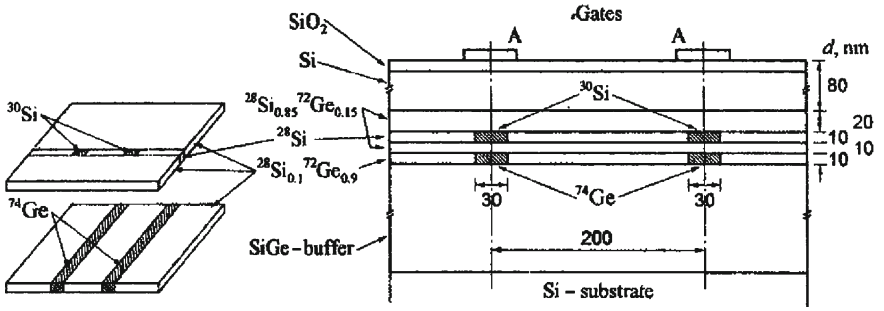

Fig. 4.22 Schematics of the proposed device. After NTD, ^{31}P donors appear only inside the ^{30}Si-spots and underlying ^{74}Ge strips will be heavily doped with ^{75}As donors. All sizes are shown in nm (after [126–128])

In the first scheme [125], A-gates would modulate the electron g-factor by polarizing its ground state into Ge-rich regions of a SiGe heterostructure for selective ESR rotations, while two-qubit electron exchange is induced through wavefunction overlap. In the studies of Shlimak et al. [126–128] was used the new technology to growth of SIGE heterostructures. Recent achievements in Si/Ge technology allow one to obtain high quality heterojunctions with a mobility of about (1–5) $\times$ 10^5 $cm^2V^{-1}s^{-1}$ [126–128]. Using *Si/Ge heterostructures* has several advantages concerning semiconductor-based nuclear spin quantum computers (S-NSQCs). First, the concentration of nuclear spins in Ge and Si crystals is much lower, because only one *isotope* (^{73} Ge and ^{29} Si [130]) has a nuclear spin, and the natural abundance of this isotope is small (see, also [131]). Second, the variation of isotopic composition for Ge and Si will lead to the creation of a material with a controlled concentration of nuclear spin, and even without nuclear spins. Utilization of isotopically engineered Ge and Si elements in the growth of the active Si/Ge layers could help realize an almost zero *nuclear spin* layer that is coplanar with the 2DEG. Then, one might deliberately vary the isotopic composition to produce layers, wires, and dots that could serve as nuclear spin qubits with a controlled number of nuclear spins (see also [15]).

The key point of a novel technology is the growth of the central Si and barrier $Si_{0.85}Ge_{0.15}$ layers from different isotopes: the $Si_{0.85}Ge_{0.15}$ layers from isotope ^{28}Si and ^{72}Ge and the central Si layer from isotope ^{28}Si with ^{30}Si spots introduced by means of the *nano-litography* (see Fig. 4.22) [132]. the formation of quasi-1D Si wires will be achieved in a subsequent operation by the etching of Si layer between wires and the filling of the resulting gaps by the $Si_{0.85}Ge_{0.15}$ barrier composed from isotopes ^{28}Si and ^{72}Ge. Because different isotopes of Si and Ge are chemically identical, this technology guarantees the high quality of the grown structures [133]. After preparation, these structures will be irradiated with a neutron flux in a nuclear reactor by the fast annealing of radiation damage (see [15] and references cited therein).

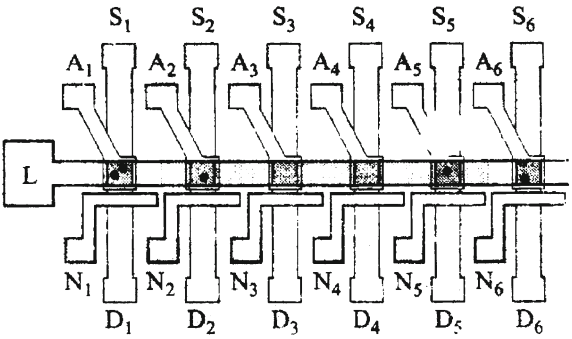

Fig. 4.23 Schematics of a ^{28}Si nanovire L with an array of ^{30}Si spots (qubits and non-qubits after NTD). Each spot is supplied by overlying A-gate, underlying source-drain-channel and lateral N-gate. This device architecture allows to realize an indirect coupling between any distant qubits (for details see text) (after [126–128])

As was shown by Di Vincenzo [134, 135] two-bit gates applied to a pair of electron or nuclear spins are universal for the verification of all principles of quantum computation. Because direct overlap of wavefunctions for electrons localized on P donors is negligible for distant pairs, the authors of paper [126–128] proposed another principle of coupling based on the placement of qubits at fixed positions in a quasi 1D Si nanowire and using the indirect interaction of ^{31}P nuclear spins with spins of electrons localized in the nanowire which they called as "1D-electrons". This interaction depends on the amplitude of the wavefunction of the "1D-electron" estimated at the position of the given donor nucleus $\Psi_n(\mathrm{r_i})$ and can be controlled by the change in the number of "1D-electrons" N in the wire. At N = 0, the interqubit coupling is totally suppressed, each ^{31}P nuclear spin interact only with its own donor electron. This situation is analogous to that suggested in the Kane proposal [124, 125] and therefore all *single-qubit operations* and estimates of the decoherence time are valid also in the model by Shlimak et al. [126–128].

Below, we briefly analyze the schematics of the device architecture which satisfy the *scalability* requirements of the quantum computer suggested in paper [125]. Figure 4.23 shows schematics of the device architecture which allows one to vary l (length of quantum wire) and N. The device consists of a ^{28}Si *nanowire* with an array of ^{30}Si spots. Each spot is supplied by the overlying A-gate, the underlying source-drain-channel, and the lateral N-gate. After NTD, P donors will appear in most of the spots (which transforms these spots into qubits) and not appear in other spots (non-qubits). In Fig. 4.23 it is assumed that the spots 3 and 4 are non-qubits (0-spots) and one needs to provide coupling between qubits 2 and 5. For this purpose, it is necessary to connect the gates N_2, N_3, N_4, and N_5. The negative voltage applied between other N-gates and the wire contact L will lead to pressing-out "1D electrons" from all corresponding areas and formation of the nanowire with $l = 800\,\mathrm{nm}$ between the sites 2 and 5 only (shown in grey in Fig. 4.23). The coupling between qubits 2 and 5 will be realized via injection in the wire of the necessary number of electrons N, using the positive voltage applied to the gates $N_2 - N_5$. According [126–128], the maximal coupling will be realized at $N = 7$, while at $N = 0$, the coupling will be totally suppressed.

All the charged-based schemes mentioned so far use single charged *semiconductor quantum dot*. The associated strong Coulomb interaction provides a convenient means for fast qubit manipulation, but can also lead to fast decoherence. One way to alleviate this problem is to use neutral excitations such as excitons as qubits, where there is the added benefit that excitons can be precisely controlled optically (see, e.g. [136]. Indeed , uncharged quantum dots have been proposed as possible candidates for quantum information processing [137, 138] and many experiments have been done to demonstrate exciton coherence and control in single quantum dot [139, 140]. Here single excitons are optically excited in individual quantum dots and can be coherently manipulated optically. The presence and absence of an *exciton* in a quantum dot provide two states of a qubit. Again, entanglement between different qubits is based on *Coulomb renormalization* of the energy levels. The exciton-based quantum computer in isotope-mixed crystals [141] proposals clearly illustrate the dichotomy faced by all quantum computer architectures: excitons are neutral, therefore are more insulated from their environment and decohere more slowly than the single charge-based schemes. However, the charge neutrality also strongly reduces the interaction between spatially separated excitons, thus rendering it more difficult to preform entangling operation. We should add that an optically controlled exciton transfer process was shown to lead to the generation of Bell and Greenberg–Horne–Zeilinger state in systems comprising two and three couple dots, respectively [142].

4.6.3.3 Color Centers Processor

The authors of [143] have proposed a new approach to constructing gates for quantum information processing, exploiting the properties of deep impurities in silicon (*color centers*). Localized spins in solids have properties suitable for representing quantum information. Quantum gates require mutual coherent evolution of such states, necessitating interactions between them. Indicated schemes (see above) to control interactions required gate electrodes positioned near to specific highly polarizable defects which would be readily ionized except at low temperatures. The formidable fabrication (see Fig. 4.20) requirements may introduce further significant sources of decoherence. Novel control, proposed in [143] avoids electrodes. According to the results of this paper interactions are controlled by electronic excitations [130]. One implementation embodies qubits in electron spins of deep donors (A, B), not ionized at working temperature. Typical A, B spacings should be large enough for ground-state interactions between donor spins to be small, perhaps 7–10 nm for a deep donor like Si:Bi [143]. Controlled optical excitation of a charge-transfer transition [144] from a nearby control impurity C, possibly Er, promotes a control electron from C into a molecular state of A and B, analogous to the hydrogen molecular ion H_2^- . In this excited state, there is an effective exchange interaction between the qubit spins. Qubit–qubit interactions are switched on by optical excitation and off by stimulated de-excitation of the control electron (see Fig. 4.24). The sup [posed approach has two key features. Clearly, the *spins* encoding the quantum information must have an acceptable time. Further, there must be an electronic excited state in which the

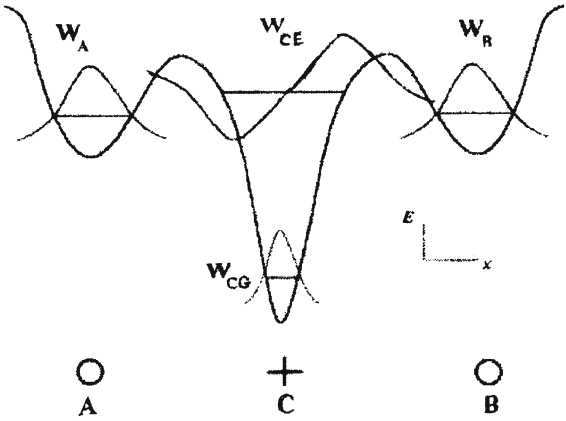

Fig. 4.24 A schematic diagram of the *quantum gate*. The qubit spins are on deep donors A and B (◯) with wavefunctions W_A and W_B. The control atom, C(+) is the source of a control electron. In the ground state, the control electron is in the state W_{CG}, whose wavefunction and potential well ar shown schematically. In the excited state, the control electron is in a charge-transfer, molecular-like , state, W_{CE}, which overlaps both qubit electrons. Neither the qubits nor the control electron interact significantly in the ground state, but interact causing entanglement in the excited state (after [143])

entanglement is changed significantly. This scheme has two major advantages. First, ground-state *quantum information storage* is largely separated from excited-state informational control. Second, no small energy scale is involved in the gate operation: it might operate at liquid nitrogen temperatures or even near room temperature. The cited authors indicate that processors following their approach might be made in near-future semiconductor fabrication plants.

4.7 Quantum Error Corrections

Quantum error correction (QEC) aims at protecting the*coherence* of quantum states in a quantum computation against noise. This noise is due to some physical interaction of the quantum systems forming the quantum computer with their environment, an interaction which can never be entirely avoided [144–148]. It turns out that reliable quantum computation is indeed possible in the presence of noise, which was one of genuinely remarkable insights in this research field. The general idea of QEC is to encode logical qubits into a number of physical qubits. The whole quantum computation is hence performed in a subspace of a larger dimensional Hilbert space, called the error correcting code subspace. Any deviation from this subspace guides into an orthogonal error subspace, and can hence be detected and corrected without losing the coherence of the actual encoded states [146]. Quantum error correcting codes have the ability to correct a certain finite *dimensional subspace* of error syndromes. These error syndromes could for example correspond to bit - flip error on

a single qubit. Such bit-flip errors are, however, by no means the only type of error that can occur to a single qubit. In a phase flip error the relative phase of $|0\rangle$ and $|1\rangle$ is interchanged. *Quantum error correcting codes* can be constructed that correct for such bit-flip and phase errors or both. In a quantum computing context, this error correction capability is still not sufficient. It is a beauty of the theory of quantum error correcting codes that indeed, codes can be constructed that have ability to correct for a general error on a single qubit.

The simplest possible encoding that protects at least against a very restricted set of errors is the following: Given a pure state of a single qubit with state vector $|\Psi\rangle = \alpha|0\rangle + \beta|1\rangle$. This state can be protected against bit-flip errors of single qubits by means of the *repetition encoding* $|0\rangle \longrightarrow |0, 0, 0\rangle$ and $|1\rangle \longrightarrow |1, 1, 1\rangle$, such that $|\Psi\rangle$ is encoded as

$$|\Psi\rangle = \alpha|0\rangle + \beta|1\rangle \longrightarrow \alpha|0, 0, 0\rangle + \beta|1, 1, 1\rangle. \tag{4.51}$$

This encoding, the idea of which dates back to work as early as 1985 [149] (see, also [150]), can be achieved by means of two sequential CNOT gates to qubit systems initially prepared in $|0\rangle$. Note that it does not amount to a copying of the input state, which would be impossible anyway [151, 152]. If an error occurs that manifests itself in a single bit-flip operation to any of three qubits, one can easily verify that one obtains one out of four mutually orthogonal states: These states correspond to no error at all, and a single bit-flip error to any of the three qubits. This encoding, while not yet being a quantum error correcting code in the actual sense, already exemplifies an aspect of the theory: With a subsequent measurement that indicates the kind of error that has occurred, no information can be inferred about the values of the coefficients α and β. A measurement may hence enquire about the error without learning about the data. While already incorporating a key idea, it is nevertheless not a particularly good encoding to protect against errors, if a different error than a bit-flip occurs, then the measurement followed by an error correction cannot Moreover, and maybe more seriously, the state cannot be disentangled from the *environment*, if the error is due to some physical interaction *entangling* the state with its environment. Further, we consider the map involving the qubit undergoing the error and the environment, modeled as a system starting with state vector $|\Psi_0\rangle$, according to

$$|0, \Psi_0\rangle \longrightarrow |1, \Psi_0\rangle, \text{and} |1, \Psi_0\rangle \longrightarrow |0, \Psi_0\rangle, \tag{4.52}$$

such that the environment becomes correlated with the qubit undergoing the error. This is a process typically referred to as decoherence. The above encoding cannot correct for such an error and recover the original state. Such an entangling error, however corresponds rather to the generic situation happening in realistic errors. According to Preskill. The manifesto of *quantum error correction* is to fight entanglement with entanglement [146]. What is meant is that the unwanted but unavoidable entanglement of the system with its environment should be avoided by means of skillfully entangling the systems in a quantum error correcting code, followed by appropriate correction.

There are, notably error correcting codes that can correct for any error inflicted on a single qubit of the code block. that such quantum error correcting codes exist was first noted by Steane [114] and Shor [153, 154] in independent seminal work in 1995 and 1996 (see, also reviews [145–147]). Shor's 9 qubit code is related to the above repetition code by encoding again each of the qubits of the code words into three other qubits, according to $|0\rangle \longrightarrow (|0,0,0\rangle + 1,1,1\rangle)/\sqrt{2}$ and $|1\rangle \longrightarrow (|0,0,0\rangle - |1,1,1\rangle)/\sqrt{2}$. In effect, in the total encoding each logical qubit is encoded in the state of 9 physical qubits, the codewords being given by

$$|0\rangle \longrightarrow (|0,0,0\rangle + |1,1,1\rangle)\,(|0,0,0\rangle + |1,1,1\rangle)\,(|0,0,0\rangle + |1,1,1\rangle)\,\sqrt{8}, \tag{4.53}$$

$$|1\rangle \longrightarrow (|0,0,0\rangle - |1,1,1\rangle)\,(|0,0,0\rangle - |1,1,1\rangle)\,(|0,0,0\rangle - |1,1,1\rangle)\,\sqrt{8}. \tag{4.54}$$

In a sense, the additional encoding of the repetition code mends the weaknesses of the repetition code itself. Such an encoding of the encoding is called a concatenation of codes, which plays an important role in QEC. What errors can it now correct? If the environment is initially again in in a pure state associated with state vector $|\Psi_0\rangle$, then the most general error model leads to the joint state vector

$$\begin{aligned}(\alpha|0\rangle + \beta|1\rangle)\,|\Psi_0\rangle = (\alpha|0\rangle + \beta|1\rangle)\,|\Psi_0\rangle + (\alpha|1\rangle + \beta|0\rangle)\,|\Psi_1\rangle \\ + (\alpha|0\rangle - \beta|1\rangle)\,|\Psi_2\rangle + (\alpha|1\rangle - \beta|0\rangle)\,|\Psi_3\rangle,\end{aligned} \tag{4.55}$$

where no assumption is made concerning the state vectors $|\Psi_0\rangle, |\Psi_1\rangle, |\Psi_2\rangle$ and $|\Psi_3\rangle$. One particular instance of this map is the one where

$$|\Psi_0\rangle = |\Psi_2\rangle = |0\rangle, |\Psi_1\rangle = |1\rangle, |\Psi_3\rangle = -|1\rangle. \tag{4.56}$$

One can convince oneself that when disregarding the state of the environment (reflected by the partial trace), that this error is quite a radical one: in effect, it is as if the qubit is discarded right away and replaced by a new one, prepared in $|0\rangle$. The key point now is that the Shor code has the ability to correct for any such error if applied to only one qubit of the codeword, and completely disentangle the state again from the environment. This includes the complete loss of a qubit as in the previous example. In a sense, one might say that the continuum of possible errors is discretized leading to orthogonal error syndromes that can be reliably distinguished with measurements, and then reliably corrected for. But then, one might say, typical errors not only affect one cubit in such a strong manner, but rather, all qubits of the codeword are exposed to errors.

Stean's seven qubit quantum error correcting code is a good example of how the techniques and the intuition from classical error correction can serve as a guideline to construct good quantum error correcting codes [145, 147]. It Is closely related to a well known classical code, the [4, 5, 8]—Hamming code [155]. The starting point

is the parity check matrix of the [4, 5, 8]—Hamming code given by

$$h = \begin{bmatrix} 0\,0\,0\,1\,1\,1\,1 \\ 0\,1\,1\,0\,0\,1\,1 \\ 1\,0\,1\,0\,1\,0\,1 \end{bmatrix}. \tag{4.57}$$

Codewords of the classical *Hamming code* are all binary words v of length 7 that satisfy $\mathrm{hv}^{\mathrm{T}} = 0$, which is meant as addition in Z_2. It is straighforward exercise to verify that there are in total 16 legitimate codewords (the cernel of h is four dimensional). In the classical setting, if at most a single unknown bit-flip error occurs to a word v, leading to the word v′, it can be easily detected: if the error happens on the *i*th bit, then, from the very construction of h, $\mathrm{hv}'T$ is nothing but a binary representation of i, indicating the position of the error. If $\mathrm{hv}'^{T} = 0$, one can conclude that $v' = v$, and no error has occurred.

The 7 qubit *Steane code* draws from this observation. It is now defined as follows: for the logical $|0\rangle$, the quantum codeword is the superposition of the eight codewords of the classical *Hamming code* with odd number of 0s, represented in terms of state vectors. The latter term means that the binary word $\mathrm{x}_1, \ldots \mathrm{x}_7$ is represented as$|\mathrm{x}_1, \ldots x_7\rangle$. The logical $|1\rangle$ is encoded in a similar state vector corresponding to the even number of 0s. That is,

$$\begin{aligned} |0\rangle \longrightarrow (&|0,0,0,0,0,0,0\rangle + |0,0,0,1,1,1,1\rangle + \\ &|0,1,1,0,0,1,1\rangle + |0,1,1,1,1,0,0\rangle + \\ &|1,0,1,0,1,0,1\rangle + |1,0,1,1,0,1,0\rangle + \\ &|1,1,0,0,1,1,0\rangle + |1,1,0,1,0,0,1\rangle)/\sqrt{8}, \end{aligned} \tag{4.58}$$

$$|1\rangle \longrightarrow (|0,0,1,0,1,1,0\rangle + |0,0,1,1,0,0,1\rangle + \tag{4.59}$$

$$|0,1,0,0,1,0,1\rangle + |0,1,0,1,0,1,0\rangle + \tag{4.60}$$

$$|1,0,0,0,0,1,1,\rangle + |1,0,0,1,1,0,0\rangle + \tag{4.61}$$

$$|1,1,1,0,0,0,0\rangle + |1,1,1,1,1,1,1\rangle\sqrt{8}. \tag{4.62}$$

The central idea is now that in the quantum situation one can make use of the idea of how the syndrome is computed in the classical case. When appending a system consisting of three qubits, the transformation

$|\mathrm{v}'\rangle|0,0,0\rangle \longrightarrow |\ \mathrm{v}'\rangle|hv'\rangle$ can be realized in a unitary manner, and the measurement of the state of the additional qubits reveals the syndrome. But this procedure, one might be tempted to think, is merely sufficient to correct for bit-flip errors, from the construction of the [4, 5, 8] Hamming code. This is not so, a rotation of each qubit of the quantum codewords with a *Hadamard gate* H as described early will yield again a superposition of binary words. In fact, it is again a superposition of Hamming codeword, and bit-flip errors in this rotated basis correspond to phase flips

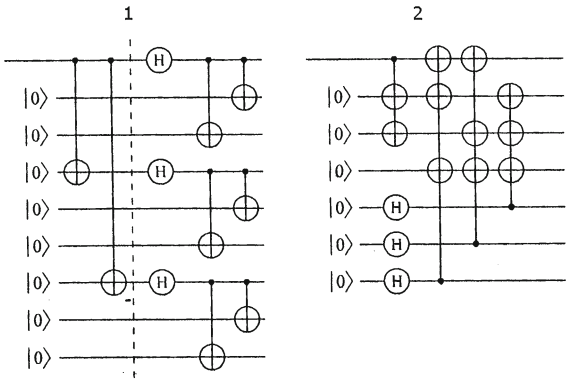

Fig. 4.25 The encoding circuits of the Shor *1* and Steane *2* quantum codes. To the left of the *dotted line*, the depicted circuit corresponds to the repetition code. The first line corresponds to the input qubit. H is Hadamard gate

in the original basis. So applying the same method again will in fact detect all errors. The encoding of the *Shor and Steane code* are shown in Fig. 4.25. The error correction methods briefly described here are not only type possible (for more details see reviews [145–148]).

References

1. M.A. Nielsen, I.L. Chuang, *Quantum Computation and Quantum Information* (Cambridge University Press, New York, 2000)
2. O. Morsch, *Quantum Bits and Quantum Secrets: How Quantum Physics Revolutionizing Codes and Computers* (Wiley, Weinham, 2008)
3. B. Schumacher, Quantum coding. Phys. Rev. **A51**, 2738–2747 (1995)
4. V.G. Plekhanov, Quantum information and quantum computation. in *Transaction of Computer Science College*, Tallinn, 2004, pp. 161–282
5. B.B. Kadomtsev, *Dynamics and Information* (UFN, Moscow, 1997). (in Russian)
6. D.P. Di Vincenzo, The physical implementation of quantum computation. Fortschr. der Physik (Prog. Phys.) **48**, 771–783 (2000)
7. C.A. Perez-Delgado, P. Kok, Quantum computers: definition and implementation. Phys. Rev. **A83**, 012303–012315 (2011)
8. K. Goser, P. Glösekötter, J. Dienstuhl, *Nanoelectronics and Nanosystems* (Springer, Berlin, 2004)
9. G.E. Moore, Cramming more components onto integrated circuits. Electronics **38**, 114–117 (1965)
10. M. Lacham, M.E. Newman, C. Moore, Why any sufficiently advanced technology is indistinguishable from noise. Am. J. Phys. **72**, 1290–1293 (2004)
11. P.A.M. Dirac, *The Principles of Quantum Mechanics* (Oxford University Press, Oxford, 1958)
12. A. Barenco, C.H. Bennett, R. Cleve et al., Elementary gates for quantum computation. Phys. Rev. **A52**, 3457–3467 (1995)
13. ArXiv, quant - ph/9503016
14. S.L. Braunstein, *Quantum Computations, Encyclopedia of Applied Physics, Update* (Wiley, New York, 1999), pp. 239–256
15. V.G. Plekhanov, Fundamentals and applications of isotope effect in solids. Prog. Mat. Sci. **51**, 287–426 (2006)

16. D. Aharonov, Quantum Computation. in *Annual Reviews of Computational Physics VI*, ed. by D. Stauffer (Singapore, World Scientific, 1998), pp. 143–184
17. D. Aharonov, Adiabatic quantum computer. SIAM J. Comput. **37**, 166–194 (2007)
18. D. Aharonov, Lanl/arXiv/ quant-ph/0405098
19. D. DiVincenzo, Topics in quantum computers. in *Mesoscopic Electron Transport*, Vol. 345, NATO ASI Series E, ed. by L. Sohn, L. Kouwenhoven, G. Schon, (Dordrecht, Kluwer, 1997), p. 657
20. D. DiVincenzo, arXiv: cond-mat/9612125. Vol. **1**, 12 (Dec 1996)
21. D. DiVincenzo, Quantum computers and quantum coherence. J. Magn. Magn. Mats. **200**, 202–216 (1999)
22. H.-K. Lo, T. Spiller, S. Popescu (eds.), *Introduction to Quantum Computation and Quantum Information* (World Scientific, London, 1998)
23. Pellizari T., Quantum computers, error-correction and networking: quantum optical approaches, in [22], pp. 270–311
24. Toffoli T., Reversible computing. in *Automata, Languages and Programming, Seventh Colloqium*, Lecture Notes in Computer Science, Vol. 84, ed. by J. de Bakker, J. van Leeuven (Berlin, Springer, 1980), pp. 632–644
25. T. Toffoli, Bicontinuous extensions of invertible combinatorial functions. Math. Syst. Theory **14**, 13–23 (1981)
26. J. Grashka, *Quantum Computing* (McGraw-Hill, New York, 1999)
27. D. Deutsch, Quantum computational networks. Proc. R. Soc. (Lond.) **A425**, 73–90 (1989)
28. V. Vedral, M. Plenio, Basics of quantum computation. Prog. Quant. Electron. **22**, 1–40 (1998)
29. M.V. Plenio, P.L. Knight, Limits to quantum computation due to decoherence, in [31], pp. 227–232
30. C. Macchiavello, G.M. Palma, Error correction and fault-tolerant computation, ibid, pp. 232–242
31. D. Bouwmeester, A.K. Ekert, A. Zeilinger (eds.), *The Physics of Quantum Information: Quantum Cryptography, Quantum Teleportation, Quantum Computation* (Springer, New York, 2000)
32. S. Datta, B. Das, Electronic analog of the electro optic modulator. Appl. Phys. Lett. **56**, 665–671 (1990)
33. M. Johnson, Bipolar spin switch. Science **260**, 320–323 (1993)
34. M. Johnson, The all-metal spin transistor. IEEE Spectr. **31**, 47–51 (1994)
35. M. Johnson (ed.), *Magnetoelectronics* (Academic Press, New York, 2004)
36. D. DiVincenzo, Quantum computing and single-qubit measurements using the spin-filter effect. J. Appl. Phys. **85**, 4785–4787 (1999)
37. S.Das Sarma, J. Fabian, X. Hu, I. Žutic , Spin electronics and spin computation, Solid State Commun. 119, 207–215, 2001
38. D.D. Awschalom, D. Loss, N. Samarth (eds.), *Semiconductor Spintronics and Quantum Computation* (Springer, Berlin, 2002)
39. N. Samarth, An introduction to semiconductor spintronics. in *Solid State Physics*, Vol. 58, ed. by H. Ehrenreich, F. Spaepen (Academic Press, New York, 2004)
40. G.A. Prinz, Magnetoelectron. Sci. **282**, 1660–1663 (1998)
41. I. Zutic, J. Fabian, S. Das Sarma, Spintronics: fundamentals and applications. Rev. Mod. Phys. **78**, 323–410 (2004)
42. M.E. Flatte, J.M. Byers, W.H. Lau, in *Semiconductor Spintronics and Quantum Computation*, ed. by D.D. Awschalom, D. Loss, N. Samarth (Springer, New York, 2002)
43. B.P. Zakharchenya, V.L. Korenev, Integrating magnetism into semiconductor electronics, Uspekhi Fiz. Nauk (Mosc.) **175**, 629–635, 2005 (in Russian)
44. M. Johnson, Spintronics. J. Phys. Chem. **B109**, 14278–14291 (2005)
45. M.I. Dyakonov (ed.), *Spin Physics in Semiconductors* (Springer, New York, 2008)
46. S. Bandyopadhyay, M. Cahay, *Introduction to Spintronics* (CRC, Broken Sound Parkway, 2008)

47. S. Das Sarma, J. Fabian, X. Hu, et al., Theoretical perspectives on spintronics and spin-polarized transport. IEEE Trans. Magn. **36**, 2821–2827 (2000)
48. S. Maekawa (ed.), *Concepts in Spin Electronics* (Oxford UniversityPress, Oxford, 2006)
49. G. Burkhard, H.A. Engel, D. Loss, Spintronics and quanrum dots for quantum computing and quantum communication. Fortsch. Phys. **48**, 965–980 (2000). This is a special issue on Experimental Proposals for Quantum Computations. ed. by S.L. Braunstein, H.-K. Lo
50. G. Burkhard, H.A. Engel, D. Loss, Spintronics, quantum computing, and quantum communication in quantum dots, in [31], pp. 241–265
51. D.P. DiVincenzo, D. Loss, Quantum computers and quantum coherence. J. Magn. Magn. Matls. **200**, 202–215 (1999)
52. R. Hanson, Electron Spin in Semiconductor Quantum Dot, Ph.D. Thesis, Delft University of technology, The Netherland, 2005
53. D. Deutsch, Quantum theory, the church—turing principle and the universal quantum computer. Proc. Roy. Soc. (Lond.) **400**, 97–117 (1985)
54. D. Deutsch, *The Fabric of Reality* (Penguin Press, Allen Line, 1998)
55. P. Benioff, The computer as a physical system: a microscopic quantum mechanical Hamiltonian model of computers as represented by turing machine. J. Stat. Phys. **22**, 563–591 (1980)
56. P. Benioff, Quantum mechanical Hamiltonian models of Turing machine, ibid, **29**, 515–546 (1982)
57. D. Deutsch, R. Jozsa, Rapid solution of problems by quantum computation. Proc. R. Soc. (Lond.) **A439**, 553–448 (1992)
58. R. Cleve, A. Ekert, C. Macciavello, M. Mosca, Quantum algorithms revisited. Proc. R. Soc. (Lond.) **A454**, 339–354 (1998)
59. D.R. Simon, On the power of quantum computation. in *Proceedings of the 35th Annual Symposium on Foundations of Computer Science*, Los Alamitos, IEEE Computer Society Press, !994, pp. 116–123
60. D.R. Simon, On the power of quantum computation. SIAM J. Comput. **26**, 1474–1483 (1997)
61. P. Shor, Polynomial-time algorithms for prime factorization and dicrete logarithms on a quantum computer. in *Proceedings of the 35th Annual Symposium on Foundations of Computer Science*, Los Alamitos, IEEE Computer Society Press, !994, pp. 124–134
62. Lanl/arXiv/quant-ph/ 9508027
63. P. Shor, IEEE Press SIAM J. Comp. **26**, 1484–1509 (1997)
64. V.G. Plekhanov, Isotopes in Condensed Matter. (Springer, Heidelberg, 2012)
65. K.A. Valiev, A.A. Kokin, *Quantum Computers: Hopes and Reality* (RC Dynamics, Moscow, 2001). (in Russian)
66. L.K. Grover, A fast quantum mechanica algorithm for database search. in *Proceedings of the 28th ACM Symposium on Theory of Computation*, New York, Association for Computing, Machinery, 1999, pp. 212–219
67. L.K. Grover, Lanl, arXiv/quant-ph/9605043
68. L.K. Grover, Quantum mechanics helps in searching for a needle in a haystack. Phys. Rev. Lett. **79**, 325–328 (1997)
69. M. le Bellac, *A Short Introduction to Quantum Information and Quantum Computation* (Cambridge University Press, Cambridge, 2006)
70. A. Ekert, R. Jozsa, Quantum computation and Shor's factoring algorithm. Rev. Mod. Phys. **68**, 733–753 (1996)
71. D. Beckman, A.N. Chari, S. Devabhaktuni et al., Efficient networks for quantum factoring. Phys. Rev. **A54**, 1034–1063 (1996)
72. A. Ekert, P. Hayden, H. Inamori, Basic concepts in quantum computation, Lanl/ArXiv/quant-ph/ 0011013
73. S.J. Lomomnaco, Jr., Shor's quantum factoting algorithm version, Lanl/ArXiv/quant-ph/0010034
74. Steane A., Quantum Computing (RCD Press, Moscow, 2000) (in Russian)

75. J. Eisert, M.M. Wolf, Quantum Computing. in *Handbook of Nature-Inspired and Innovative Computing*, Berlin, 2006
76. J. Stolze, D. Suter, *Quantum Computing* (A Short Course from Theory to Experiment)(Wiley, Weiheim, 2008)
77. N. Yanofsky, M. Manucci, *Quantum Computing for Computer Scientists* (Cambridge University Press, Cambridge, 2008)
78. D.E. Knuth, *The Art of Computer Programming: Semiempirical Algorithms*, vol. 2 (Addison-Wesley, New York, 1981)
79. D. Coppersmith, An approximate Fourier transform useful in quantum factiringm IBM Research Report RC 19642, 1994
80. S. Hallgren, Polynomial-time quantum algorithmz for Pell's equation and the principal ideal problem. in *Proceedings of the 35th Annual ACM Symposium on Theory of Computing*, New York, Association for Computing Machinery Press, 2002, pp. 653–658
81. O. Regev, Quantum computation and lattice problems. in *Proceedings of the 43th Annual Symposium on the Foundation of Computer Science* Los Alamitos, IEEE Computer Science Press, 2002, pp. 520–530
82. M. Gridni, L. Schulman, M. Vasirani et al., Quantum mechanical algorithms for the non-abelian hidden subgroup problem. in *Proceedings of the 33rd ACM Symposium on Theory of Computing*, New York, ACM Press, 2001, pp. 68–74
83. M. Ettinger, P. Hoyer, E. Knill, The quantum query complexity of the hidden subgroup problem is polynomial, Lanl/arXiv/quant-ph/0401083
84. A. Kuperberg, Subexponential-time quantum algorithm for the dihedral hidden subgroup problem. Lanl/arXiv/quant-ph/0302112
85. E. Farhi, J. Goldstone, S. Guthman, et al., Quantum computation by adiabatic evolution, Lanl/arXiv/quant-ph/ 0001106
86. W. van Dam, M. Mosca, U. Vasirani, How powerful is adiabatic quantum computation? in *Proceedings of the 42nd Annual Symposium on the Foundations of Computer Science*, Los Alamitos, IEEE Computer Society Press, 2001, pp. 279–287
87. W. van Dam, U. Vazirani, Limits on quantum adiabatic optimization. in *5th Workshop on Quantum Information Processing (QIP 2002)*, Yorktown Heights, New York
88. B. Reichrardt, The quantum adiabatic optimization algorithm and local minima. in *Proceedings of the 36th Annual ACM Symposium on Theory of Computing*, Chicago, 2004
89. D. Aharonov, A. Ta-Shma, Adiabatic quantum state generation and statistical zero knowledge, Lanl/arXiv/quant-ph/ 0301023
90. D. Aharonov, W. van Dam, J. Kempe et al., Adiabatic quantum computation is equivalent to standard computation. SIAM J. Comput. **37**, 166–194 (2007)
91. D. Aharonov, W. van Dam, J. Kempe et al., Lanl/arXiv/quant-ph/ 0405098 (2008)
92. G. Beneti, G. Casati, G. Strini, *Principles of Quantum Computation and Information* (World Scientific Publishing, Singapore, 2005)
93. J.W. Emsley, J.C. Lindon, *NMR Spectroscopy Using Liquid Crystals Solvents* (Pergamon Press, Oxford, 1975)
94. M. Levitt, *Spin Dynamics* (Basics of Nuclear Magnetic Resonance (Wiley, New York, 2001)
95. R.R. Ernst, G. Bodenhausen, A. Wokaun, *Principles of Nuclear Magnetic Resonance in One and Two Dimensions* (Oxford University Press, Oxford, 1987)
96. R. Freeman, Shaped radiofrequency pulses in high resolution NMR. Prog. NMR Spectr. **32**, 59–106 (1998)
97. I.L. Chuang, N. Gershenfeld, M. Kubinec, Experimental implementation of fast quantum searching. Phys. Rev. Lett. **80**, 3408–3411 (1998)
98. I.L. Chuang, N. Gershenfeld, M. Kubinec, Bulk quantum computation with NMR: theory and experiment. Proc. R. Soc. (Lond.) **A454**, 447–467 (1998)
99. I. Chuang, Y. Yamamoto, Simple quantum computer. Phys. Rev. **A52**, 3489–3496 (1995)
100. L. Vandersypen, M. Steffen, G. Breita et al., Experimental realization of Shor's quantum factoring algorithm using NMR. Nature **414**, 883–887 (2001)

101. D. Esteve, J.M. Raimond, J. Dalibard (eds.), *Quantum Coherence and Information Processing* (Elsevier, London, 2004)
102. I. Bloch, Ultracold quantum gases in optical lattices. Nat. Phys. **1**, 23–27 (2005)
103. T.C. Ralph, Quantum optical systems for the implementation of quantum information processing. Rep. Prog. Phys. **69**, 853–898 (2006)
104. Steane A.M., The ion trap quantum information processor, Appl. Phys. **B64**, 623–642 (1997)
105. H. Häffner, C.F. Roos, R. Blatt, Quantum computing with trapped ions. Phys. Rep. **469**, 155–203 (2008)
106. J.I. Cirac, P. Zoller, Quantum computations with cold trapped ions. Phys. Rev. Lett. **74**, 4091–4094 (1995)
107. C. Monroe, D.M. Meekhof, B.E. King et al., Demonstration of a universal quantum logic gate. Phys. Rev. Lett. **75**, 4714–4717 (1995)
108. D.J. Wineland, M. Barret, J. Britton et al., Quantum information processing with trapped ions. Phil. Trans. R. Soc. (Lond.) **A361**, 1349–1362 (2003)
109. T. Spiller, Quantum information processing: cryptography, computation, and teleportation. Proc. IEEE **84**, 1719–1746 (1996)
110. V.V. Schmidt, *Introduction in Physics of Superconductors* (Science, Moscow, 1982). (in Russian)
111. Yu. Makhlin, G. Schön, A. Shnirman, Quantum-state engineering with Josephson-junction devices. Rev. Mod. Phys. **73**, 357–400 (2001)
112. J.H. Platenberg, P.C. de Groot, C.J.P.M. Harmands et al., Demonstration of controlled-NOT quantum gates on a pair of superconducting quantum bits. Nat. (Lond.) **447**, 836–839 (2007)
113. P. Benioff, Quantum mechanical models of turing machines that dissipate no energy. Phys. Rev. Lett. **48**, 1681–1684 (1982)
114. A.M. Steane, Error correcting codes in quantum theory. Phys. Rev. Lett. **77**, 793–797 (1996)
115. J. Preskill, Reliable quantum computers. Proc. R. Soc. (Lond.) **A454**, 385–410 (1998)
116. B.E. Kane, A silicon-based nuclear spin quantum computer. Nature **393**, 133–137 (1998)
117. Lanl/arXiv:quant-ph/0003031
118. B.E. Kane, Silicon-based quantum computation, Fortschr. Phys. **48**, 1023–1041 (2000)
119. A.M. Tyryshkin, S.A. Lyon, A.V. Astashkin, A.M. Raitsining, Electron spin relaxation times of phosphorus donors in silicon. Phys. Rev. **B68**, 193207–4 (2003)
120. D.K. Wilson, G. Feher, Electron spin resonance on donors in silicon. Phys. Rev. **124**, 1068–1083 (1961)
121. V.G. Plekhanov, Isotopetronics-new direction of nanoscience, Lanl/ArXiv/gen.phys/1007.5386
122. J.S. Waugh, C.P. Slichter, Mechanism of nuclear spin-lattice relaxation in insulators at very low temperatures. Phys. Rev. **B37**, 4337–4339 (1988)
123. B.E. Kane, N.S. McAlpine, A.S. Dzurak, B.G. Clark, Single Spin measurement using single-electron transistors to probe two-electron systems. Phys. Rev. **B61**, 2961–2972 (2000)
124. A.J. Skinner, M.E. Davenport, B.E. Kane, Hydrogenic spin quantum computing in silicon. Phys. Rev. Lett. **90**, 087901–4 (2003)
125. R. Vrijen, E. Yablonovich, K. Wang et al., Electron spin resonance transistors for quantum computing in Silicon–Germanium heterostructures. Phys. Rev. **A62**, 12306–12309 (2000)
126. I. Shlimak, V.I. Safarov, I. Vagner, Isotopically engineered Si/SiGe nanostructures as basic elements for a nuclear spin quantum computer. J. Phys. Condens. Matter **13**, 6059–6065 (2001)
127. I. Shlimak, I. Vagner, Quantum information processing based on ^{31}P nuclear spin qubits in a quai-one-dimensional ^{28}Si nanowire. Phys. Rev. **B75**, 045336–6 (2007)
128. I. Shlimak, V. Ginodman, A. Butenko et al., Electron transport in a slot-gate Si MOSFET, Lanl/ArXiv: cond-mat./0803.4432
129. F. Schäffler, High-electron-mobility Si/SiGe heterostructures: influence of the relaxed buffer layer. Semicond. Sci. Technol. **7**(n 2), 260–267 (1992)
130. V.G. Plekhanov, Elementary excitations in isotope -mixed crystals. Phys. Rep. **410**, 1–235 (2005)

131. V.G. Plekhanov, Manifestation and origin of the isotope effect. Lanl/ArXiv/gen. phys./0907.2024
132. V.G. Plekhanov, Isotopes in quantum information, Preprint N 2 of Computer Science College, Tallinn, 2007. (in Russian)
133. D. Bimberg, M. Grundman, N.N. Ledenzov, Quantum Dot Heterostructure, (Wiley, Chichester, 1999)
134. D.P. DiVincenzo, Two-bit are universal for quantum computation. Phys. Rev. **A51**, 1015–1022 (1995)
135. D.P. DiVincenzo, Quantum computation, Science **270**, 256–261 (1995)
136. Special issue of Solid State Communications, Vol. 149,2009
137. A. Olaya-Castro, N.F. Johnson, Quantum information processing in nanostructures, Lanl/Arxiv/quant-ph/0406133
138. D. Gammon, D.G. Steel, Optical studies of single quantum dots, Phys. Today **55**,36–41 (2002)
139. P. Michler (ed.), *Single Semiconductor Quantum Dots* (Springer, Berlin, 2009)
140. S. Kiravittaya, A. Rastelli, O.G. Schmidt, Advanced quantum dot configurations. Rep. Prog. Phys. **72**, 046502–046534 (2009)
141. V.G. Plekhanov, Isotope-based quantum information, Lanl/ArXiv/quant-ph/0909.0820
142. L. Quiroga, N.F. Johnson, Entangled Bell and Greenberg-Horne-Zeilinger state of excitons in coupled quantum dots. Phys. Rev. **83**, 2270–2273 (1999)
143. A.M. Stoneham, A.J. Fisher, P.T. Greenland, Optically driven silicon-based quantum gates with potential for high-temperature operation. J. Phys. Condens. Matter **15**, L447–L451 (2003)
144. A.M. Stoneham, *Theory of Defects in Solids* (Oxford University Press, Oxford, 1975)
145. A.M. Steane, Introduction to quantum error correction. Phil Transac. (Lond.) **356**, 1739–1758 (1998)
146. J. Preskill, Fault-tolerant quantum computation, in [22], pp. 213–269
147. A.M. Steane, Quantum error correction, in [22], pp. 184–212
148. J. Kempe, Approach to quantum error correction, Lanl/ArXiv/quant-ph/0612185
149. A. Peres, Reversible logic and quantum computers. Phys. Rev. **A32**, 3266–3276 (1985)
150. A. Peres, *Quantum Theory: Concepts and Methods* (Kluwer Academic Publishers, Dodrecht, 1993)
151. W.K. Wooters, W.H. Zurek, A single quantum state cannot be cloned. Nature **299**, 802–803 (1982)
152. D. Dieks, Communications by electron-paramagnetic-resonance devices. Phys. Lett. **A92**, 271–272 (1982)
153. P.W. Shor, Scheme for reducing decoherence in quantum computer memory. Phys. Rev. **A52**, R2493–R2496 (1995)
154. A.R. Calderbrank, P.W. Shor, Good quantum error-correcting codes exist. Phys. Rev. **A54**, 1098–1105 (1996)
155. R.W. Hamming, *Coding and Information Theory*, 2nd edn. (Prentice Hall, Englewood Cliffs, 1986)

Index

DOI: 10.1007/978-3-642-28750-3, © The Author(s) 2012